Towards a Universal Size Distribution in a Polymer Network. Implications for Drug Delivery and Plasmonic Nanoparticle Transport Phenomena in Polysaccharide and Synthetic Hydrogels.

SUPPORTING INFORMATION

Stefano A. Mezzasalma[a,b], Michela Abrami[c], Gabriele Grassi[d], Mario Grassi*[c]

[a]*Materials Physics Division, Ruđer Bošković Institute, Bijeniška cesta 54, 10000 Zagreb, Croatia*
[b]*Institute for advanced Neutron and X-ray Science (LINXS), Lund University, Ideon Building, Delta 5, Scheelevägen 19, 223 70 Lund, Sweden*
[c]*Department of Engineering and Architecture, Trieste University, via Valerio 6, I-34127 Trieste, Italy*
[d]*Clinical Department of Medical, Surgical and Health Sciences, Cattinara University Hospital, Strada di Fiume 447, I-34149 Trieste, Italy*

Contents

*Corresponding Author; e-mail: mario.grassi@dia.units.it

1. Statistical Mechanics of Rubber Elasticity

1.1. Summary of the Gaussian Model of Polymer Elasticity

The first integral in Flory's elasticity theory is a configurational entropy term accounting for the probability distribution of random end-to-end chain vectors in the deformed state, $W = W(\mathbf{r})$:[1]

$$\tfrac{1}{\nu} \ln \Omega_{_1} = \ln \mathrm{J} + \int_{\Re^3} W(\mathbf{R}) \ln \frac{W(\mathbf{r})}{W(\mathbf{R})} \, d\mathbf{R} \tag{1.1}$$

where ν is the number of cross-linked strands, meant to be homogeneously distributed in a continuum space, and J is the Jacobian determinant of the deformation gradient,[2] assessing the material point transformation that maps the undeformed network into a stretched state, $\mathbf{R} = (X, Y, Z) \rightarrow (x, y, z) = \mathbf{r}$. Further details can be found in seminal works on the subject[3–5] and in our recent study.[6] Formally, it suffices to recall that undeformed and stretched configurations can be represented in Cartesian basis $\{\mathbf{e}_x, \mathbf{e}_y, \mathbf{e}_z\}$ as $x_i = \alpha_i X_i$, with $\mathrm{J} = \prod_i \alpha_i$. The coordinates $x_i = (\mathbf{e}_i \cdot \mathbf{r})$ transform into $X_i = (\mathbf{e}_i \cdot \mathbf{R})$ by means of positive elongation coefficients (or extension ratios) $\alpha_i = \alpha_x, \alpha_y, \alpha_z$, characterizing the homogeneous deformation.

Behind Eq. (1.1) is an entropy-driven elastic response. As there is only one exactly straight conformation, against a large number of curled ones, stretching a flexible chain lowers its conformational entropy to yield an opposing force. Networks are normally modelled by letting the persistence length $\lambda_{_P} \leq$ contour length L_c (i.e. the length scale for the tangent–tangent correlation decay does not exceed the distance between cross-link points), disregarding rigid strands with no entropic elasticity. Highly flexible chains ($\lambda_{_P} \ll L_c$) display in this case a purely entropic response, although semiflexible ones ($\lambda_{_P} \approx L_c$) still undergoes relevant bending fluctuations of thermal nature. Eq. (1.1) instead does not take into account the repulsive bulk interactions of chemical links, as it is only the entropy part related to the chain system.[7] Excluded volumes are presupposed to be *totally* screened by the attractive force between segments generally foreseen by the "Perturbation-Attraction Theorem" (also known in polymer physics as Flory's theorem).[8]

In Flory's view, $\Omega_{_1}$ is anyway not enough to write the full partition function of an elastic network, as a second "perfect gas" contribution, $\Omega_{_2}$, is required.[9] It comes from the likelihood to

find all the cross-linked units juxtaposed in a network of volume V_0 which deforms into $V = JV_0$, and turns out to be $\frac{1}{\nu}\ln\Omega_2 = -\frac{1}{2}\ln J + \text{const}$. The total entropy ($S$) in Boltzmann's constant units (k_B), to be evaluated differentially between initial and final mechanical states, finally is:

$$\frac{S}{k_B}(\{\alpha_k\}; W) \equiv \ln\Omega = \ln\Omega_1 + \ln\Omega_2 \tag{1.2}$$

In our former work,[6] the derivation of Ω_2 was recast to allow for a reconsideration of cross-link fluctuations in a finite elemental volume. To avoid further hypotheses in addition to that present (i.e. testing a universal distribution function), we won't deal here with our modified perfect gas term. This means focusing on systems kept at a constant volume (J = const), an isochoric condition that recurs in many experiments.

Following Flory's assumption, and ignoring enthalpic contributions, it is generally acknowledged that the Gaussian density $W_g(|\mathbf{R}| = R)$, i.e.:

$$W_g(R) = \prod_i W_{gi}(X_i) \tag{1.3}$$

$$W_{gi}(X_i) = \frac{\beta}{\sqrt{\pi}}\exp(-\beta^2 X_i^2) \tag{1.4}$$

generates a Helmholtz free energy per unit referential volume (F) which is essentially of entropic nature:[10,11]

$$\frac{1}{V_0}F(\{\alpha_k\}) = -\frac{T}{V_0}S(\{\alpha_k\}; W_g) = -\rho k_B T s_g(\{\alpha_k\}) \tag{1.5}$$

where T is the absolute temperature, $\rho = \nu/V_0$ is the density of cross-linked strands in undeformed states (in our experiments T, ρ = constant), and the notation:

$$s_g(\{\alpha_k\}) \equiv \tfrac{1}{\nu}(\ln\Omega_{1n})_{T,V} = -\tfrac{1}{2}\sum_i \alpha_i^2 + \text{const} \tag{1.6}$$

denotes the first configurational integral for a Gaussian system (const = $\frac{3}{2}$). We remember that $\beta^2 = 3/(2\langle\mathbf{R}^2\rangle)$ depends on intrinsic polymer features (contour length and Kuhn's step size, $\langle\mathbf{R}^2\rangle = L_c l_k$) but does not appear in Eq. (1.6). Consequently, a quadratic form in α_i, regardless

of the disorder in distribution (expressed by the variance), can be considered indicative of normal statistics. A guide on how to perform the explicit computation of the first configuration integral is detailed in SI (2.1).

Networks are taken to be homogeneous, isotropic, straining uniformly and formed by strands obeying a given force-extension curve. From Eqs. (1.5, 1.6), the popular relationships for Young's (E) and shear (G) moduli follow:[11]

$$E \;=\; 3\mathrm{Q}^{-\frac{1}{3}}\rho k_{_B}T\;, \quad G \;=\; \tfrac{1}{3}E \tag{1.7}$$

applying respectively to uniaxial and pure shear deformation geometries in swollen ($\mathrm{J} \equiv \mathrm{Q} =$ swelling factor) and unswollen ($\mathrm{Q} = 1$) materials:[1,10]

$$\alpha_x \equiv \mathrm{Q}^{\frac{1}{3}}\alpha, \quad \alpha_y = \alpha_z = \mathrm{Q}^{\frac{1}{3}}\alpha^{-\frac{1}{2}} \qquad \text{(u.d.)} \tag{1.8}$$

$$\mathrm{Q}^{-\frac{1}{3}}\alpha_x = \mathrm{Q}^{\frac{1}{3}}\alpha_y^{-1} \equiv \alpha, \quad \alpha_z = \mathrm{Q}^{\frac{1}{3}} \quad \text{(p.s.)} \tag{1.9}$$

No torques are supposed to take place at cross-link points (strands either stretch or compress, but do not bend). In the first case (u.d.), E stems from the uniaxial stress component (f_σ):

$$E \;\approx\; \frac{f_\sigma}{\varepsilon}\;, \quad f_\sigma \;=\; -\,\frac{\rho k_{_B}T}{\mathrm{Q}}\left(\frac{\partial s_g}{\partial \alpha}\right)_{_{T,V}} \tag{1.10}$$

the engineering strain $\varepsilon = \alpha - 1$ being taken in the limit of small deformations ($\alpha \approx 1$). In the second (p.s.), G descends from the shearing stress (τ_0):

$$G \;\approx\; \frac{\tau_0^g}{\gamma^s}\;, \quad \tau_0^g \;=\; -\,\frac{\rho k_{_B}T}{\mathrm{Q}}\left(\frac{\partial s_g}{\partial \gamma^s}\right)_{_{T,V}} \tag{1.11}$$

where the shear strain $\gamma^s = \alpha - 1/\alpha$ is still regarded near $\alpha = 1$. Such calculations clearly focus on the low-strain regime, where the entropic character of elasticity prevails. It is important to remark that a distribution of polymer lengths would imply that individual filaments no longer experience a zero force (as they would do when all lengths equal the mean value): a fraction of

these will be stretched, others will be compressed relative to the relaxed state. On this basis, the bulk mechanical equilibrium at zero isotropic stress would not develop at zero strain, but at some finite value of it. This is another reason for inquiring a distribution function that does not necessarily reflect the Gaussian equilibrium state. For explicitly non-Gaussian distributions, and networks that are far from ideality, the entropic contribution in Flory's configurational integral thus acquires a more thermodynamic significance.

1.2. Pierced Gaussian (Near the Origin)

We verify now how the former calculations vary when the most flexible configurational states are removed from the distribution of end-to-end polymer lengths. The simplest way to proceed is "piercing" the Gaussian near the origin, $\mathbf{R} \notin \mathbf{C}\ [\mathbf{0}, u]$, i.e. by disallowing chain vectors to lie in a closed cube of given side $(2u)$ centred at the origin $(\mathbf{0})$. Let $W_h = W_h(\mathbf{R})$ be such a distribution, we still factorize it with respect to each (Cartesian) coordinate:[6,9]

$$W_h(\mathbf{R}) \ = \ \prod_i W_{hi}(X_i) \tag{1.12}$$

now with:

$$W_{hi}(X_i) \ = \ \frac{\beta}{\sqrt{\pi}[1-\Phi(q)]} \exp(-\beta^2 X_i^2) \tag{1.13}$$

Φ denoting the error function (erf) evaluated at $q = \beta u$. The density function $W_h = W_h(\mathbf{R})$ has clearly zero average ($\langle \mathbf{R} \rangle = 0$) and the new variance:

$$\sigma_h^2 \ = \ \left[1 \ + \ \frac{2q\exp(-q^2)}{\sqrt{\pi}(1-\Phi(q))}\right]\sigma^2 \tag{1.14}$$

To carry out the three-dimensional integral in Eq. (1.1) as a function of extension ratios requires some integral calculus, reported in SI (2.2). In the end:

$$\begin{aligned} s_h\left(\{\alpha_i\}\right) \ = \ \int_{\Re^3 - \mathbf{C}\,[\mathbf{0},u]} W_h(\mathbf{R}) \ln \frac{W_h(\mathbf{r})}{W_h(\mathbf{R})}\, d\mathbf{R} \ = \ \frac{s_g}{[1-\Phi(q)]^3}\left[1 \ - \prod_k \Phi\left(q/\alpha_k\right)\right] + \\ - \ \frac{q}{\sqrt{\pi}[1-\Phi(q)]^3} \sum_{k\neq h\neq p} \gamma_k^s \exp(-q^2/\alpha_k^2)\Phi(q/\alpha_h)\Phi(q/\alpha_p) \end{aligned} \tag{1.15}$$

where $k, h, p \in \{x, y, z\}$, each addendum in the sum is taken only once, and $\gamma_i^s = \alpha_i - 1/\alpha_i$ is the i-th shear deformation component. We observe that, as s_h is resumed from letting $W_g \to W_h$ in Eq. (1.6), then $s_h \to s_g$ upon $q \to 0^+$, as expected. On the basis of the integral in Eq. (1.15), the exact solution for the mechanical moduli in the pierced Gaussian case (subindex h) therefore is:

$$\frac{G_h}{\rho k_{_B} T} = \frac{\exp\left(-3q^2/\mathrm{Q}^{\frac{2}{3}}\right)}{\pi^{\frac{3}{2}}\left[\Phi(q)-1\right]^3 \mathrm{Q}^{\frac{8}{3}}} \left\{ \pi^{\frac{3}{2}} \left[\Phi^3(q/\mathrm{Q}^{\frac{1}{3}}) - 1\right] \mathrm{Q}^{\frac{7}{3}} \exp\left(3q^2/\mathrm{Q}^{\frac{2}{3}}\right) - \pi \Phi^2(q/\mathrm{Q}^{\frac{1}{3}}) q \exp\left(2q^2/\mathrm{Q}^{\frac{2}{3}}\right) \times \right.$$
$$\times \left[2q^4(\mathrm{Q}^{\frac{2}{3}} - 1) + q^2(3\mathrm{Q}^{\frac{4}{3}} + \mathrm{Q}^{\frac{2}{3}}) + \mathrm{Q}^{\frac{4}{3}} - \mathrm{Q}^2\right] - \sqrt{\pi}\Phi(q/\mathrm{Q}^{\frac{1}{3}}) q^2 \mathrm{Q}(7\mathrm{Q}^{\frac{2}{3}} - 3) \exp\left(q^2/\mathrm{Q}^{\frac{2}{3}}\right)$$
$$\left. + 2q^3(\mathrm{Q}^{\frac{2}{3}} - 1)\mathrm{Q}^{\frac{2}{3}} \right\} \quad (1.16)$$

still with $E_h = 3G_h$ and regaining Flory's prediction, $G = \rho k_{_B} T \mathrm{Q}^{-\frac{1}{3}}$, for $q \to 0^+$. The calculations bringing to Eq. (1.16) were tested numerically, the main results being documented in SI (2.2.1). For an unswollen material ($\mathrm{Q} = 1$), the former equation simplifies into:

$$\frac{G_h}{\rho k_{_B} T} = \frac{1 - \Phi^3(q)}{\left[1 - \Phi(q)\right]^3} + \frac{4q^2 \Phi(q) \exp(-2q^2)}{\pi \left[1 - \Phi(q)\right]^3} + \frac{4q^3 \Phi^2(q) \exp(-q^2)}{\sqrt{\pi}\left[1 - \Phi(q)\right]^3} \quad (1.17)$$

1.3. Maxwell-Boltzmann Averaging of the Pierced Gaussian

In an alternative derivation of the final moduli, it can be noted that q may be conceived as a random variable, connected with the modulus of an aleatory vector as $q \sim |\mathbf{q}|/\sqrt{3}$, with $\mathbf{q} = \beta \mathbf{u}$. Averaging Eq. (1.15) presents great formal difficulties, thus it is more convenient starting from the power series of q in the first derivatives $(\partial s_h / \partial \alpha_i)$, ruling here all the essential mechanical quantities. At fourth order in q, one obtains:

$$\left(\frac{\partial s_h}{\partial \alpha_i}\right)_{T,V} = -\alpha_i \left[1 + \frac{6}{\sqrt{\pi}}\, q + \frac{24}{\pi}\, q^2 + \frac{2(40-\pi)}{\pi^{3/2}}\, q^3 + \frac{16(15-\pi)}{\pi^2}\, q^4\right] + O(5) \quad (1.18)$$

To remain as general as possible, we would like to regard an isotropic distribution that conforms to a maximally disordered system (as in molecular chaos and Markov's processes).[12] A suitable choice is given by the Maxwell-Boltzmann distribution, which has in fact semi-infinite support,

$|\mathbf{q}| \in [0, +\infty)$, it is infinitesimal in zero and is unimodal:

$$P(\bar{q}, z) \;=\; \frac{2}{\bar{q}} \left(\frac{2z}{\pi}\right)^2 \exp(-z^2/\pi) \tag{1.19}$$

where $\bar{q}z \equiv 2|\mathbf{q}|$ and $\bar{q}$ is the mean value. In SI (2.2.2), each term in Eq. (1.18) is averaged over z to get:

$$\left\langle \left(\frac{\partial s_h}{\partial \alpha_i}\right) \right\rangle_{T,V} \;=\; -\,\alpha_i \left[1 \;+\; 2\sqrt{\frac{3}{\pi}}\,\bar{q} \;+\; 3\bar{q}^2 \;+\; \frac{40-\pi}{3\sqrt{3\pi}}\,\bar{q}^3 \;+\; 5\frac{15-\pi}{12}\,\bar{q}^4\right] \;+\; O(5) \tag{1.20}$$

Since $\sqrt{3/\pi} = 0.97720(5)$, $(40-\pi)/3\sqrt{3\pi} = 4.0020(2)$, $(15-\pi)/12 = 0.98820(1)$, we conjecture that the previous expansion can be approximated by a sum of powers as ky^k ($k \in \mathrm{N}$), so that:

$$\left\langle \left(\frac{\partial s_h}{\partial \alpha_i}\right) \right\rangle_{T,V} \sim\; -\,\frac{\alpha_i}{(1-\bar{q})^2} \tag{1.21}$$

The accuracy of this expression is the better the more $\bar{q}$ is lesser than unity, i.e. $\bar{u}/\sigma \ll \sqrt{2/3} \;\approx$ 0.816. Since the values of these derivatives uniformly increase in each elongation ratio by the constant term $(1-\bar{q})^{-2}$, the mechanical moduli for both unswollen and swollen materials will also exhibit this uniform expansion, i.e.:

$$\frac{E_h}{E} \;=\; \frac{G_h}{G} \;=\; \frac{1}{(1-\bar{q})^2} \;>\; 1 \tag{1.22}$$

1.4. Weibull Distribution

Weibull's distribution, together with Gumbel's and Fréchet's, are typically used in extreme value statistics (EVS).[13] Let the rectangular coordinate $X_i \in [u, \infty)$ ($u \geq 0$), it has the form:[14]

$$W_{wi}(X_i) \;=\; \frac{\delta}{\eta}\left(\frac{X_i - u}{\eta}\right)^{\delta-1} \exp\left[-\,(\tfrac{X_i-u}{\eta})^{\delta}\right] \tag{1.23}$$

where δ and η are positive coefficients bearing the name, respectively, of shape and scale parameters. Eq. (1.23) coincides, evidently, with $(1/\eta)$ times the derivative with respect to X_i of

the stretched exponential contribution. Average value, mode and variance over $[u,\infty)$ are given respectively by:

$$\mu_0 \;=\; \frac{\eta}{\delta}\Gamma_{\frac{1}{\delta}} \tag{1.24}$$

$$M_O \;=\; u \;+\; \frac{\eta}{2}\left(\frac{\delta-1}{\delta}\right)^{\frac{1}{\delta}} \tag{1.25}$$

$$\sigma_w^2 \;=\; \frac{\eta^2}{\delta}\left(2\Gamma_{\frac{2}{\delta}} \;-\; \tfrac{1}{\delta}\Gamma_{\frac{1}{\delta}}^2\right) \tag{1.26}$$

Γ_z generally denoting Euler's gamma function with argument z. In line with our extended conformational calculations,[6] Weibull's law can be extended by continuity to embrace the negative axis:

$$\widetilde{W_{wi}}(X_i) \;\equiv\; \tfrac{1}{2}W_{wi}(X_i) \;+\; \tfrac{1}{2}W_{wi<}(X_i) \tag{1.27}$$

with $W_{wi<}(X_i) = W_{wi}(-X_i)$ in $X_i \in (-\infty,-u]$. Averaging over positive or negative values of X_i will clearly return the same value, therefore the functional:

$$s_w\left(\{\alpha_i\}\right) \;=\; \int_{\Re^{+3}\,\setminus\,\mathbf{C}^+\,[\mathbf{0},u]} W_w(\mathbf{R})\ln\frac{W_w(\mathbf{r})}{W_w(\mathbf{R})}\,d\mathbf{R} \tag{1.28}$$

still furnishes an adequate definition of the entropy per strand in a network undergoing deformation, where the subset $\mathbf{C}^+$ expresses the restriction of $\mathbf{C}$ to the positive semi-axes, and:

$$W_w(\mathbf{R}) \;=\; \prod_{X_i=x,y,z} W_{wi}(X_i) \tag{1.29}$$

As the entropy integral s_w produces strongly non-linear α_i-derivatives, uniaxial deformation (u.d.; Eq. 1.8) and pure shear (p.s.; Eq. 1.9) geometries are treated separately. In SI (2.3), a general expansion is derived for small values of (u/η) near $\alpha = 1$:

$$\left(\frac{\partial s_w}{\partial\alpha}\right)_{\mathrm{Q},T,\Xi} \;=\; -\,e_\Xi\delta^2\mathrm{Q}^{\frac{\delta}{3}}(\alpha-1)\left(1+\tfrac{u}{\eta}Y\right) \;+\; \mathrm{O}(2) \tag{1.30}$$

that is function of a geometry-dependent parameter, $e_\Xi = 3/2$ ($\Xi =$ u.d.) and $e_\Xi = 2$ ($\Xi =$ p.s.). A nontrivial expression of δ and Q for the first-order perturbation coefficient:

$$Y(\delta, \mathrm{Q}) \;=\; \delta\Gamma_{3-\frac{1}{\delta}} \;+\; \left[(1-\delta)(1+\mathrm{Q}^{-\frac{1}{3}}) + (1-\tfrac{1}{\delta})\mathrm{Q}^{-\frac{1}{3}}\right]\Gamma_{2-\frac{1}{\delta}} \;+\; \tfrac{1}{\delta}\left(1-\tfrac{1}{\delta}\right)\mathrm{Q}^{-\frac{1+\delta}{3}}\Gamma_{1-\frac{1}{\delta}} \quad (1.31)$$

reflects a strong deviation of the distribution from the normal behaviour. Consistently with the model constraints (see SI 3.1), the above equation is not defined for $\delta \leq 1$. For $\delta > 1$, it can be simplified by means of the fundamental properties of Euler's Gamma function, $\Gamma_{z+1} = z\Gamma_z$ ($\mathrm{Re}\{z\} > 0$) and $\Gamma_{1-z}\Gamma_z = \pi/\sin(\pi z)$ ($z \notin \mathrm{Z}$).[15] Some algebraic developments first return:

$$Y(\delta, \mathrm{Q}) \;=\; (1-\tfrac{1}{\delta})\left[\delta \;+\; (2-\delta-\tfrac{1}{\delta})\mathrm{Q}^{-\frac{1}{3}} \;+\; \tfrac{1}{\delta}\mathrm{Q}^{-\frac{1+\delta}{3}}\right]\Gamma_{1-\frac{1}{\delta}} \qquad (\delta > 1) \quad (1.32)$$

that, for unswollen materials, reduces to:

$$Y(\delta, 1) \;=\; 2\,(1-\tfrac{1}{\delta})\,\Gamma_{1-\frac{1}{\delta}} \qquad (\delta > 1) \quad (1.33)$$

with constant Rayleigh's and null exponential behaviour, i.e. $Y(2,1) = \sqrt{\pi}$ and $Y(1^+, 1) = 0$, respectively. Note, however, that an experimental analysis of the perturbation term is beyond the scope of the present investigation.

Finally, the mechanical moduli calculated from Eq. (1.10) and Eq. (1.11) under the Weibullian statistics (subindex w) are:

$$E_w \;=\; \tfrac{3}{2}\delta^2\mathrm{Q}^{\frac{\delta}{3}-1}\rho k_{_B}T(1+\tfrac{u}{\eta}Y)\,, \quad G_w \;=\; \tfrac{1}{3}E_w \quad (1.34)$$

still standing in the same proportion $(1:3)$ of the Gaussian case, with:

$$\frac{E_w}{E} \;=\; \frac{G_w}{G} \;=\; \tfrac{1}{2}\delta^2\mathrm{Q}^{\frac{\delta-2}{3}}(1+\tfrac{u}{\eta}Y) \quad (1.35)$$

Such a relation could also be set in a form explicitly independent of the length scale parameter (η), as it enters the distribution mean (μ_0). A parametric plot of the perturbation term (Y) is

Figure 1: Representation of the perturbation term $Y(\delta > 1)$ as a function of the shape parameter for a number of swelling ratios.[16] For $Q^* = 1$, a crude approximation over ample δ intervals is $Y \approx 2$. The perturbation tends overall to increase/decrease with increasing δ when $Q^* < 1/Q^* > 1$. However, this does not apply to the range $1 < \delta \leq 2$, where $Y(\delta \sim 1^+)$ shows a decreasing behavior with maximum excursion $|\Delta Y| < 0.5$.

finally illustrated in Fig. (1) and Fig (2) in a rather wide range for δ and Q.

1.5. Generalized Weibull Distribution (with Statistical Dependence Parameter a)

Weibull's law can be generalized to the following expression:[17]

$$W^*_{wi}(X_i) \;=\; \frac{\delta}{\Gamma_a \eta}\left(\frac{X_i - u}{\eta}\right)^{a\delta-1} \exp\left[-\,(\tfrac{X_i-u}{\eta})^{\delta}\right] \;. \tag{1.36}$$

Together with Gumbel's and Fréchet's generalized laws, it finds applications to sums of random variables, the parameter $a > 0$ providing a measure of their statistical dependence (or, eventually, correlation). For instance, within a Gumbel-like statistics, the case $a = 1$ corresponds to the (highly correlated) $1/f$ noise.[17,18]

With this (slight) modification, the same calculation schemes in SI (2.3) simply transform the mechanical moduli in Eqs. (1.34) into:

$$E_a \;=\; \tfrac{3}{2}\delta^2 \mathrm{Q}^{\frac{\delta}{3}-1} a\rho k_{_B} T(1 + \tfrac{u}{\eta} Y_a) \;, \quad G_a \;=\; \tfrac{1}{3} E_a \tag{1.37}$$

with:

$$\frac{E_a}{E} \;=\; \frac{G_a}{G} \;=\; \tfrac{1}{2} a\delta^2 \mathrm{Q}^{\frac{\delta-2}{3}}(1 + \tfrac{u}{\eta} Y_a) \tag{1.38}$$

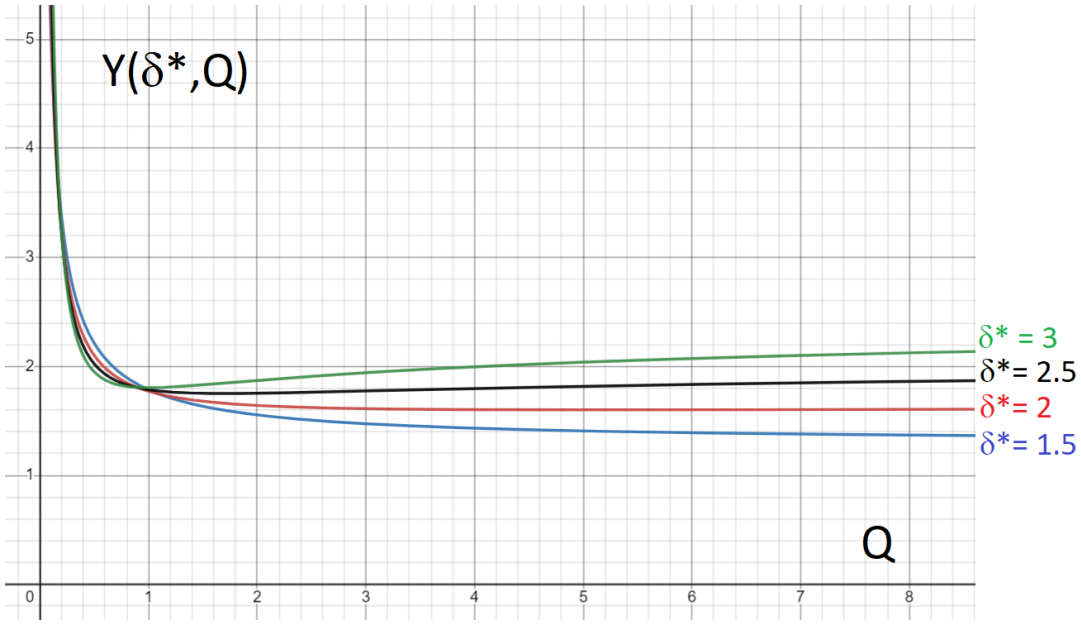

Figure 2: Representation of the perturbation term $Y(Q \geq 0)$ as a function of the swelling ratio for a number of shape parameter values.[16] Note that, consistently with Fig. (1), the Y behaviours revert their comparative trend at $\mathrm{Q} = 1$ (the smallest becomes the largest and vice versa). Near the unswollen state, perturbations do not differ that much.

and:

$$Y_a(\delta, Q) \;=\; \frac{1}{\Gamma_{1+a}} \left[a\delta \;+\; (2 - \delta - \tfrac{1}{\delta})\mathrm{Q}^{-\frac{1}{3}} \;+\; \tfrac{1}{\delta}\mathrm{Q}^{-\frac{1+\delta}{3}} \right] \Gamma_{1+a-\frac{1}{\delta}} \qquad (\delta > 1,\; a > 0) \tag{1.39}$$

recovering the former Eq. (1.32) upon $a \to 1$ and applying the Euler function properties $\Gamma_{1+z} = z\Gamma_z$ $(z \notin \mathbb{Z}^- \cup \{0\})$, $\Gamma_{1+n} = n!$ $(\forall n \in \mathbb{N})$. Other limiting perturbation behaviours are:

$$\lim_{\delta \to 1^+,\, a \neq 1} Y_a \;=\; 1 \;+\; \frac{\mathrm{Q}^{-\frac{2}{3}}}{a}\,, \qquad \lim_{\mathrm{Q} \to 1} Y_a \;=\; \left(1 + \tfrac{2}{a\delta} - \tfrac{1}{a}\right) Y_\infty \tag{1.40}$$

$$Y_\infty \;\equiv\; \lim_{\mathrm{Q} \to \infty} Y_a \;=\; a\delta\, \frac{\Gamma_{1+a-\frac{1}{\delta}}}{\Gamma_{1+a}} \;=\; (\delta a - 1)\frac{\Gamma_{a-\frac{1}{\delta}}}{\Gamma_a} \tag{1.41}$$

the last equality clearly holding for $a - 1/\delta \notin \mathbb{Z}^- \cup \{0\}$. A parametric inspection of the generalized perturbation Y_a has been drawn in Fig. (3) and Fig. (4) according to a number of characteristic values for δ and Q.

Other statistical properties of the generalized Weibull distribution stem from its definition, and are not reported here. Observe that, to reduce the number of phenomenological coefficients,

the proportionality factor in the exponential argument was still set to unity [i.e. $\exp(-1 \cdot x^{\delta})$] and thus omitted from Eq. (1.36).

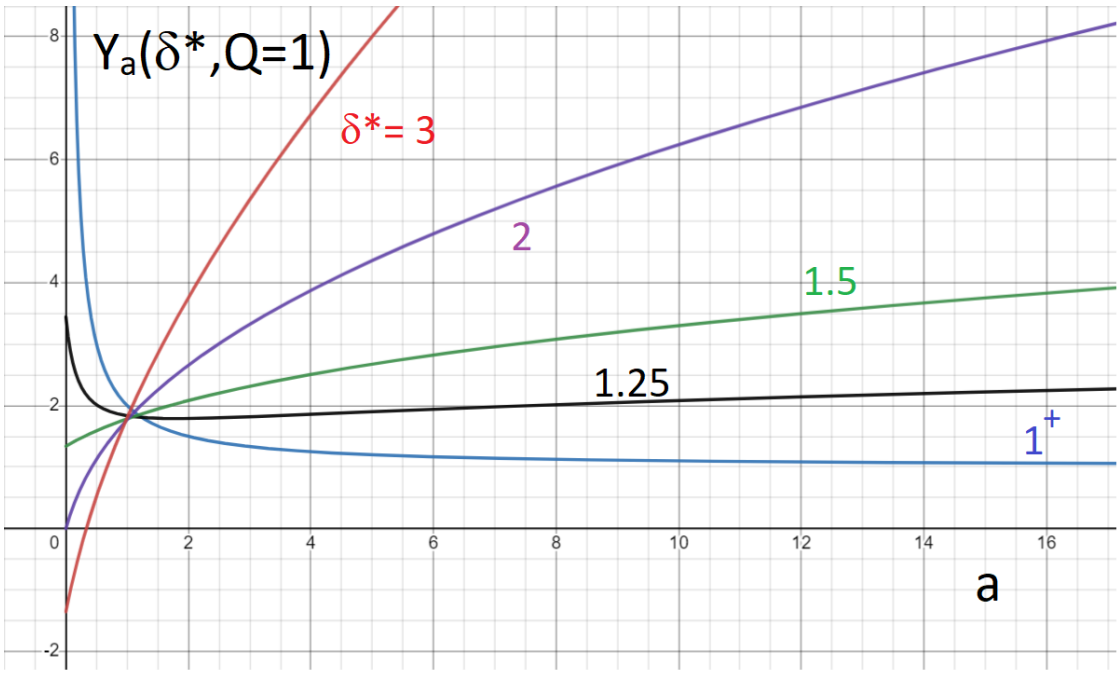

Figure 3: Representation of the perturbation Y_a as a function of the statistical dependence parameter ($a > 0$) for a number of δ values in the unswollen state ($Q = 1$).[16] Changing δ eventually reverts the sign of the perturbation derivative, suggesting a strong interplay between δ and a.

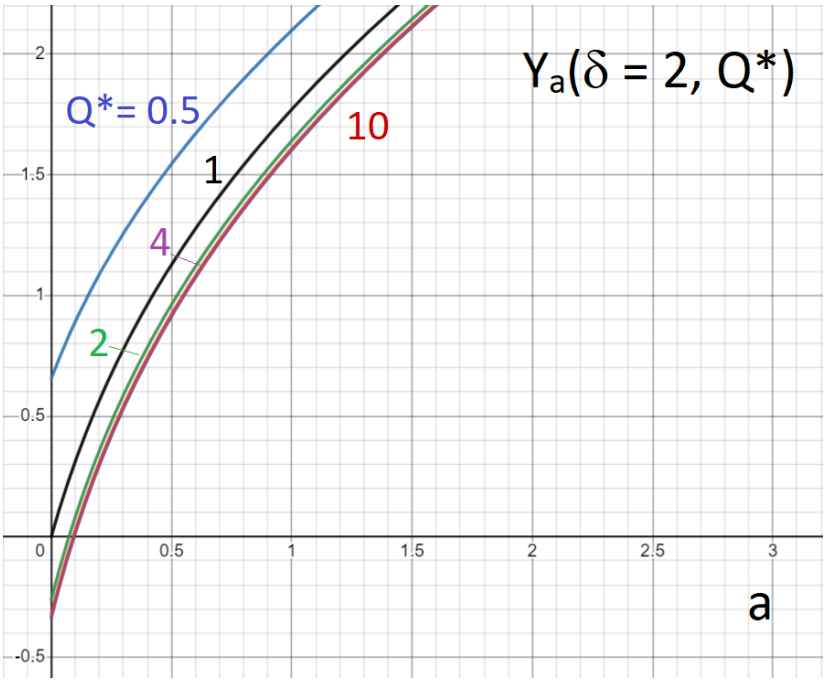

Figure 4: Representation of the perturbation Y_a as a function of $a > 0$ for a number of Q values when $\delta = 2$.[16] Changing the swelling ratio has little or no effect on the general trend of $Y_a = Y_a(a)$.

2. Further on Formal Details

2.1. Notes on Flory's Configuration Integral

The integral in Eq. (1.1) stands for six contributions, explicitly written in Cartesian coordinates as:

$$\iiint W_x\left(\tfrac{x}{\alpha_x}\right) W_y\left(\tfrac{y}{\alpha_y}\right) W_z\left(\tfrac{z}{\alpha_z}\right) \left[\ln W_x(x) + \ln W_y(y) + \ln W_z(z)\right] \tfrac{dx\,dy\,dz}{\alpha_x\alpha_y\alpha_z} \; + \\ - \iiint W_x\left(\tfrac{x}{\alpha_x}\right) W_y\left(\tfrac{y}{\alpha_y}\right) W_z\left(\tfrac{z}{\alpha_z}\right) \left[\ln W_x\left(\tfrac{x}{\alpha_x}\right) + \ln W_y\left(\tfrac{y}{\alpha_y}\right) + \ln W_z\left(\tfrac{z}{\alpha_z}\right)\right] \tfrac{dx\,dy\,dz}{\alpha_x\alpha_y\alpha_z} \quad (2.1)$$

which, by a simple variable change ($x_k = \alpha_k\vartheta$), can be rearranged into a sum of one-dimensional integrals:[6]

$$\int_{\Re^3} W(\mathbf{R}) \ln \frac{W(\mathbf{r})}{W(\mathbf{R})}\, d\mathbf{R} \;=\; \sum_{i=x,\,y,\,z} \int_{D_i} W_i(\vartheta) \ln W_i(\alpha_i\vartheta)\; d\vartheta \;-\; \sum_{i=x,\,y,\,z} \int_{D_i} W_i(\vartheta) \ln W_i(\vartheta)\; d\vartheta \quad (2.2)$$

D_i denoting the i-th conformational domain over which such averages are to be carried out and the Jacobian, $\mathrm{J} = \alpha_x\alpha_y\alpha_z$, cancelling out in the final relationship. In the Gaussian case, integrals in the first sum on the right of Eq. (2.2) return evidently $-\frac{\alpha_i^2}{2}$ each, while the second sum contributes with $-3 \times \frac{1}{2}$. In what follows we report the central details to calculate the configuration integral for the other two statistical distributions put forward by this study.

2.2. Pierced Gaussian

The first step is to calibrate the distribution by a proper normalisation term ($\mathcal{N}$):

$$\mathcal{N}\frac{\beta}{\sqrt{\pi}} \left[\int_{-\infty}^{-u} + \int_{u}^{\infty}\right] \exp\left(-\beta^2\vartheta^2\right) d\vartheta \;=\; 1 \quad (2.3)$$

which turns out to stem from the Gauss error function Φ:

$$\mathcal{N}^{-1} = \; -\,2\left[\tfrac{\sqrt{\pi}}{\beta}\;\Phi(\beta u) \;-\; \tfrac{\sqrt{\pi}}{\beta}\right] \tfrac{\beta}{2\sqrt{\pi}} \quad (2.4)$$

or, let $q \equiv \beta u$:

$$\mathcal{N}(q) \;=\; [1-\Phi(q)]^{-1} \tag{2.5}$$

here with:

$$\Phi(q) \;=\; \tfrac{2}{\sqrt{\pi}} \int_0^q \exp(-\vartheta^2)\, d\vartheta \tag{2.6}$$

and it is clear that Flory's configuration integral is recovered upon $q \to 0^+$, i.e. $\mathcal{N}(0) = 1$. Eq. (2.5) explains the prefactor in Eq. (1.13), piercing the Gaussian law.

To proceed, since all polymer states in $\mathbf{C}\,[\mathbf{0}, u] \equiv C_x \cup C_y \cup C_z$ are to be ruled out, we exploit the symbolic relation:

$$\left[\int_{-\infty}^{-u} + \int_u^{\infty}\right] d\vartheta_i \;=\; \left[\int_{-\infty}^{\infty} - \int_{C_i}\right] d\vartheta_i \qquad\qquad \vartheta_i \;=\; x,\; y,\; z \tag{2.7}$$

the sums over the whole domain on the right being characteristic of the Gaussian case. Thereby, one may simply subtract from Flory's results the integrals over $C_i = (-u, u)$ for each coordinate ϑ_i of the pierced functions W_{hi} in Eq. (1.13). Replacing $W_i \to W_{hi}$ in Eq. (2.2) upon $D_i \equiv C_i$ and exploiting the property in Eq. (2.7) bring to the following decomposition:

$$\begin{aligned} s_h\left(\{\alpha_i\}\right) \;=\; & \frac{s_g\left(\{\alpha_i\}\right)}{\left[1-\Phi(q)\right]^3} \;-\; \frac{s_g\left(\{\alpha_i\}\right)}{\left[1-\Phi(q)\right]^3}\, \Phi(\tfrac{q}{\alpha_x})\Phi(\tfrac{q}{\alpha_y})\Phi(\tfrac{q}{\alpha_z}) \;-\; \frac{q}{\sqrt{\pi}[1-\Phi(q)]^3} \times \\ & \times \left[\gamma_x^s \exp(-\tfrac{q^2}{\alpha_x^2})\Phi(\tfrac{q}{\alpha_y})\Phi(\tfrac{q}{\alpha_z}) + \gamma_y^s \exp(-\tfrac{q^2}{\alpha_y^2})\Phi(\tfrac{q}{\alpha_x})\Phi(\tfrac{q}{\alpha_z}) + \gamma_z^s \exp(-\tfrac{q^2}{\alpha_z^2})\Phi(\tfrac{q}{\alpha_x})\Phi(\tfrac{q}{\alpha_y})\right] \end{aligned} \tag{2.8}$$

where the first addendum on the right reproduces Flory's result (s_g) weighted by the new normalisation factor ($\mathcal{N}$), while the other two, combining error functions, derive from the integrations on the left of Eq. (2.7). Eq. (2.8) is obviously identical to Eq. (1.15) (SI 1.2) and, for $q \to 0^+$, gets back to $s_h \to s_g$.

2.2.1. Computational Details

The expressions for $(\partial s_h/\partial\alpha)$ were derived analytically in uniaxial deformation and pure shear conditions. They were afterwards tested symbolically in a SageMath environment.[19] The purpose is to confirm the exact relationships for the mechanical moduli and to check their

consistency with the pure Gaussian results. The calculation routes, from $(\partial s_h/\partial\alpha)$ to E_h and G_h, are illustrated in Figs. (5-6). At the two points 3.) in these illustrations are the equations taking place of Flory's E and G (Eq. 1.16). Their Maclaurin expansions in q (the piercing width) are found in items 4.). It can be seen the predictions of rubber elasticity theory are respected, with shear and Young's moduli standing correctly in a $1:3$ proportion. Their dependence on Q is monotonic, with first derivative $\propto -\mathrm{Q}^{-\frac{4}{3}}$ (i.e. no minima or maxima with respect to the swelling parameter).

Uniaxial Deformation Geometry

1. Conformational Derivative ($\partial s_h/\partial\alpha$). It is proportional to the uniaxial stress (second of Eqs. 3.8, in units of $\rho k_B T$).

```
sage:
-Q^(1/3)*((erf(sqrt(a)*q/Q^(1/3))^2*erf(q/(Q^(1/3)*a))-1)*Q^(1/3)*a
/(erf(q)-1)^3-2*(2*q*(sqrt(a)/Q^(1/3)-Q^(1/3)/sqrt(a))*erf(sqrt(a)*q/
Q^(1/3))*e^(-a*q^2/Q^(2/3))/sqrt(pi)-(q^2*(1/(Q^(2/3)*a^2)-1)-Q^(2/3)
*a^2-Q^(2/3)/a+1)*erf(sqrt(a)*q/Q^(1/3))^2)*q*e^(-q^2/(Q^(2/3)*a^2))
/(sqrt(pi)*Q^(2/3)*a^2*(erf(q)-1)^3))+Q^(1/3)*(((2*q^2*(a/Q^(2/3)-1)-
Q^(2/3)*a^2-3*Q^(2/3)/a +2)*erf(sqrt(a)*q/Q^(1/3))*erf(q/(Q^(1/3)*a))-
2*((sqrt(a)/Q^(1/3)-Q^(1/3)/sqrt(a))*erf(q/(Q^(1/3)*a))*e^(-a*q^2/
Q^(2/3))-(Q^(1/3)*a-1/(Q^(1/3)*a))*erf(sqrt(a)*q/Q^(1/3))*e^(-q^2/
(Q^(2/3)*a^2)))*q/sqrt(pi))*a*q*e^(-a*q^2/Q^(2/3))/(sqrt(pi)*Q^(2/3)*
(erf(q)-1)^3)+(erf(sqrt(a)*q/Q^(1/3))^2* erf(q/(Q^(1/3)*a))-1)*Q^(1/3)
/(sqrt(a)*(erf(q)-1)^3))/a^(3/2)
```

2. Ratio(E) = $-(\partial s_h/\partial\alpha)/Q/(\alpha - 1)$ (first of Eqs. 3.8, units of $\rho k_B T$).

```
sage:
(Q^(1/3)*((erf(sqrt(a)*q/Q^(1/3))^2*erf(q/(Q^(1/3)*a))-1)*Q^(1/3)*a
/(erf(q)-1)^3-2*(2*q*(sqrt(a)/Q^(1/3)-Q^(1/3)/sqrt(a))*erf(sqrt(a)
*q/Q^(1/3))*e^(-a*q^2/Q^(2/3))/sqrt(pi)-(q^2*(1/(Q^(2/3)*a^2)-1)-
Q^(2/3)*a^2-Q^(2/3)/a+1)*erf(sqrt(a)*q/Q^(1/3))^2)*q*e^(-q^2/
(Q^(2/3)*a^2))/(sqrt(pi)*Q^(2/3)*a^2*(erf(q)-1)^3))-Q^(1/3)*(((2*q^2*
(a/Q^(2/3)-1)-Q^(2/3)*a^2-3*Q^(2/3)/a+2) *erf(sqrt(a)*q/Q^(1/3))*
erf(q/(Q^(1/3)*a))-2*((sqrt(a)/Q^(1/3)-Q^(1/3)/ sqrt(a))*erf(q/
(Q^(1/3)*a))*e^(-a*q^2/Q^(2/3))-(Q^(1/3)*a-1/(Q^(1/3)*a))*erf(sqrt(a)
*q/Q^(1/3))*e^(-q^2/(Q^(2/3)*a^2)))*q/sqrt(pi))*a*q*e^(-a*q^2/Q^(2/3)
)/(sqrt(pi)*Q^(2/3)*(erf(q)-1)^3)+(erf(sqrt(a)*q/Q^(1/3))^2* erf(q/
(Q^(1/3)*a))-1)*Q^(1/3)/(sqrt(a)*(erf(q)-1)^3))/a^(3/2))/(Q*(a-1))
```

3. Taylor expansion of Ratio(E) at the lowest order in $(\alpha - 1)$, giving the exact expression of Young's modulus Eh in units of $\rho k_B T$ and for small deformations.

```
sage: Eh=Ratio(E).taylor(a,1,0)
3*(pi^2*(erf(q/Q^(1/3))^3-1)*Q^(8/3)*e^(3*q^2/Q^(2/3))-2*(pi^(3/2)*Q*
erf(q/Q^(1/3))^2*e^(2*q^2/Q^(2/3))-pi^(3/2)*Q^(1/3)*erf(q/Q^(1/3))^2*
e^(2*q^2/Q^(2/3)))*q^5-(pi^(3/2)*erf(q/Q^(1/3))^2*e^(2*q^2/Q^(2/3))+
(3*pi^(3/2)*erf(q/Q^(1/3))^2*e^(2*q^2/Q^(2/3))-2*sqrt(pi))*Q^(2/3)+2*
sqrt(pi))*Q*q^3-(7*pi*Q^2*erf(q/Q^(1/3))*e^(q^2/Q^(2/3))-3*pi*Q^(4/3)
*erf(q/Q^(1/3))*e^(q^2/Q^(2/3)))*q^2+(pi^(3/2)*Q^(7/3)*erf(q/Q^(1/3))
^2*e^(2*q^2/Q^(2/3))-pi^(3/2)*Q^(5/3)*erf(q/Q^(1/3))^2*e^(2*q^2/Q^(2/
3)))*q)/(pi^2*Q^3*erf(q)^3*e^(3*q^2/Q^(2/3))-3*pi^2*Q^3*erf(q)^2*e^(
3*q^2/Q^(2/3))+3*pi^2*Q^3*erf(q)*e^(3*q^2/Q^(2/3))-pi^2*Q^3*
e^(3*q^2/Q^(2/3)))
```

4. Taylor expansion of Young's elastic modulus (units of $\rho k_B T$) to fourth order in q. The underlined term is equivalent to Flory's prediction.

```
sage: Eh.taylor(a,1,0)
-48*(pi-15)*q^4/(pi^2*Q^(1/3))+72*q^2/(pi*Q^(1/3))+18*q/(sqrt(pi)*
Q^(1/3))-6*(pi^3-40*pi^2)*q^3/(pi^(7/2)*Q^(1/3))+3/Q^(1/3)
```

Figure 5: Summary of symbolic calculations for the uniaxial deformation geometry (Eqs. 1.8, 1.10).

Shear Deformation Geometry

1. Conformational Derivative ($\partial s_h/\partial\alpha$). It is proportional to the shear stress (second of Eqs. 3.9, in units of $\rho k_B T$).

```
sage:
-Q^(1/3)*((erf(a*q/Q^(1/3))*erf(q/Q^(1/3))*erf(q/(Q^(1/3)*a))-1)*Q^ (1
/3)*a/(erf(q)-1)^3+((2*q^2*(1/(Q^(2/3)*a^2)-1)-2*Q^(2/3)*a^2-Q^(2/3)-
Q^(2/3)/a^2+2)*erf(a*q/Q^(1/3))*erf(q/Q^(1/3))-2*((a/Q^(1/3)-Q^(1/3)/
a)*erf(q/Q^(1/3))*e^(-a^2*q^2/Q^(2/3))-(Q^(1/3)-1/Q^(1/3))*erf(a*q/Q^
(1/3))*e^(-q^2/Q^(2/3)))*q/sqrt(pi))*q*e^(-q^2/(Q^(2/3)*a^2))/(sqrt(
pi)*Q^(2/3)*a^2*(erf(q)-1)^3))+Q^(1/3)*(((2*(a^2/Q^(2/3)-1)*q^2-Q^(2/
3)*a^2-Q^(2/3)-2*Q^(2/3)/a^2+2)*erf(q/Q^(1/3))*erf(q/(Q^(1/3)*a))+2*(
(Q^(1/3)-1/Q^(1/3))*erf(q/(Q^(1/3)*a))*e^(-q^2/Q^(2/3))+(Q^(1/3)*a-1/(
Q^(1/3)*a))*erf(q/Q^(1/3))*e^(-q^2/(Q^(2/3)*a^2)))*q/sqrt(pi))*a^2*q*
e^(-a^2*q^2/Q^(2/3))/(sqrt(pi)*Q^(2/3)*(erf(q)-1)^3)+(erf(a*q/Q^(1/3)
)*erf(q/Q^(1/3))*erf(q/(Q^(1/3)*a))-1)*Q^(1/3)/(a*(erf(q)-1)^3))/a ^2
```

2. Ratio(G) = $-(\partial s_h/\partial\alpha)/Q/(\alpha-1/\alpha)/(1+\alpha^{-2})$ (first of Eqs. 3.9, $\rho k_B T$ units).

```
sage:
(Q^(1/3)*((erf(a*q/Q^(1/3))*erf(q/Q^(1/3))*erf(q/(Q^(1/3)*a))-1)*Q^(1
/3)*a/(erf(q)-1)^3+((2*q^2*(1/(Q^(2/3)*a^2)-1)-2*Q^(2/3)*a^2-Q^(2/3)-
Q^(2/3)/a^2+2)*erf(a*q/Q^(1/3))*erf(q/Q^(1/3))-2*((a/Q^(1/3)-Q^(1/3)/
a)*erf(q/Q^(1/3))*e^(-a^2*q^2/Q^(2/3))-(Q^(1/3)-1/Q^(1/3))*erf(a*q/Q^
(1/3))*e^(-q^2/Q^(2/3)))*q/sqrt(pi))*q*e^(-q^2/(Q^(2/3)*a^2))/(sqrt(
pi)*Q^(2/3)*a^2*(erf(q)-1)^3))-Q^(1/3)*(((2*(a^2/Q^(2/3)-1)*q^2-Q^(2/
3)*a^2-Q^(2/3)-2*Q^(2/3)/a^2+2)*erf(q/Q^(1/3))*erf(q/(Q^(1/3)*a))+2*(
(Q^(1/3)-1/Q^(1/3))*erf(q/(Q^(1/3)*a))*e^(-q^2/Q^(2/3))+(Q^(1/3)*a-1/
(Q^(1/3)*a))*erf(q/Q^(1/3))*e^(-q^2/(Q^(2/3)*a^2)))*q/sqrt(pi))*a^2*q
*e^(-a^2*q^2/Q^(2/3))/(sqrt(pi)*Q^(2/3)*(erf(q)-1)^3)+(erf(a*q/Q^(1/3
))*erf(q/Q^(1/3))*erf(q/(Q^(1/3)*a))-1)*Q^(1/3)/(a*(erf(q)-1)^3))/a^2
)/(Q*(a-1/a)*(1/a^2 + 1))
```

3. Taylor expansion of Ratio(G) at the lowest order in (α - 1), giving the exact expression of the shear modulus Gh in units of $\rho k_B T$ and for small deformations.

```
sage: Gh=Ratio(G).taylor(a,1,1)
(pi^2*Q^(8/3)*erf(q/Q^(1/3))^3*e^(3*q^2/Q^(2/3))-pi^2*Q^(8/3)*e^(3*q^2
/Q^(2/3))+2*(sqrt(pi)*Q^(2/3)-sqrt(pi))*Q*q^3-(7*pi*Q^2-3*pi*Q^(4/3))*
q^2*erf(q/ Q^(1/3))*e^(q^2/Q^(2/3))-(2*(pi^(3/2)*Q-pi^(3/2)*Q^(1/3))*
q^5+(3*pi^(3/2)*Q^ (2/3)+pi^(3/2))*Q*q^3-(pi^(3/2)*Q^(7/3)-pi^(3/2)*Q^
(5/3))*q)*erf(q/Q^(1/3))^2* e^(2*q^2/Q^(2/3)))/(pi^2*Q^3*erf(q)^3*e^(
3*q^2/Q^(2/3))-3*pi^2*Q^3*erf(q)^2*e^(3*q^2/Q^(2/3))+3*pi^2*Q^3*erf(q
)*e^(3*q^2/Q^(2/3))-pi^2*Q^3*e^(3*q^2/Q^(2/3)))
```

4. Taylor expansion of the shear modulus in units of $\rho k_B T$ to the fourth order in q. It can be seen it is 1/3 of the former Eh.taylor(a,1,0). The underlined term is equivalent to Flory's prediction.

```
sage: Gh.taylor(q,0,4)
-16*(pi-15)*q^4/(pi^2*Q^(1/3))+24*q^2/(pi*Q^(1/3))+6*q/(sqrt(pi)*
Q^(1/3))-2*(pi^3-40*pi^2)*q^3/(pi^(7/2)*Q^(1/3))+1/Q^(1/3)
```

Figure 6: Summary of symbolic calculations for the pure shear deformation geometry (Eqs. 1.9, 1.11).

2.2.2. Maxwell-Boltzmann Averaging

The starting point is Eq. (1.18):

$$\left(\frac{\partial s_h}{\partial \alpha_i}\right)_{T,V} = -\alpha_i \left[1 + \frac{6}{\sqrt{\pi}}\, q + \frac{24}{\pi}\, q^2 + \frac{2(40-\pi)}{\pi^{3/2}}\, q^3 + \frac{16(15-\pi)}{\pi^2}\, q^4\right] + O(5) \qquad (2.9)$$

with q intended to be a one-dimensional random variable. We will therefore rescale $q \to q/\sqrt{3}$ and weigh the former relation statistically, through a Maxwell-Boltzmann distribution of values.

In this way, the coefficients become respectively:

$$2\sqrt{\frac{3}{\pi}} \quad (q) \qquad \frac{8}{\pi} \quad (q^2) \qquad \frac{2\,(40-\pi)}{(3\pi)^{\frac{3}{2}}} \quad (q^3) \qquad \frac{16\,(15-\pi)}{9\pi^2} \quad (q^5) \tag{2.10}$$

Now we consider a probability density of the form:[12]

$$P(q) \;=\; \sqrt{\frac{2}{\pi}}\,\frac{q^2\exp(-\,q^2/2a^2)}{a^3} \tag{2.11}$$

with mean value $\bar{q} \equiv 2a\sqrt{2/\pi}$, and average Eq. (1.18) at each order:

$$\frac{2\sqrt{6}}{\pi a^3}\int_0^\infty q^3\exp(-\,q^2/2a^2)\;dq \;=\; 2\sqrt{\frac{3}{\pi}}\;\bar{q} \tag{2.12}$$

$$\frac{8}{\pi a^3}\sqrt{\frac{2}{\pi}}\int_0^\infty q^4\exp(-\,q^2/2a^2)\;dq \;=\; 3\bar{q}^2 \tag{2.13}$$

$$\frac{2(40-\pi)}{(3\pi)^{\frac{3}{2}}a^3}\sqrt{\frac{2}{\pi}}\int_0^\infty q^5\exp(-\,q^2/2a^2)\;dq \;=\; \frac{40-\pi}{3\sqrt{3\pi}}\;\bar{q}^3 \tag{2.14}$$

$$\frac{16(15-\pi)}{9\pi^2a^3}\sqrt{\frac{2}{\pi}}\int_0^\infty q^6\exp(-\,q^2/2a^2)\;dq \;=\; \frac{5(12-\pi)}{12}\;\bar{q}^4 \tag{2.15}$$

Such results provide the final coefficients of the mean derivative in Eq. (1.20), to be regarded in the re-evaluations of mechanical moduli.

2.3. Weibull Distribution

Unlike the pierced Gaussian law, whose extended configurational integral can be explicitly carried out, the pronounced non-linearity of the Weibull distribution does not permit a closed-form evaluation of s_w. We will therefore resort to some useful Taylor expansion. Inserting Eq. (1.23) into Eq. (2.7) leads, after several algebraic manipulations, to an expression that can be written as:

$$s_w\left(\{\alpha_i\}\right) \;=\; \tfrac{\delta(\delta-1)}{\eta}\sum_{k=x,y,z}\mathrm{H}_k\left(\{\alpha_i\}\right) \;-\; \tfrac{\delta}{\eta^{\delta+1}}\sum_{k=x,y,z}\mathrm{L}_k\left(\{\alpha_i\}\right) \tag{2.16}$$

with the two functions H_k, L_k defined as:

$$H_k \;=\; \int_{\Re \setminus C_k^+} \left(\frac{t-u}{\eta}\right)^{\delta-1} \exp\left[-\left(\tfrac{t-u}{\eta}\right)^{\delta}\right] \ln\left(\frac{\alpha_k t-u}{t-u}\right) dt \tag{2.17}$$

$$L_k \;=\; \int_{\Re \setminus C_k^+} \left(\frac{t-u}{\eta}\right)^{\delta-1} \exp\left[-\left(\tfrac{t-u}{\eta}\right)^{\delta}\right] \left[(\alpha_k t-u)^{\delta}-(t-u)^{\delta}\right] dt \tag{2.18}$$

where C_k^+ obviously means the restriction of $\mathbf{C}$ to the positive k-th semiaxis. As expected, since $t = x_k/\alpha_k$ and η stand for a length, s_w turns out to be dimensionless. However, to these author's knowledge, H_k and L_k cannot be resolved analytically. It is therefore convenient to go straight to the point and calculate the mechanical moduli according to Eq. (1.10) and Eq. (1.11). We need to apply the chain rule for differentiation:

$$\left(\frac{\partial s_w}{\partial \alpha}\right)_{T,V,\Xi} = \sum_i \left(\frac{\partial \alpha_i}{\partial \alpha}\right)_{\Xi} \left(\frac{\partial s_w}{\partial \alpha_i}\right)_{T,V} \tag{2.19}$$

to Eq. (2.16) for the deformation geometries Ξ = u.d. (Eq. 1.8) and Ξ = p.s. (Eq. 1.9).

2.3.1. Uniaxial Deformation

In a material undergoing uniaxial stress, Eq. (2.19) returns:

$$\left(\frac{\partial s_w}{\partial \alpha}\right)_{T,V,\Xi} = \tfrac{\delta(\delta-1)}{\eta} \sum_{i=x,y,z} \int \frac{M(t)}{\alpha_i t-u} \left(\frac{\partial \alpha_i}{\partial \alpha}\right)_{\Xi} dt \;-\; \tfrac{\delta^2}{\eta^{\delta+1}} \sum_{i=x,y,z} \int M(t)\,(\alpha_i t-u)^{\delta-1} \left(\frac{\partial \alpha_i}{\partial \alpha}\right)_{\Xi} dt \tag{2.20}$$

with:

$$M(t,u) \;=\; \left(\frac{t-u}{\eta}\right)^{\delta-1} t \exp\left[-\left(\tfrac{t-u}{\eta}\right)^{\delta}\right] \;, \tag{2.21}$$

and (see Eq. 1.8):

$$\left(\frac{\partial \alpha_x}{\partial \alpha}\right) \;=\; \mathrm{Q}^{\frac{1}{3}}, \;\; \left(\frac{\partial \alpha_y}{\partial \alpha}\right) \;=\; \left(\frac{\partial \alpha_z}{\partial \alpha}\right) \;=\; -\,\tfrac{1}{2}\mathrm{Q}^{\frac{1}{3}}\alpha^{-\frac{3}{2}} \tag{2.22}$$

After summing over i and a number of algebraic manipulations, Eq. (2.20) becomes:

$$\left(\frac{\partial s_w}{\partial \alpha}\right)_{T,V,\Xi} = \frac{\delta(\delta-1)}{\eta}\mathrm{Q}^{\frac{1}{3}}\int_u^\infty M(t,u)\; g_u(t,\alpha,u)\; dt \;-\; \frac{\delta^2}{\eta^{\delta+1}}\mathrm{Q}^{\frac{1}{3}}\int_u^\infty M(t,u)\; f_u(t,\alpha,u)\; dt \quad (2.23)$$

where:

$$g_u(t,\alpha,u) = \frac{1}{\alpha\mathrm{Q}^{\frac{1}{3}}t-u} - \frac{1}{\alpha\mathrm{Q}^{\frac{1}{3}}t-\alpha^{\frac{3}{2}}u} \quad (2.24)$$

$$f_u(t,\alpha,u) = (\alpha\mathrm{Q}^{\frac{1}{3}}t-u)^{\delta-1} - \alpha^{-\frac{3}{2}}(\alpha^{-\frac{1}{2}}\mathrm{Q}^{\frac{1}{3}}t-u)^{\delta-1} \quad (2.25)$$

These two functions are expanded at first order in $\alpha - 1$:

$$g_u(t,\alpha,u) = -\frac{3}{2}\frac{u}{(\mathrm{Q}^{\frac{1}{3}}t - u)^2}\;(\alpha - 1) + O(\alpha-1)^2 \quad (2.26)$$

$$f_u(t,\alpha,u) = \frac{3}{2}(\mathrm{Q}^{\frac{1}{3}}t - u)^{\delta-2}\;(\delta\mathrm{Q}^{\frac{1}{3}}t - u)\;(\alpha - 1) + O(\alpha-1)^2 \quad (2.27)$$

and put back into Eq. (2.23), which becomes:

$$\left(\frac{\partial s_w}{\partial \alpha}\right)_{T,V,\Xi} = -A_\alpha\int_u^\infty N(t,u)\; dt + O(\alpha-1)^2 \quad (2.28)$$

being:

$$N(t,u) = \frac{M(t,u)}{(\mathrm{Q}^{\frac{1}{3}}t-u)^2}\left[(\delta-1)\;u + \frac{\delta}{\eta^\delta}(\delta\mathrm{Q}^{\frac{1}{3}}t - u)(\mathrm{Q}^{\frac{1}{3}}t - u)^\delta\right], \quad (2.29)$$

$$A_\alpha = \frac{3}{2}\,\frac{\mathrm{Q}^{\frac{1}{3}}\delta}{\eta}\;(\alpha - 1) \quad (2.30)$$

We can now expand the integral in Eq. (2.28) at first-order in Weibull's parameter u:

$$\int_u^\infty N(t,u)\; dt = \int_0^\infty N(t,0)\; dt + u\left(\frac{d}{du}\int_u^\infty N(t,u)\; dt\right)_{u=0} \quad (2.31)$$

the derivative on the right following from Leibniz's integral rule:

$$\left(\frac{d}{du}\int_u^\infty N(t,u)\; dt\right)_{u=0} = -N(0,0) + \int_0^\infty\left[\frac{\partial N(t,u)}{\partial u}\right]_{u=0} dt \quad (2.32)$$

Since $N(t,u) \to 0$ upon $(t,u) \to (0,0)$ ($\delta > 1$), we are left with two contributions to Eq. (2.28). The first is:

$$- A_\alpha \int_0^\infty N(t,0)\, dt \;=\; - \delta^2 \eta A_\alpha \mathrm{Q}^{\frac{\delta-1}{3}} \Xi_{2\delta-1} \tag{2.33}$$

where Ξ_z ($z \in \Re^+$) denotes the shorthand notation for the following integral in the dimensionless variable $x = t/\eta$:

$$\Xi_z \;\equiv\; \int_0^\infty x^z \exp(-x^\delta)\, dx \;=\; \tfrac{1}{\delta}\Gamma_{\frac{z+1}{\delta}} \tag{2.34}$$

and Γ_y is Euler's gamma function with argument y,[15] yielding $\Xi_{2\delta-1} = \frac{1}{\delta}$. In the second contribution:

$$- A_\alpha u \int_0^\infty \left[\frac{\partial N(t,u)}{\partial u}\right]_{u=0} dt \tag{2.35}$$

after some integro-differential elaboration, one obtains:

$$\begin{aligned}\int_0^\infty \left[\frac{\partial N(t,u)}{\partial u}\right]_{u=0} dt \;=\; & (\delta-1)\mathrm{Q}^{-\frac{2}{3}}\Xi_{\delta-2} - \;\delta(\delta^2+1)\mathrm{Q}^{\frac{\delta-2}{3}}\Xi_{2\delta-2} + \\ & + \;2\delta^2\mathrm{Q}^{\frac{\delta-2}{3}}\Xi_{2\delta-2} + \;\delta^3\mathrm{Q}^{\frac{\delta-1}{3}}\Xi_{3\delta-2} - \;\delta^3\mathrm{Q}^{\frac{\delta-1}{3}}\Xi_{2\delta-2} + \;\delta^2\mathrm{Q}^{\frac{\delta-1}{3}}\Xi_{2\delta-2}\end{aligned} \tag{2.36}$$

The final expression for the derivative in Eq. (2.28) comes from adding Eq. (2.33) to Eq. (2.36). Then, in order to get Young's modulus (at small deformations), we need to recall Eq. (1.10):

$$E_w \;\approx\; \frac{\sigma_w}{\varepsilon}\,, \quad \sigma_w = \; - \frac{\rho k_{_B} T}{\mathrm{Q}} \left(\frac{\partial s_w}{\partial \alpha}\right)_{T,V} \tag{2.37}$$

where it is clear that the u-independent contribution to E_w originates from Eq. (2.33):

$$E_w^* = \; \tfrac{3}{2}\delta^2 \mathrm{Q}^{\frac{\delta}{3}-1} \rho k_{_B} T \tag{2.38}$$

Eq. (2.36) leads instead to a first-order perturbation (ΔE_w) in the parameter u which, employing Eq. (2.34), finally becomes:

$$\frac{\Delta E_w}{E_w^*} \;=\; \frac{u}{\eta}\left\{\delta\Gamma_{\,3-\frac{1}{\delta}} \;+\; [(1-\delta)(1+\mathrm{Q}^{-\frac{1}{3}})+(1-\tfrac{1}{\delta})\mathrm{Q}^{-\frac{1}{3}}]\Gamma_{\,2-\frac{1}{\delta}} \;+\; \tfrac{1}{\delta}\left(1-\tfrac{1}{\delta}\right)\mathrm{Q}^{-\frac{1+\delta}{3}}\Gamma_{\,1-\frac{1}{\delta}}\right\} \tag{2.39}$$

Accordingly, Eq. (1.34) of SI (1.4) is regained in the simple form:

$$E_w \;=\; E_w^* \;+\; \Delta E_w \tag{2.40}$$

2.3.2. Pure Shear

Pure shear expressions rest on a different deformation geometry (Eq. 1.9), transforming Eq. (2.22) into:

$$\left(\frac{\partial\alpha_x}{\partial\alpha}\right) \;=\; \mathrm{Q}^{\frac{1}{3}},\;\; \left(\frac{\partial\alpha_y}{\partial\alpha}\right) \;=\; -\,\frac{\mathrm{Q}^{\frac{1}{3}}}{\alpha^2},\;\; \left(\frac{\partial\alpha_z}{\partial\alpha}\right) \;=\; 0\,, \tag{2.41}$$

and on a different final calculation, for the shear modulus G_w (Eq. 1.11):

$$G_w \;\approx\; \frac{\tau_0^w}{\gamma^s}\,,\quad \tau_0^w = \,-\,\frac{\rho k_{_B} T}{\mathrm{Q}}\left(\frac{\partial s_w}{\partial\gamma^s}\right)_{T,V} \tag{2.42}$$

Apart from this, the procedure is identical to that set out in the former SI (2.3). The only point to be made is on the first-order expansion of the functions f and g (Eq. 2.23), becoming:

$$g_s(t,\alpha,u) \;=\; \frac{1}{\alpha\mathrm{Q}^{\frac{1}{3}}t-u} \;-\; \frac{1}{\alpha\mathrm{Q}^{\frac{1}{3}}t-\alpha^2 u} \tag{2.43}$$

$$f_s(t,\alpha,u) \;=\; (\alpha\mathrm{Q}^{\frac{1}{3}}t-u)^{\delta-1} - \alpha^{-2}(\alpha^{-1}\mathrm{Q}^{\frac{1}{3}}t-u)^{\delta-1} \tag{2.44}$$

Once they are expanded at first order in $\alpha-1$:

$$g_s(t,\alpha,u) \;=\; -\,\frac{2u}{(\mathrm{Q}^{\frac{1}{3}}t \;-\; u)^2}\,(\alpha \;-\; 1) \;+\; O(\alpha-1)^2 \tag{2.45}$$

$$f_s(t,\alpha,u) \;=\; 2(\mathrm{Q}^{\frac{1}{3}}t \;-\; u)^{\delta-2}\,(\delta\mathrm{Q}^{\frac{1}{3}}t \;-\; u)\,(\alpha \;-\; 1) \;+\; O(\alpha-1)^2 \tag{2.46}$$

we can promptly see that the coefficient $\frac{3}{2}$ in g_u, f_u has turned into 2 in g_s, f_s. On developing Eq. (2.42), the shear modulus stems straight away from a comparison with the expression for E_w:

$$G_w \;=\; \tfrac{2}{3/2}E_w \lim_{\alpha\,\to\,1}\left(\frac{\varepsilon}{\gamma^s}\right)\left(\frac{\partial\varepsilon}{\partial\gamma^s}\right) \;=\; \tfrac{4}{3}E_w \lim_{\alpha\,\to\,1}\left(\frac{\alpha-1}{\alpha-1/\alpha}\right)\left[\frac{\partial(\alpha-1/\alpha)}{\partial\alpha}\right]^{-1} = \\ = \;\tfrac{4}{3}E_w \lim_{\alpha\,\to\,1}\frac{\alpha^3}{(\alpha^2+1)(\alpha+1)} \;=\; \tfrac{1}{3}E_w \quad (2.47)$$

as expected from the fundamentals of elasticity theory.

2.4. Generalized Weibull Distribution

The presence of the parameter a in Eq. (1.36) slightly modifies Eq. (2.16) into a generalized entropy equation:

$$s_a\left(\{\alpha_i\}\right) \;=\; \tfrac{\delta(a\delta-1)}{\Gamma_a\eta}\sum_{k=x,y,z}\mathrm{H}_{ka}\left(\{\alpha_i\}\right) \;-\; \tfrac{\delta}{\Gamma_a\eta^{\delta+1}}\sum_{k=x,y,z}\mathrm{L}_{ka}\left(\{\alpha_i\}\right) \quad (2.48)$$

now with:

$$\mathrm{H}_{ka} \;=\; \int_{\Re\,\setminus\,C_k^+}\left(\frac{t-u}{\eta}\right)^{a\delta-1}\exp\left[-\left(\tfrac{t-u}{\eta}\right)^{\delta}\right]\ln\left(\frac{\alpha_k t-u}{t-u}\right)dt \quad (2.49)$$

$$\mathrm{L}_{ka} \;=\; \int_{\Re\,\setminus\,C_k^+}\left(\frac{t-u}{\eta}\right)^{a\delta-1}\exp\left[-\left(\tfrac{t-u}{\eta}\right)^{\delta}\right]\left[(\alpha_k t-u)^{\delta}-(t-u)^{\delta}\right]dt \quad (2.50)$$

Sticking to the formal procedure in SI (2.3), we observe that the uniaxial and shear deformation expansions for the functions g_u, f_u, g_s, f_s, do not depend on a. With these premises, the derivative in Eq. (1.30) becomes:

$$\left(\frac{\partial s_a}{\partial\alpha}\right)_{\mathrm{Q},T,\Xi,a} \;=\; -\,e_{\Xi}\tfrac{\Gamma_{a+1}}{\Gamma_a}\delta^2\mathrm{Q}^{\frac{\delta}{3}}(\alpha-1) \;-\; e_{\Xi}\tfrac{u\delta}{\Gamma_a\eta}(\alpha-1)\left[2\delta\mathrm{Q}^{\frac{1}{3}(\delta-1)}\Gamma_{1+a-\frac{1}{\delta}} \;+\; \delta^2\mathrm{Q}^{\frac{\delta}{3}}\Gamma_{2+a-\frac{1}{\delta}} \;+\right. \\ \left. -\,\delta^2\mathrm{Q}^{\frac{\delta}{3}}\Gamma_{1+a-\frac{1}{\delta}} \;+\; \delta\mathrm{Q}^{\frac{\delta}{3}}\Gamma_{1+a-\frac{1}{\delta}} \;+\; \left(a-\tfrac{1}{\delta}\right)\mathrm{Q}^{-\frac{1}{3}}\Gamma_{a-\frac{1}{\delta}} \;-\; (1+\delta^2)\mathrm{Q}^{\frac{1}{3}(\delta-1)}\Gamma_{1+a-\frac{1}{\delta}}\right] \;+\; \mathrm{O}(2) \quad (2.51)$$

from which a little algebra brings the relationships in Eqs. (2.38) and (2.39) to take the following form:

$$E_a^* \;=\; \tfrac{3}{2}\delta^2 \mathrm{Q}^{\frac{\delta}{3}-1} a\rho k_{_B} T \tag{2.52}$$

$$\frac{\Delta E_a}{E_a^*} \;=\; \frac{u}{\eta\Gamma_{1+a}}\left\{\delta\Gamma_{\,2+a-\frac{1}{\delta}} + \;[(1-\delta)(1+\mathrm{Q}^{-\frac{1}{3}}) + (1-\tfrac{1}{\delta})\mathrm{Q}^{-\frac{1}{3}}]\Gamma_{\,1+a-\frac{1}{\delta}} + \;\tfrac{1}{\delta}\left(a-\tfrac{1}{\delta}\right)\mathrm{Q}^{-\frac{1+\delta}{3}}\Gamma_{\,a-\frac{1}{\delta}}\right\} \tag{2.53}$$

The expression for the new shear modulus, $G_a = G_a^* + \Delta G_a$, is clearly immediate. By employing the properties $\Gamma_{1+z} = z\Gamma_z$, $\Gamma_{1+n} = n!$ $(n \in \mathbb{N})$, $G_a = \frac{1}{3}E_a$, with $E_a = E_a^* + \Delta E_a$, Eqs. (1.37) and Eqs. (1.38) are finally recovered, i.e.:

$$G_a \;=\; \tfrac{1}{2}a\delta^2 \mathrm{Q}^{\frac{\delta-2}{3}} G(1 + \tfrac{u}{\eta}Y_a) \tag{2.54}$$

where G still denotes Flory's expression and Y_a is given by Eq. (1.39). Note that every result descending from the (ordinary) Weibull distribution is consistently regained in the limit $a \to 1$, particularly the mechanical moduli $E_a \to E_w$ and $G_a \to G_w$.

3. Polymer Physics and Distribution Laws

3.1. Weibull's Coefficients versus Scaling Exponents

3.1.1. Shape and Scale Parameters δ and η in Weibull's Law ($a = 1$)

To fix the ideas, we commence the discussion for the non-generalized Weibull's law. A radial behavior close to Eq. (1.23) was applied to a real self-avoiding chain with radius $R_{_F}$ in a good solvent. Fisher,[20] des Cloizeaux[21] and de Gennes[22] regarded a length distribution similar to Eq. (1.23), involving two independent coefficients, δ_1 and δ_2 (i.e. $\delta - 1 \to \delta_1$, $\delta \to \delta_2$), which connect the scaling exponents of the polymer molecule known as ν and γ, derived in the limit of large numbers of repeat units ($n \gg 1$).[23]

In short, while the identification $\eta \sim R_{_F}$ is immediate, one can deduce $\delta_1 = (\gamma - 1)/\nu$ and $\delta_2 = (1 - \nu)^{-1}$, where ν governs the size, $R_{_F} \sim n^{\nu}$, and γ rules ("enhances") the total number of self-avoiding walks of n steps on a lattice,[24] scaling as $\sim z^n n^{\gamma - 1}$ (z = fugacity coefficient). If $\delta \geq 1$, ν and γ are both monotonically increasing with δ, which is physically sound (Fig. 7). If $\delta < 1$, it leads to $\nu < 0$, resulting into a decreasing number of self-avoiding walks as ν increases. This behavior is not acceptable in our hydrogel problem and should be regarded as a limitation of the referenced interpretation. The case $\delta = 1$ returns an exponential function (i.e. Laplace's), thoroughly investigated elsewhere.[6]

3.1.2. Statistical Dependence Parameter (a) in the Generalized Weibullian

For a generalized Weibullian, the coefficient a in principle can take any positive value. Remaining in the framework of Subsection (3.1.1), the equation of ν would be unaffected by a, but γ modify into $\gamma = a(\delta - 1) + \delta^{-1}$. One has in this case a function of two variables (of which Fig. (7) represents the level curve for $a = 1$), with partial derivative:

$$\left(\frac{\partial \gamma}{\partial \delta}\right)_a = a - \delta^{-2} \, . \tag{3.55}$$

As it is required to be positive, the physically meaningful domain here would be set by:

$$\delta > \tfrac{1}{\sqrt{a}} \tag{3.56}$$

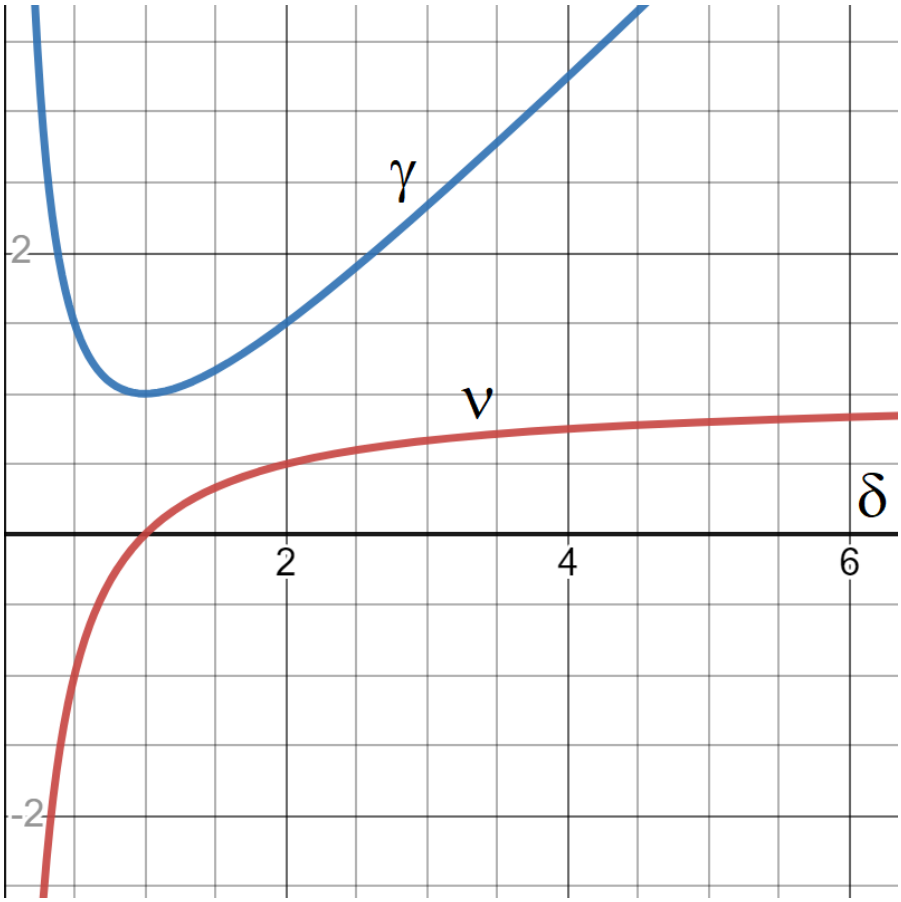

Figure 7: Plots of scaling exponents for the chain size ($\nu = 1 - 1/\delta$; red curve) and the number of self-avoiding walks ($\gamma = \delta - 1 + 1/\delta$; blue curve) against δ in the (ordinary) Weibullian distribution ($a = 1$).[16] The physically significant domain is given here by $\delta \geq 1$, when $\nu \geq 0$ and γ is monotonically increasing. Note that the exponent δ is recovered as $\frac{1}{2}(\nu + \gamma) \equiv \delta$. For a generalized Weibull law, the second exponent extends to a function of two variables, $\gamma(\delta, a) = a(\delta - 1) + 1/\delta$, of which the present plot is the two-dimensional cross-section for $a = 1$. Here's a refined version of your sentence: These behaviors arise from the scaling laws described in Subsection (3.1.1) and may not fully apply to realistic systems.

These constraints could also reflect a model limitation, at least in our context. The exponent ν (chain size) should not be independent of a (monomer correlation). However, it may be striking to realize that Eq. (3.56) was always fulfilled by our best-fitting results (Tab. 1, main text).

3.2. Discussion of the Microscopic Interpretation of Aleatory Variables

3.2.1. Pierced Gaussian

From a formal viewpoint, a way to get W_h from a sum of random variables (here, repeat unit vectors $\mathbf{r}_i$) is to restrict its domain at each step towards convergence. Consider the distribution

$(W_g^{(n)})$ for $\mathbf{R}_n = \sum_{i=1}^{n} \mathbf{r}_i \equiv \mathbf{r}_n + \mathbf{R}_{n-1}$ in a standard CLT scheme:

$$W_g^{(n)} = w_{g,n} \otimes W_g^{(n-1)} \tag{3.57}$$

where $\otimes$ is the convolution product and $w_{g,n}$ is the Gauss function governing $\mathbf{r}_n$. An additional constraint piercing the conformational space in $[-u, u]$ would give:

$$W_h^{(n)} = W_g^{(n)} \prod_{X_i = x,y,z} \left[1 - \mathbf{1}_{[-u,u]}(X_i)\right] \tag{3.58}$$

since $\mathbf{1}_{[x_a,x_b]}(X_i)$ is the so-called indicator (or characteristic) function for the subset $[x_a, x_b] \subseteq \Re$ of the X_i-axis, and:

$$W_h = \lim_{n\to\infty} W_h^{(n)} \,. \tag{3.59}$$

The microscopic interpretation of the product in Eq. (3.58) is evidently a conformational cut-off function for the absolute value of the end-to-end vector distribution at any step n, and should be regarded aside from Eq. (3.57). If convolution and productory were not running independently, CLT would eventually lead to $\lim_{n\to\infty} W_h^{(n)} = W_g$. In simpler terms, the conformational restriction scheme described here only affects the domains of the random variables (for example, by introducing an external hard-sphere potential with an infinite energy barrier whenever $|X_i| \leq u$).

3.2.2. Weibull Distributions

The implications of the Weibull laws on the interplay between random variables and interaction potentials within the polymer system are yet to be explored. An established framework within which discussing such an aspect is Rouse's bead-spring model (and its modification credited to Zimm),[22] where a high-molecular weight molecule is described as n beads, each separated from the next by the aleatory vector $\mathbf{r}_k$ ($k = 1, \ldots n$) and mechanically linked by $n - 1$ massless springs. Let the force field between any two consecutive beads (k, $k + 1$) be purely harmonic,

with finite $\langle \mathbf{r}_k^2 \rangle \equiv l_k^2$ and $\langle \mathbf{r}_k \rangle = 0$ $(\forall k)$:

$$u_{\mathrm{el}}(\mathbf{r}_k) \;=\; \frac{3k_{_B}T}{2}\left(\frac{\mathbf{r}_k^2}{l_k^2}\right) \tag{3.60}$$

application of Maxwell-Boltzmann's statistics to the distribution of bond probabilities (p):

$$p\left(\mathbf{r}_k\right) \;\propto\; \exp\left[-u_{\mathrm{el}}/(k_{_B}T)\right] \tag{3.61}$$

simply returns, upon normalization, a Gauss function for each single segment. The law for end-to-end vectors, $\mathbf{R}_n$, will be clearly Gaussian as well, although this conclusion does not require the elastic hypothesis in Eq. (3.60). CLT in fact guarantees any sum of independent, equidistributed random variables (with finite variance) to converge in distribution to a normal law, here identified to $\mathrm{N}(0, nl_k^2) \equiv W_g(|\mathbf{R}_n| = R)$.[25]

We find that the Weibullian statistics models the hydrogel network better than the Gaussian, and thus expect the assumptions leading to CLT to be invalidated. Weibull's law belongs in particular to the distribution class ruling the so-called extreme value statistics (EVS).[26] As any extreme value problem can be generally translated in terms of a sum of non-independent random variables,[27] a distribution of end-to-end vectors obeying a Weibull law will be insightful e.g. of polymer correlations at the level of repeat units. Our findings allow to include hydrogel networks into the wealth of systems successfully interpreted by EVS distributions (see e.g. bibliographies in[13,18]), meant to form a class of *universal laws for statistically dependent phenomena*.

In such a case, the joint probability P_w for n aleatory variables $\mathbf{r}_k$ should obey:[18]

$$P_w\left(\mathbf{r}_1,\ \ldots\ \mathbf{r}_n\right) \;=\; Z_n^{-1}\Omega\left[F\left(\mathbf{R}_n\right)\right]\prod_{k=1}^{n} p\left(\mathbf{R}_n - \mathbf{R}_{k-1}\right) \tag{3.62}$$

where $\Omega\ (x) \sim x^{a-1}$ $(x \to 0^+)$ is an arbitrary positive function, with $a > 0$ characterizing the statistical dependence, $F = F(y)$ is a cumulative probability distribution:

$$F(y) \;=\; \int_y^{\infty} p(x)\ dx \tag{3.63}$$

and Z_n denotes a partition function given by:

$$Z_n \;=\; \frac{1}{\Gamma_n}\int_0^1 \Omega(x)(1-x)^{n-1}dx \tag{3.64}$$

The explicit form of the productory is:

$$\prod_{k=1}^{n} p\left(\mathbf{R}_n-\mathbf{R}_{k-1}\right) \;=\; p\left(\mathbf{R}_n\right)p\left(\mathbf{R}_n-\mathbf{R}_1\right)\;...\,p\left(\mathbf{R}_n-\mathbf{R}_{n-1}\right)$$

$$=\; p\left(\mathbf{r}_1+\;...\;+\mathbf{r}_n\right)p\left(\mathbf{r}_2+\;...\;+\mathbf{r}_n\right)\;...\,p\left(\mathbf{r}_n\right) \tag{3.65}$$

the origin for the end-to-end vector being set here to $\mathbf{R}_0 \equiv \mathbf{0}$.

Now, for an asymptotic distribution of fluctuations to comply with a generalized Weibull law, say:

$$W_w^*(x) \;\propto\; x^{a\delta-1}\exp(-x^{\delta}) \tag{3.66}$$

the probability p needs to fade out above a given value $x_{_M}$ and to behave as $p(x)\sim[(x_{_M}-x)/\lambda]^{\delta-1}$ for $x\to x_{_M}$ (and some typical length, λ). This is accomplished, for instance, by a (rigid) potential wall, with energy diverging at $x\to x_{_M}^-$. For mere illustration purposes, wishing to combine the steric hindrance and Rouse's phenomenologies, a local potential field $u=u_w+u_{\rm el}$ is redesigned (in one dimension) in Fig. (8) below. It sketches out an elastic interaction that i.) never returns to its resting state (due e.g. to excluded volumes) and ii.) prevents the repeat units from moving apart beyond a maximum extension (e.g. by a non-linear spring getting hugely stiff). We impose the mathematical continuity of values, first and second derivatives of the two potentials, $u_{\rm el}\sim\frac{1}{2}k_{_B}T(x/l_k)^2$ $(-x_c\le x\le x_c)$ and $u_w\sim(1-\delta)k_{_B}T\ln[(x_{_M}-x)/\lambda]$ $(-x_{_M}<x<-x_c\vee x_c<x<x_{_M})$, at some cross-over points $\pm x_c$. Weibull's force field is clearly extended by continuity to the negative axis (Eq. 1.27) upon $x_{_M}-x\to x-x_{_M}$. Interestingly, given δ and $x_{_M}$, the mean size of the subchain unit and the length scale parameter turn out to be $(l_k/x_c)=(\delta-1)^{-\frac{1}{2}}$ and $\lambda/x_c=\exp(\frac{1}{2})\approx 1.65$, being $x_c=x_{_M}/2$. Therefore, $l_k\approx\frac{1}{2}(\delta-1)^{-\frac{1}{2}}x_{_M}$ would be the optimal monomeric size suggested by the generalized Weibull statistics presented here.

In summary, in order to switch from a Gaussian to a Weibullian description, the joint distribution function for the polymer conformation, generally written for random-flight models as:[28]

$$P_g\left(\{\mathbf{r}_k\}\right) \;=\; \prod_k p\left(\mathbf{r}_k, \mathbf{r}_{k+1},\; \ldots\, \mathbf{r}_n\right) \tag{3.67}$$

needs to be mapped into Eq. (3.62), i.e. $P_g\left(\{\mathbf{r}_k\}\right) \rightarrow P_{_J}\left(\{\mathbf{r}_k; a\}\right)$. This introduces a statistical

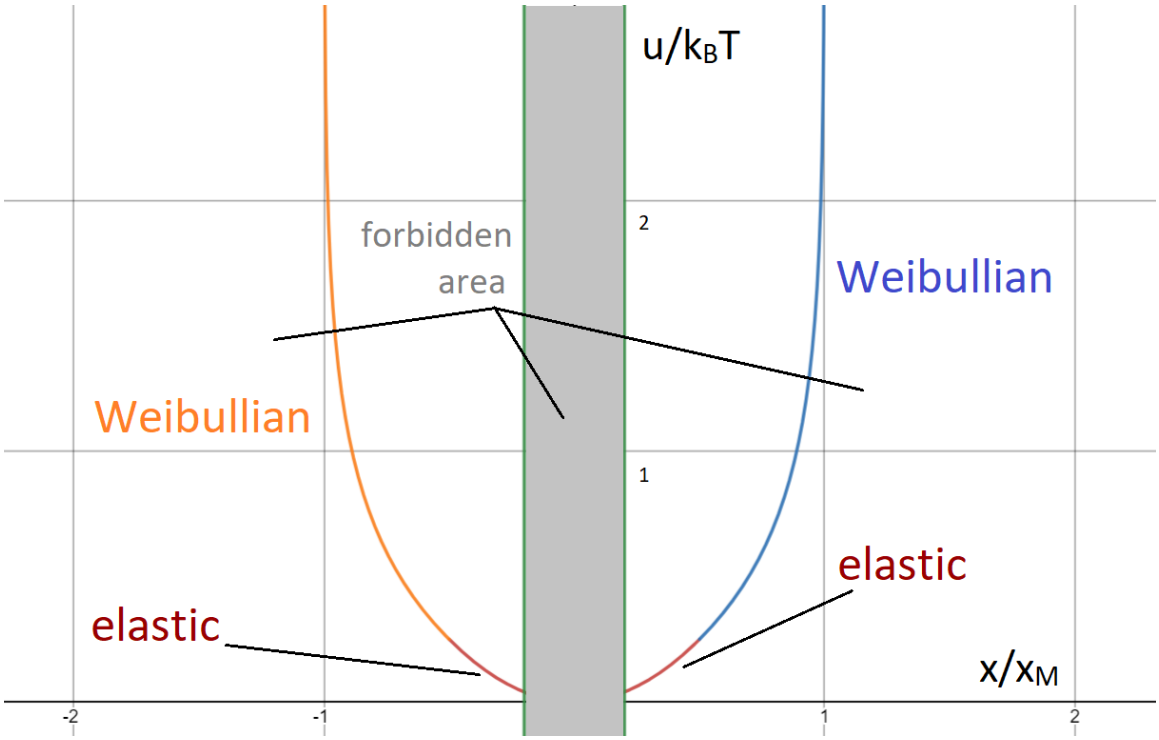

Figure 8: Building a modified repeat unit potential for a Weibullian hydrogel description, consisting of a Rouse-like elastic and Weibull-like contributions in $k_{_B}T$ units (u_{el}, magenta curve; u_w, blue and orange curves).[16] Two are the forbidden conformational areas: close to the origin (see e.g. the iteration scheme in SI 3.2.1) and beyond a given extension ($\pm x_{_M}$). The positions $x_c/x_{_M} = \pm\frac{1}{2}$, at which the colour of the curve changes, identify two (equivalent) continuous cross-over points between u_{el} and u_w.

dependence between random variables. The probability p (and, equivalently, the local force field) then should transform so as to guarantee the asymptotic fluctuation behaviour in Eq. (3.66).

3.3. Interpretation in terms of an External Potential

3.3.1. Non-Generalized Weibullian

The conformational entropy is independent of the nature of forces fixing the state of a polymeric system.[7] A complementary description, to the one in the previous subsection, thus can be

afforded by introducing a fictitious external potential (V_e) acting on ideal hydrogel strands, guaranteeing that any given macroscopic state attains equilibrium. It is known in fact the end-to-end vector distribution of a macromolecular system obeys a diffusion equation where time is sent into the repeat unit number, $t \to n$.[22] While $V_e = 0$ returns the Gaussian chain, a non-trivial potential $V_e \neq 0$ should generally arise from the following relationship:[28]

$$\frac{V_e W}{k_{_B} T} \;=\; \frac{l_k^2}{6} \nabla_{\mathbf{r}}^2 W \;-\; \left(\frac{\partial W}{\partial n} \right) \tag{3.68}$$

which here we specialize in one dimension to the non-generalized $W \equiv W_{wi}(x_i)$:

$$V_e \;=\; k_{_B} T \left[\frac{l_k^2}{2} \left(\frac{\partial \ln W_{wi}}{\partial x_i} \right) \left(\frac{\partial \ln W'_{wi}}{\partial x_i} \right) \;-\; \left(\frac{\partial \ln W_{wi}}{\partial n} \right) \right] \tag{3.69}$$

prime indicating the first derivative with respect to x_i. With the assumption that δ is not (or is negligibly) dependent on n, on defining $\xi = l_k/\eta$ a first result for V_e is:

$$V_e(\Lambda_i) \;=\; k_{_B} T \left\{ \tfrac{\xi^2}{2} \Lambda_i^{-2} \left[(\delta - 1)(\delta - 2) \;-\; 3\delta(\delta - 1)\Lambda_i^{\delta} \;+\; \delta^2 \Lambda_i^{2\delta} \right] \;-\; \delta \left(\tfrac{\partial \ln \eta}{\partial n} \right) \left(1 - \Lambda_i^{\delta} \right) \right\} \tag{3.70}$$

where, for convenience, $\Lambda_i = (x_i - u)/\eta$. This expression can be elaborated to take the form:

$$\tfrac{2}{\xi^2 k_{_B} T} V_e(\Lambda_i) \;=\; \Lambda_i^{-2} \left(\Lambda_i^{\delta} \;-\; \Lambda_+ \right) \left(\Lambda_i^{\delta} \;-\; \Lambda_- \right) \;+\; \tfrac{\epsilon \delta}{n_{_\xi}} \left(\Lambda_i^{\delta} \;-\; 1 \right) \tag{3.71}$$

$n_{_\xi}$ being the unit number per polymer strand, $\epsilon/2$ denoting for convenience the scaling exponent for the length scale Weibull's parameter ($\eta \propto n^{\frac{\epsilon}{2}}$), and:

$$\Lambda_{\pm} = \; \frac{3(\delta - 1) \pm \sqrt{(5\delta - 1)(\delta - 1)}}{2\delta} \tag{3.72}$$

The solution in Eq. (3.71) comprises a family of leading functions perturbed at the $\sim 1/n_{_\xi}$ order, with $n_{_\xi} \sim 10^2 - 10^3$ and $\epsilon \in [\frac{1}{2}, 2]$ ranging overall between globular and stiff polymer values.[11]

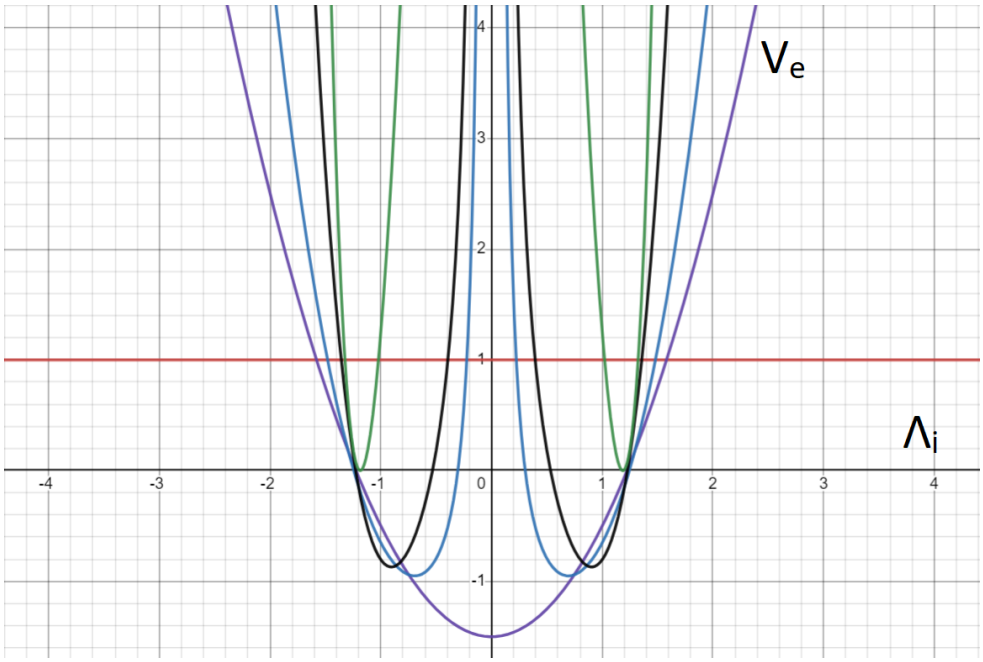

Figure 9: Coloured representation of the unperturbed (n_ξ-independent) part of the one-dimensional external field in $k_B T\zeta^2$ units (Eq. 3.71) against the rescaled coordinate when δ varies as a parameter: $\delta \to 1^+$ (magenta), $\delta = 2$ (violet), 2.4 (blue), 3.2 (black), 4.4 (green).[16] When δ (> 2) increases, pairs of energy minima, increasingly distant from the origin, appear.

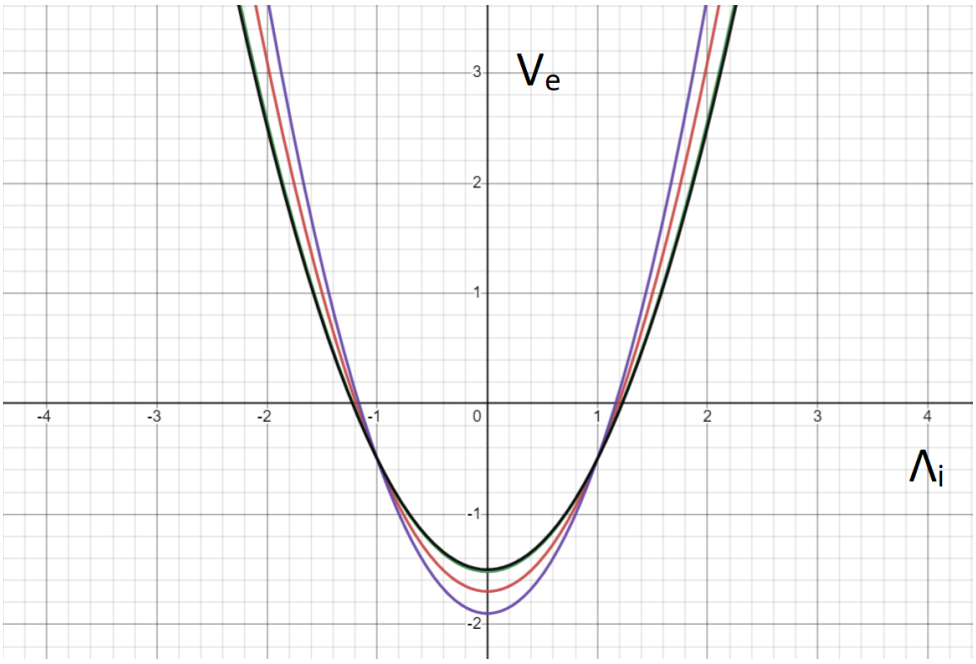

Figure 10: Coloured representation of the one-dimensional external potential in $k_B T\zeta^2$ units (Eq. 3.71) against the rescaled coordinate when n_ξ varies as a parameter: $n_\xi = 5$ (violet), 10 (magenta), 10^2 (green), 10^3 (black).[16] The scaling coefficient ϵ is set to come from the size exponent for excluded volume polymers predicted by renormalization group theory (RGT),[29] i.e. $\epsilon = 1.176$. The strand molecular weight effect on the potential shape is not remarkable.

For instance, in the special cases given by:

$$\tfrac{2}{\zeta^2 k_B T} V_e(\Lambda_i) \;=\; 1 \;+\; \tfrac{\epsilon}{n_\xi}\,(\Lambda_i - 1) \qquad\qquad (\delta \;\to\; 1^+) \tag{3.73}$$

$$\tfrac{2}{\zeta^2 k_B T} V_e(\Lambda_i) \;=\; \Lambda_i^2 \;-\; \tfrac{3}{2} \;+\; \tfrac{2\epsilon}{n_\xi}\left(\Lambda_i^2 - 1\right) \qquad\qquad (\delta \;=\; 2). \tag{3.74}$$

Figs. (9) and (10) report a parametric illustration of the external potential for particular values of δ and n_ξ. The doubling of V_e along the negative Λ_i-axis follows evidently the prolongation of Weibull's distribution in Eq. (1.27). We underline, however, that assuming a large-scale external field acting on every polymer segment in the hydrogel (whereas, in practice, there is none) is mostly an equivalent description, an artifact. Thus, although we showed here that V_e formally exists, the previous microscopic/molecular approach is preferable to explain the emergence of Weibull's statistics.

3.3.2. Generalized Weibullian

To explicitly understand the effect of the statistical dependence between repeating units, now consider the condition $0 < a \neq 1$. As we have seen, the quantity a is normally assigned a heuristic value, lacking an adequate molecular characterization on an experimental basis. Nevertheless, in our polymer problem, SI (3.1.2) would suggest as a reasonable approximation to treat it as an intrinsic coefficient, independent of n whenever $n \gg 1$. Recalculating the derivatives with the generalized function W_{wi}^*, the main calculations to be regarded are:

$$\frac{l_k^2}{2}\left(\frac{W_{wi}^{*\prime\prime}}{W_{wi}^*}\right) \;=\; \frac{\zeta^2}{2}\Lambda_i^{-2}\left\{\delta^2\Lambda_i^{2\delta} -\; \delta\left[(2a+1)\delta - 3\right]\Lambda_i^{\delta} \;+\; a^2\delta^2 \;-\; 3a\delta \;+\; 2\right\} \tag{3.75}$$

$$\left(\frac{\partial \ln W_{wi}^*}{\partial n}\right) \;=\; \left(\frac{\partial \ln W_{wi}}{\partial n}\right) \;+\; (\delta \ln \Lambda_i - \psi_a)\left(\frac{\partial a}{\partial n}\right) \;-\; \delta\left(\frac{\partial \ln \eta}{\partial n}\right)(a-1) \tag{3.76}$$

where $\psi_z = \frac{\partial \ln \Gamma_z}{\partial z}$ is the digamma function with argument z. It can be seen that $a = 1$ gets back to the W_{wi} relations, while $a \neq a(n)$ implies that the only supplementary term surviving in Eq. (3.76) is the last one.

With these premises, the effective potential in Eq. (3.71) now extends to:

$$\frac{2}{\zeta^2 k_B T} V_e(\Lambda_i) \;=\; \Lambda_i^{-2}\left(\Lambda_i^{\delta} \;-\; \Lambda_{+a}\right)\left(\Lambda_i^{\delta} \;-\; \Lambda_{-a}\right) \;+\; \frac{\epsilon\delta}{n_\xi}\left(\Lambda_i^{\delta} \;+\; a \;-\; 2\right) \tag{3.77}$$

now being:

$$\Lambda_{\pm a} = \frac{(2a \;+\; 1)\delta \;-\; 3 \;\pm\; \sqrt{(2a-1)(2a+3)(\delta \;-\; \delta_{+a})(\delta \;-\; \delta_{-a})}}{2\delta} \tag{3.78}$$

$$\delta_{\pm a} = \frac{6(a^2 \;+\; \frac{1}{2}a - 1) \;\pm\; 2\sqrt{-\,a^2 \;-\; a \;+\; 3}}{a(2a \;-\; 1)(2a \;+\; 3)} \tag{3.79}$$

Since a must assume positive values, this description thus admits real force fields for $a \leq \frac{1}{2}(\sqrt{13} - 1) \approx 1.303$. This is certainly a severe model limitation, likely originating from the artificiality of the external potential, but interestingly it is always fulfilled by our numerical extrapolations (in which $a < 1.28$). A parametric view of Eq. (3.77) is finally reported in Fig. (11) for some meaningful values of a (still in the Rayleigh case).

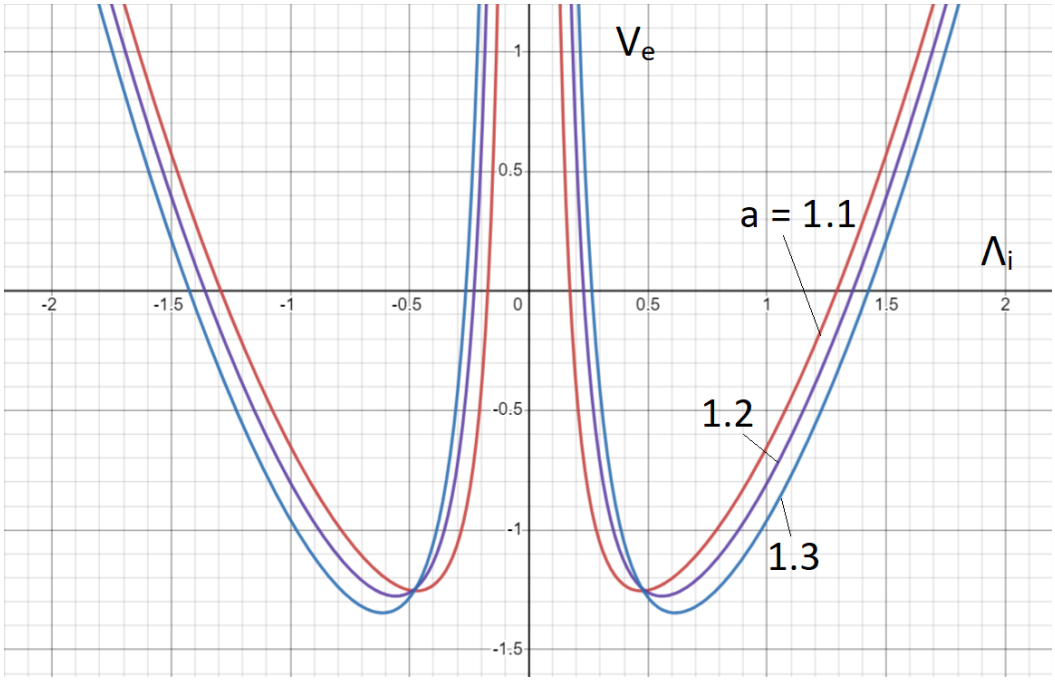

Figure 11: Coloured representation of the unperturbed (n_ξ-independent) part of the generalized potential field in $k_B T\zeta^2$ units (Eq. 3.77) for $\delta = 2$ and some values of a.[16] An increase in correlation tends to tighten V_e towards the origin, and qualitatively equals a decrease in δ. These behaviours get back to those in Fig. (10) when $a = 1$.

3.4. Discussion of the Flory-Huggins parameter

The value of the Flory-Huggins parameter (χ) for the three polysaccharides in water has been reported as $\chi = 0.2$ (alginate, Ca^{2+} concentration = 1% w/v)[30], 0.40 (agar),[31] and 0.46 (scleroglucan).[32] Regarding the macromolecules used to form covalent cross-link hydrogels, PEG, within a range of sufficiently high molecular weight values, has been attributed a roughly constant value of $\chi = 0.426$.[33] As in our hydrogel PEG and PPG form a copolymer with volume fractions ≈ 0.45 and 0.55, respectively, a reduction $\Delta\chi \approx -30\%$ in the value of PEG is expected,[34] resulting in $\chi \approx 0.3$ for the copolymer. On the other hand, an extrapolation from a study[35] on PVP still under our volume fraction conditions yields $\chi \approx 0.4$.

All these values reflect the swelling processes observed in our laboratory, where a higher χ value implies a lower tendency for the hydrogel to swell (in a good solvent, i.e. $\chi < 0.5$). However, we should remember that the Flory-Huggins theory may be a simplistic approach, and the actual behavior of χ be a more complicated function, depending for example on the polymer volume fraction, molecular weight and ionization degree, which affects the crosslink density.[36] Therefore, these numbers may be only indicative. For instance, the data reported for the alginate refers to a Ca^{2+} ion w/v concentration of 1%, whereas in the present case it is halved (0.5%). This suggests that in our alginate samples (in the same solution thermodynamic state as in ref.[30]), the value of χ should be somewhat lower.

4. Materials and Processing

The first three samples examined in this study consist of polysaccharide hydrogels − alginate, agar, and scleroglucan − which are widely used in the biomedical field due to their unique properties, such as biocompatibility and the ability to form strong or weak hydrogels under mild conditions.[37] The other two samples are synthetic polymers: poly(vinylpyrrolidone) (PVP K90) and a copolymer of poly(ethylene glycol)/propylene glycol (PEG-PPG), both of which are widely used in pharmaceutical applications.[38,39] Finally, the last two samples are derived from the sputum of cystic fibrosis patients.

4.1. Alginate

Alginate is a collective term to describe a family of polysaccharide molecules isolated from brown seaweeds and bacteria.[40] Chemically, they are linear copolymers of $(1 \rightarrow 4)$-linked β-D-mannuronic acid (MM) and its C-5 epimer, the α-L-guluronic acid (GG), arranged in a blockwise pattern, with homopolymer regions of MM and GG residues (indicated as MM- and GG-blocks, respectively) and interspersed with regions of alternating structure (MG blocks). The higher the GG content, the stiffer and more fragile the gel they form in water in the presence of divalent cations.

The ability to form stable physical hydrogels upon treatment with divalent ions, such as calcium ions,[41] have resulted in alginates that are widely used in industrial and biomedical applications. For instance, they have been used for encapsulation of insulin-producing Langerhans islets for treating type I diabetes[42] and show potential in drug delivery.[43] They absorb exudate, aid tissue repair, are non-toxic and do not trigger an inflammatory response in vivo, enhancing their appeal as delivery vehicles for pharmaceuticals, regenerative stem cells and in regenerative medicine, such as ischaemic stroke therapies (see[44] and references therein), due to their ease of administration.

4.2. Agar

Agar is a gel forming polysaccharide with a main chain consisting of alternating $(1 \rightarrow 3)$-linked β-D-galactopyranose and $(1 \rightarrow 4)$-linked $(3,6)$-anhydro-α-L-galactopyranose units.[45] It is composed by agarose and agaropectin.[46] Agarose is a neutral polysaccharide, representing the fraction with the gelling capacity, while agaropectin contains charged polysaccharide compounds. Agarose and agaropectin contents are function of the seaweed source which agar is extracted from.[47] It generally affects the physico-chemical, mechanical and rheological properties of agar gels.[46]

The agarose network was suggested to arise from double helix formation and subsequent aggregation of these helices into bundles, called suprahelices.[46,48] However, according to molecular modelling studies,[49] agarose appears to be capable of forming both single- and double-helical structures, which are left-handed and antiparallel-packed. Additionally, all the proposed crystal structures show a large enough space $(30 - 45\%)$ that can be occupied by water molecules, a fact which is expected in a gel-forming polysaccharide.

4.3. Scleroglucan

Scleroglucan is a non-ionic polysaccharide secreted exocellularly by fungi of the genus Sclerotium. Its primary structure consists of a linear backbone of $(1 \rightarrow 3)$-β-linked D-glucopyranosyl residues bearing a single $(1 \rightarrow 6)$-β-linked D-glucopyranosyl unit for every three sugar residues of the main chain.[50] Both in aqueous solution and in the solid state, scleroglucan takes on a highly ordered, rigid, triple helical tertiary structure (triplex), which consists of three individual strands composed of six residues per turn in the backbone. The three strands of the triplex are held together by inter-strand hydrogen (H-) bonds at the centre of the triplex. The $(1 \rightarrow 6)$-linked β-D-glucopyranosyl side groups protrude from the outside of the triplex, preventing intermolecular aggregation and polymer precipitation.[51–53]

The triplex conformation is only destabilized in dimethyl sulfoxide or strong alkaline conditions, and characterized by a high stiffness, responsible of the peculiar properties displayed by aqueous scleroglucan solutions in a wide range of pH values and even at relatively high tempera-

tures. As the triplex clustering proceeds, the formation of three-dimensional hydrogel networks takes place. This occurs, typically, for a polymer mass percent $\geq 0.25\%$.[54] Due to its rheological properties, scleroglucan is used as a thickener and suspending agent in several industry sectors.[55] In addition, as it is not toxic, biocompatible, biodegradable and bio-adhesive, it is widely exploited in cosmetic and pharmaceutical fields, where its main application is the release of bioactive molecules.[56–59]

4.4. Cystic Fibrosis Sputum (with notes on COPD)

Cystic Fibrosis (CF) is a prevalent fatal genetic disorder among individuals of Caucasian descent, with a frequency of about 1 in 3000 births.[60–62] It results from mutations in the gene encoding the CF Transmembrane Conductance Regulator (CFTR), an ATP-regulated chloride channel located on epithelial cell surfaces.[63] The malfunctioning CFTR leads to a reduction in surface liquid volume and an increase in mucus viscosity across various organs, predominantly affecting the airways.[63] This thick mucus impairs mucociliary clearance, leading to mucus buildup and fostering bacterial lung infections, a hallmark of CF pathology (Cystic Fibrosis Foundation Patient Registry).[60,62]

In CF patients, early childhood colonization by Staphylococcus aureus often transitions to Pseudomonas aeruginosa as the predominant pathogen over time.[62] By adulthood, approximately 80% of them are chronically infected with P. aeruginosa, leading to rapid deterioration in lung function, heightened morbidity, and reduced life expectancy.[64] Notably, in chronically infected CF patients, P. aeruginosa transitions to a mucoid phenotype due to increased production of alginates, intensifying the inflammatory response and exacerbating lung pathology.[65–67] During inflammation, the pathological mucus in CF undergoes a significant increase in solid components, primarily mucins $(1-5)\%$, which are high molecular weight ($\sim 0.1-10$ MDa), heavily glycosylated proteins comprising hydrophobic polypeptide backbones linked to multiple hydrophilic oligosaccharide chains. The size and organization of the biopolymer network within the mucus are influenced not only by the hydration level of mucus layers but also by the composition. In fact, apart from mucins, other biomacromolecules − such as alginates, antibodies, lipids

and other proteins like DNA and cellular debris − are present, organizing a three-dimensional meshwork through disulfide cross-linkages and physical entanglements, which imparts adhesive gel-like properties to sputum.[65–68] This high viscoelasticity impedes microorganism removal by cilia, fostering an ideal environment for bacterial colonization. Alongside, the mucus architecture hinders the effectiveness of in situ drug delivery devices targeting epithelial cells.[68]

Understanding the nanostructure of this network thus is crucial for evaluating patient clinical status and enhancing drug efficacy in CF therapy,[68] where antibiotics, mucolytics, bronchodilators, and anti-inflammatory agents play crucial roles. Antibiotics are essential for treating respiratory infections and are administered orally, intravenously, or via inhalation in various formulations.[69] Mucolytics like dornase alfa (Pulmozyme) thin mucus, to be commonly delivered via inhalation.[70] Bronchodilators relax airway muscles, improving breathing, and are administered via inhalation.[71] Anti-inflammatory medications reduce airway inflammation and improve lung function, available in multiple formulations.[72]

Chronic obstructive pulmonary disease (COPD) shares clinical and pathologic features with CF, including increased mucus viscosity and mucin hyperexpression.[72,73] Exposure to cigarette smoke inhibits CFTR, leading to delayed mucociliary transport and increased mucus viscosity, promoting infection (Morbidity and Mortality: 2007 Chart Book on Cardiovascular, Lung and Blood Diseases, 2007).[73] The pathological substances present in both CF and COPD lung diseases severely subvert mucus structure, with the mucus mesh size being highly heterogeneous and varying between patients and clinical conditions.[74] As previously observed, these variations affect drug permeability and efficacy.[75]

The two sputum samples under investigation were sourced from CF patients at the Burlo Garofolo Hospital (https://www.burlo.trieste.it), a scientific hospitalization and treatment institute of national significance (IRCSS), following approval by the Ethics Committee (protocol no. 000543, dated 17-02-2020, CEUR-2019-Em-408). Each patient provided written informed consent. Spontaneously expectorated sputum samples ($1 - 2$ mL in volume) were collected in sterile containers and promptly utilized for low-field nuclear magnetic resonance (LF-NMR) and rheological analysis.

4.5. Poly-vinylpyrrolidone (PVP)

Poly(vinylpyrrolidone) (PVP) is widely used both as a drug and polymeric excipient in a variety of drug dosage forms. Not only is it approved for human use, but it also exhibits the unique property of being amphiphilic, allowing it to form good interactions with both hydrophilic (body fluids) and lipophilic (drugs) environments.[76]

4.6. Poly(ethylene-glycol/propylene-glycol) (PEG-PPG)

Among the numerous applications of PEG in the biomedical field, one notable use is the creation of hydrophobically modified polymers for the synthesis of hydrophobically modified gels (HM), which are aimed at delivering hydrophobic drugs.[39] This work focuses on a precursor to HM gels that lacks the hydrophobic component, with the hydrophilic component being primarily PEG and, to a lesser extent, poly-propylene glycol (PPG). In this case, crosslinking occurs solely for chemical reasons, as physical crosslinking is only possible when the hydrophobic component is present.[77]

5. Experimental Methods

5.1. Low-Field Nuclear Magnetic Resonance (LF-NMR)

Water proton spin-spin relaxation time (T_2) was detected by a Bruker Minispec MQ20 (0.47 T, 20 MHz, Germany) at 25° C (polysaccharide hydrogels) or 37° C (sputum samples), according to the CPMG (Carr–Purcell–Meiboom–Gill) sequence $\{90^\circ\,[-\tau - 180^\circ - \tau(\text{echo})]_k - T_R\}$[78] with a 8.36 μs wide 90° pulse, $\tau = 250$ μs (i.e. the time separation between 90° and 180° pulses) and with $T_R = 10$ s (recycle delay). The quantity k denotes the number of experimental echoes and is related with good approximation to the duration (T_d) of the experimental test by $T_d = 2k\tau = 2k'(1+A)\tau$, where k', A are respectively the numbers of recorded and unrecorded echoes, linked through $k = (1 + A)k'$.

A try-and-error procedure was adopted to select k' (≤ 1000) and A (≤ 21) in such a way that, at the end of the experiment (elapsed time $t = T_d$), the intensity FID ($I_s(t)$) of the induced magnetization component in the XY plane (M_{XY}) was about 2% of the initial intensity. The time interval (T_d/k') for data acquisition, consequently, was equal to $2(1 + A)\tau$ and could differ in each sample on the basis of the different values of k', A regarded to get the necessary duration T_d (approximately, in our systems, $T_d \approx 10^3$–10^4 ms). Any relaxation experiment, comprising k' points, was repeated 36 times (four scans for any of the 9 repetitions per experiment). The glass tube (internal diameter 8 mm), in which all gel samples were accommodated, was sealed by a suitable plastic top promptly after the sample insertion and kept at 25 °C or 37 °C for about ten minutes before measuring. Finally, it was quickly put into the MQ20 sample holder, positioned just above the magnetic field.

Relying on Eq. (22) of the main text and remembering the physical meaning of $\mathcal{M}$:

$$\mathcal{M} \;=\; \frac{h}{T_{2b}} \;=\; \frac{R_c - R_f}{T_{2b}} \tag{5.1}$$

it is possible to determine both T_{2b} and a. In fact, solving Eq. (22) (main text) for $\mathcal{M}$ and equating the resulting expression to Eq. (5.1), leads to:

$$\mathcal{M} \;=\; \frac{\zeta}{2}\left[\left(\frac{1}{T_2}\right)_m - \left(\frac{1}{T_{2\mathrm{H_2O}}}\right)\right]\sqrt{\frac{c_0(1-0.58\;\phi)}{c_1\phi}} \tag{5.2}$$

Substituting in Eq. (5.2) the explicit R_f and R_c dependence on ϕ and ζ (respectively from Eq. 21 and Eq. 25 of the main text):

$$R_f \;=\; \zeta\sqrt{\frac{c_0\phi}{c_1(1-0.58\;\phi)}}\;\;,\quad R_c \;=\; \zeta\sqrt{\frac{c_0}{c_1(1-0.58\;\phi)}} \tag{5.3}$$

and solving for T_{2b}, then returns:

$$T_{2b} \;=\; \frac{2\phi}{(1-0.58\;\phi)}\left(\frac{1-\sqrt{\phi}}{\sqrt{\phi}}\right)\left[\left(\frac{1}{T_2}\right)_m - \left(\frac{1}{T_{2\mathrm{H_2O}}}\right)\right]^{-1} \tag{5.4}$$

Finally, from Eqs. (5.3):

$$h \;=\; R_c - R_f \;=\; \zeta\sqrt{\frac{c_0\phi}{c_1(1-0.58\;\phi)}}\left(\frac{1-\sqrt{\phi}}{\sqrt{\phi}}\right) \tag{5.5}$$

Table (1) reports the numbers for T_{2b} and h in alginate, agar and scleroglucan gels. For PVP-K90 and PEG-PPG hydrogels, the absence of reliable R_f values made it necessary to exclude the estimation of T_{2b} and h. Similarly, determining T_{2b} and h for the sputum samples analyzed in this study was not feasible, as the polymer volume fraction remained unknown.

5.2. Rheology

Hydrogels exhibit viscoelastic characteristics when subjected to deformation, with the degree of this behavior dependent on the frequency of deformation. Generally, when the storage modulus surpasses the loss modulus by approximately tenfold and remains relatively constant regardless of stress frequency, they are considered "strong hydrogels" due to their resilience.[79] In this study, we determined the viscoelastic properties of the analyzed samples by examining their mechanical spectra under oscillatory shear conditions, employing two rheological techniques: the stress sweep

	Agar 1%	**Alginate 1%**	**Scleroglucan 2%**
T_{2b} (ms)	20	8.8	31
h (nm)	6.0	2.6	13.8
ζ (nm)	20.2	8.5	47.5
ϕ	$6.6 \cdot 10^{-3}$	$5.7 \cdot 10^{-3}$	$12.6 \cdot 10^{-3}$
$(1/T_2)_m$ (ms^{-1})	$7.83 \cdot 10^{-3}$	$16.11 \cdot 10^{-3}$	$6.83 \cdot 10^{-3}$
T_{2H_2O} (ms)	3020	3020	3020

Table 1: Thickness (h) and relaxation time (T_{2b}) of the bound water layer, coating the surface of the polymeric chains building up the network of agar, alginate and scleroglucan gels in this study. Values of the average mesh dimension (ζ) were evaluated by assuming the generalized Weibull distribution for the polymer end-to-end length (subsection 5.4) and the corresponding shear moduli determined by means of rheology (see 5.2). The free water relaxation time (T_{2H_2O}) is derived at room temperature ($25°C$).[39] Values of the average inverse relaxation time $(1/T_2)_m$ were calculated from Eq. (23) in the main text applied to the data in Fig. (26).

test and the frequency sweep test. These experiments involve applying a sinusoidal stress to the sample to measure the corresponding oscillatory deformation (γ^s), or vice versa when obtaining stress. The experimental data were interpreted according to the generalized Maxwell model depicted in Fig. (12).

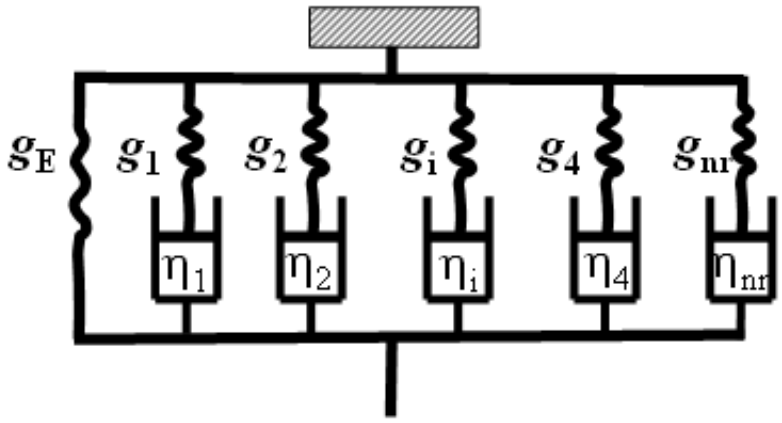

Figure 12: Schematic representation of generalized Maxwell's model. The symbol g_E denotes the elastic constant of the purely elastic Maxwell element, g_i refers to the elastic constant of the i-th element and η_i to the i-th dashpot viscosity.

5.3. Determination of the Shear Modulus

Figs. (13-16) present the stress sweep test results for alginate, scleroglucan, agar, PVP-K90, and PEG-PPG hydrogels, as well as the two sputum samples (CF167 and CF178) considered in this study. For alginate hydrogels (Fig. 13), the linear viscoelastic region extends up to

approximately 40 Pa, although this threshold is exceeded by alginate 1% and alginate $(2-3)$% g/l. Within this stress range (τ_0), both the G' (elastic or storage modulus) and G" (viscous or loss modulus) remain virtually independent of the applied shear stress, a fundamental criterion for defining the linear viscoelastic region.

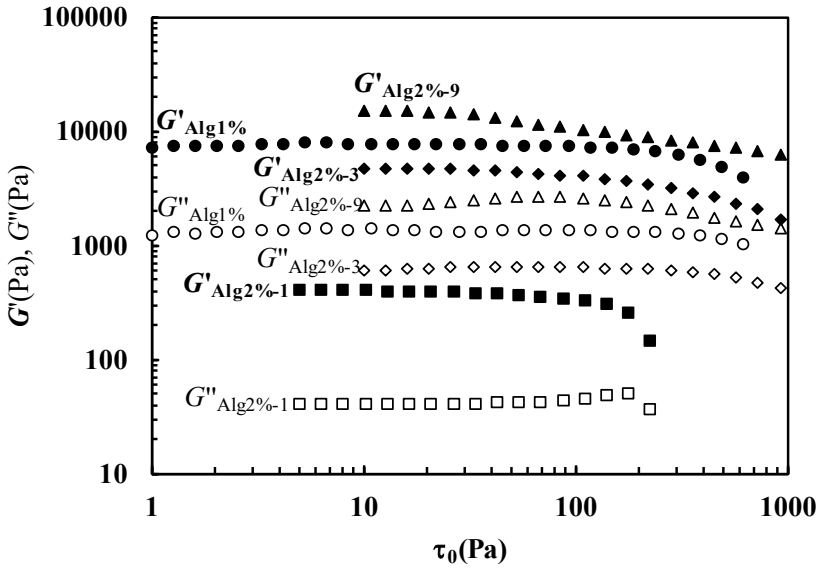

Figure 13: Stress sweep experiments relative to alginate 1 % and alginate 2 % hydrogels (at different crosslinking concentrations: 1, 3 and 9 g/L). The quantities G' (filled symbols) and G'' (open symbols) indicate, respectively, the elastic (or storage) and viscous (or loss) moduli. The applied shear stress is denoted by τ_0.

Higher stress causes variations in G' and G'' with τ_0, leading to nanostructure damage − an aspect we do not intend to explore. Our focus is on determining nanostructure characteristics (mesh size) in a nearly unperturbed state.

For Agar and scleroglucan hydrogels, the linear viscoelastic range extends to approximately $\approx 20-30$ Pa (Fig. 14), while for PVP-K90 and PEG-PPG hydrogels, it increases to around 40 Pa (Fig. 15). Regarding the two sputum samples (Fig. 16), we could not fully explore the viscoelastic range, including both the linear and nonlinear regions. Entering the nonlinear regime would irreversibly damage the sample's nanostructure, compromising the reliability of subsequent rheological tests (frequency sweep tests). Unlike other gels, where fresh samples could be prepared separately for determining the linear viscoelastic range and further rheological

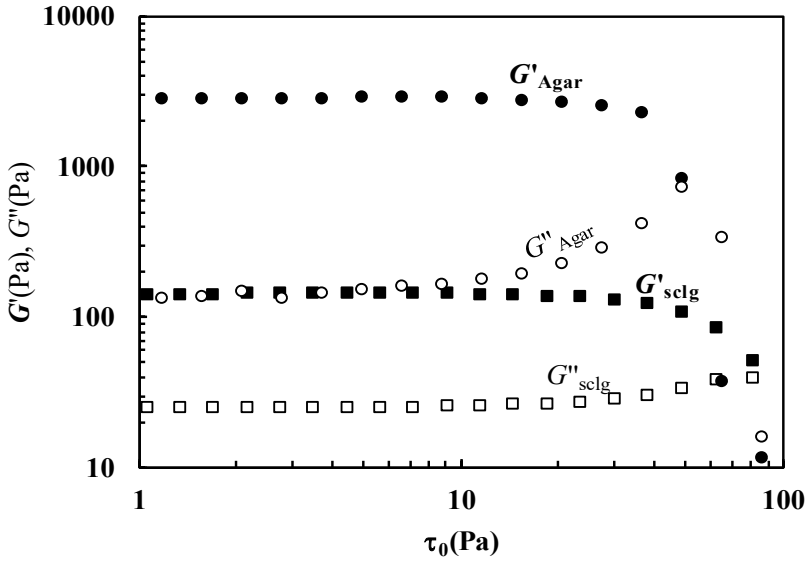

Figure 14: Stress sweep experiments relative to agar and scleroglucan hydrogels. Other symbols are as in Fig. (13).

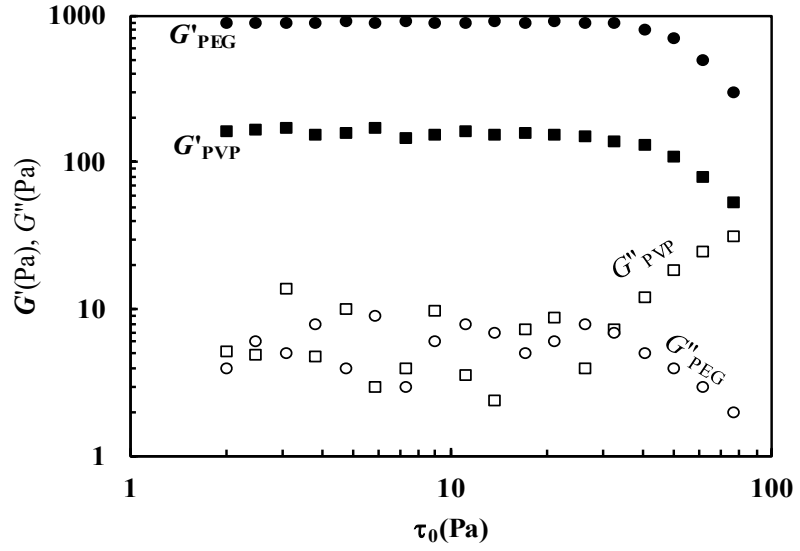

Figure 15: Stress sweep experiments relative to PVP-K90 and PEG-PPG hydrogels. Other symbols are as in Fig. (13).

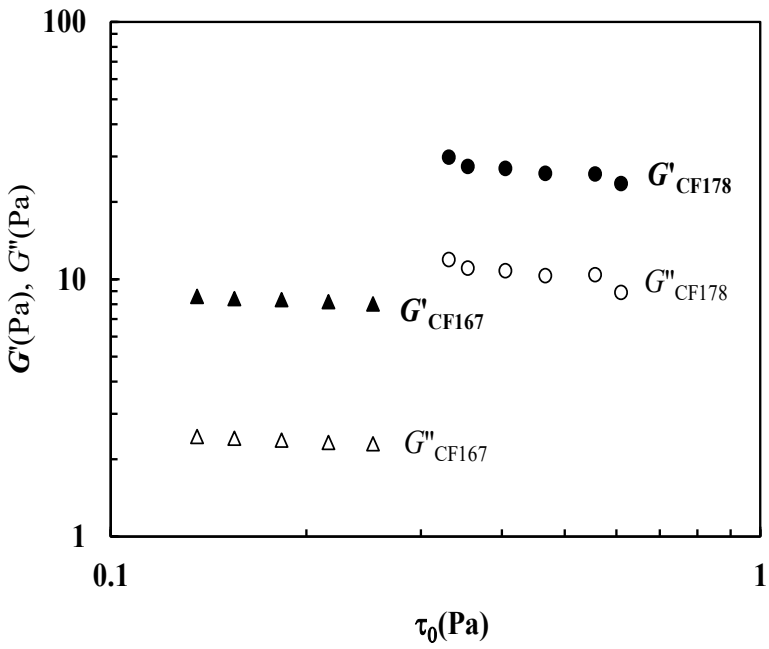

Figure 16: Stress sweep experiments on two sputum samples, CF167 and CF178. Other symbols are as in Fig. (13).

characterization, this was not possible for sputum samples, as they are unique. Since they result from patient expectoration, they cannot be replicated during the same clinical check. Therefore, we performed a limited stress sweep test to identify a stress range within the linear regime. Fig. (16) confirms that $\tau_0 \approx (0.2 - 0.3)$ Pa falls within the linear viscoelastic range for both samples (CF167 and CF178). Figs. (13-16) clearly show the predominance of the samples' elastic modulus (G') over the viscous modulus (G''), a characteristic typical of gels.[55] To stay within the linear viscoelastic region, frequency sweep tests were performed with $\tau_0 = 2$ Pa for all hydrogels, except for sputum samples, where $\tau_0 = 0.2$ Pa was used. The generalized Maxwell model (Eqs. 29 and 30 in the main text), fitted to the experimental data in Figs. (2-5) (main text), aims to determine the unknown parameters (g_E, λ_i, g_i) and the number of Maxwell models required for a statistically reliable fit.

Taking the alginate 1% as example, Fig. (17) represents the statistical approach discussed in section 3.3.2 of the main text (Rheology) by looking at the variation of $N\chi^2$ with N. It can be seen, in this particular case, that this product gets minimum when $N = 6$ fitting parameters are

(a)	**Agar 1%**	**Alginate 1%**	**Scleroglucan 2%**	**CF167/Sputum**	**CF178/Sputum**
$10^2\lambda_1$(s)	4.59 ± 0.35	1.66 ± 0.16	4.4 ± 0.45	0.9 ± 0.2	1.35 ± 0.20
g_E(Pa)	2114 ± 77	2282 ± 111	56 ± 4	—	—
g_1 (Pa)	285 ± 15	1877 ± 65	46 ± 2	9.7 ± 1.8	24.2 ± 1.4
g_2 (Pa)	186 ± 15	1371 ± 55	33 ± 2	3 ± 0.4	11.0 ± 0.6
g_3 (Pa)	225 ± 24	1269 ± 54	28 ± 2	3 ± 0.3	9.7 ± 0.5
g_4 (Pa)	546 ± 62	1953 ± 71	34 ± 4	1.5 ± 0.3	4.9 ± 1.3
g_5 (Pa)	—	—	—	4.3 ± 0.4	7.8 ± 1.0
F-test	$F(5,39) < 624$	$F(5,35) < 1154$	$F(5,35) < 542$	$F(5,31) < 207$	$F(5,31) < 652$
$G_{\rm exp}$(Pa)	3356 ± 104	8763 ± 166	196 ± 7	21.5 ± 2.0	57.6 ± 2.3

(b)	**Alg. 2% (1 g/l)**	**Alg. 2% (3 g/l)**	**Alg. 2% (9 g/l)**	**PVP-K90**	**PEG-PPG**
$10^2\lambda_1$(s)	2.1 ± 0.1	2.2 ± 0.1	1.7 ± 0.2	18.4 ± 2.0	0.25 ± 0.16
g_E(Pa)	271 ± 7	2547 ± 309	9432 ± 223	95 ± 8	899 ± 238
g_1 (Pa)	84 ± 1	1064 ± 16	4337 ± 106	11 ± 9	76 ± 43
g_2 (Pa)	45.8 ± 1.2	731 ± 19	2959 ± 106	2.6 ± 1.9	—
g_3 (Pa)	74 ± 2	1106 ± 25	3991 ± 116	3.9 ± 0.9	2.7 ± 2.6
g_4 (Pa)	—	—	—	—	6.1 ± 2.1
F-test	$F(4,21) < 664$	$F(4,21) < 34$	$F(4,21) < 542$	$F(4,19) < 44$	$F(4,27) < 28.5$
$G_{\rm exp}$(Pa)	476 ± 7	5447 ± 311	20709 ± 292	113 ± 13	984 ± 242

Table 2: (a-b). Fitting parameters and related physical quantities of the generalized Maxwell model (Eqs. 29 and 30 of the main text) fitting to experimental data shown in Figs. (2-3) of the main text and Figs. (18-20). The symbol λ_1 denotes the relaxation time of the first Maxwell element (while, for the other elements, $\lambda_i = 10^{i-1}\lambda_1$ $1 \leq i \leq 4$), g_E is the modulus of the purely elastic component, g_i are the moduli of all other elements. In the last two rows are the scores of the statistical F-test and the experimental values ($G_{\rm exp}$) of the shear modulus (calculated as the sum of g_E with all g_i).

considered, i.e. the first relaxation time (λ_1), the purely elastic term (g_E) and four additional viscoelastic components (g_i), for a total of 5 Maxwell elements. The experimental value of the

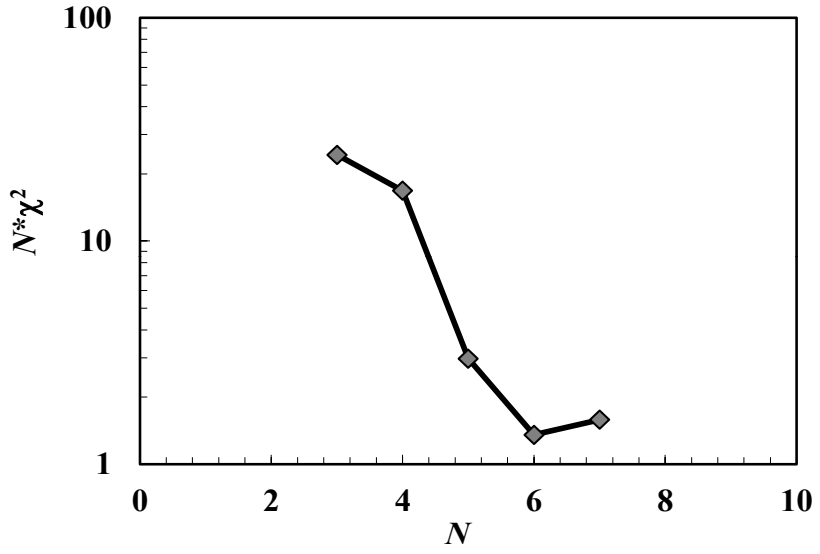

Figure 17: Graphical representation of the statistical method inferring the optimal number of generalized Maxwell elements to be regarded in data fitting (for the alginate case). The number of fitting parameters is denoted by N, χ^2 being the sum of squared errors.

shear modulus (G) is finally evaluated as the sum of g_E to the other elastic constants (g_i). Figs. (18-20) show the outcomes of the frequency sweep tests referring to the samples not shown in the main text.

Tab. (2) presents the number and values of the fitting parameters required to accurately describe the rheological behavior of all the samples considered, as confirmed by the F-test score. The shear modulus G is determined as the sum of g_E and the other elastic constants (g_i) of the viscoelastic Maxwell elements. Based on the G values, Tab. (2) indicates that agar 1%, alginate 1%, alginate 2% (3 g/L), and alginate 2% (9 g/L) are strong hydrogels, while scleroglucan and PVP-K90 form weak hydrogels. The weakest gels are the sputum samples, which lack a purely elastic element in the generalized Maxwell model ($g_E = 0$).

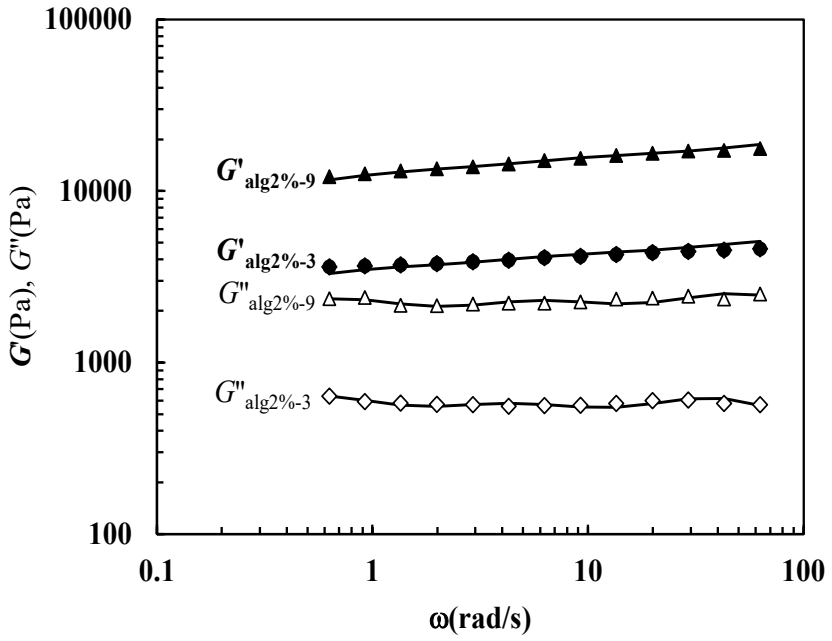

Figure 18: Frequency sweep tests referring to alginate 2 %, 3 g/l and 9 g/l. G' (filled symbols) and G'' (open symbols) indicate, respectively, the experimental elastic (or storage) and the viscous (or loss) moduli. The quantity f and ω ($= 2\pi f$) indicate, respectively, the solicitation frequency and angular frequency. The solicitation stress is equal to 2 Pa. Solid lines indicate the best fitting of the generalized Maxwell model (eq. (29) and eq. (30) of the main text).

5.4. Determination of the Polymer End-to-End Distribution

The first step we considered is the determination of the magnetic relaxation spectra of our samples. The experimental data, showing I_s vs. t for every hydrogel system, were best fitted with Eq. (19) (main text). This brings to an iterative process leading to the extrapolation of $N(= 200)$ unknowns (A_i), implemented by a Microsoft Excel file with the commands "User Defined Functions" and the "Solver" (Levenberg-Marquardt) method. Data fitting was performed first by setting a wide range of relaxation times ($T_{2\text{min}} = 1$ ms and $T_{2\text{max}} = 10^4$ ms), logarithmically subdivided into N parts. We imposed $A_i = 0$ ($1 \leq i \leq 200$) as a first choice and led the fitting procedure with the constraints $A_i > 0$ in the same i range. Indeed, as discussed later on (SI 5.9), the relaxation time of free or pure water ($T_{2\text{H}_2\text{O}}$) (i.e. water in the absence of any solid component, such as polymer) at 25 °C or 37 °C is shorter than 10^4 ms (at 20 MHz), whereas relaxation times shorter than 1 ms are not likely in hydrogel systems in the same frequency and

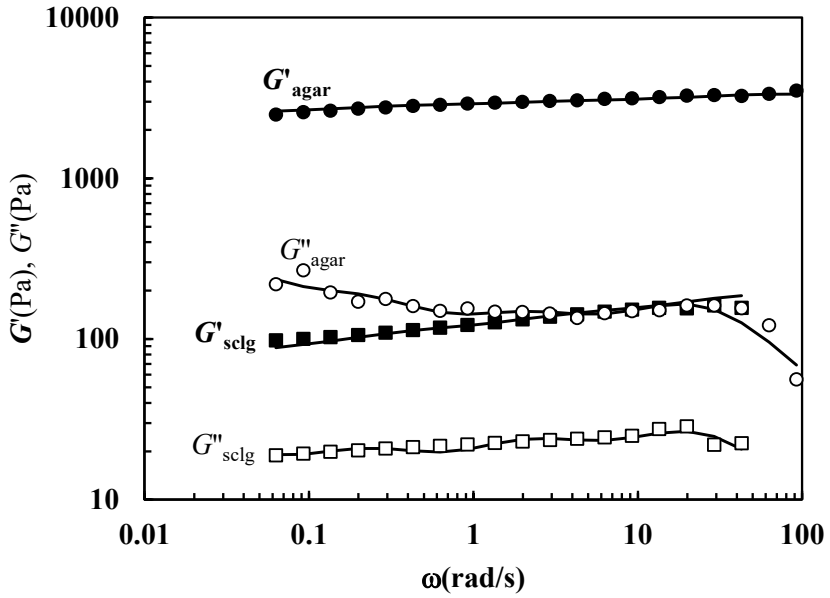

Figure 19: Frequency sweep tests referring to agar and scleroglucan. G' (filled symbols) and G'' (open symbols) indicate, respectively, the experimental elastic (or storage) and the viscous (or loss) moduli. The quantity f and ω $(= 2\pi f)$ indicate, respectively, the solicitation frequency and angular frequency. The solicitation stress is equal to 2 Pa. Solid lines indicate the best fitting of the generalized Maxwell model (eq. (29) and eq. (30) of the main text).

temperature conditions.[80] As discussed in the main text (section 3.3.1), data fitting also requires the derivation of the unknown smoothing term (w_{st}), carried out by the strategy proposed by Wang and Ni.[81] They suggest to repeat the fitting analysis by assuming different w_{st} values to get the dependence $\ln(\chi_s)$ vs. $\ln(w_{st})$. The correct w_{st} value is the one taking place just below the heel (slope variation) of this function, as depicted in Fig. (21) for the alginate gel at 1%.

Figs. (22–25) display the best fits (solid lines) of Eq. (19) from the main text to the magnetic relaxation data for the samples under consideration. This fitting procedure yields the magnetic relaxation spectrum (T_{2i}, A_i) shown in Figs. (4) and (5) of the main text. Subsequently, Eq. (26) (main text) enables the transformation of the relaxation time distribution (T_{2i}, A_i) into the corresponding dimensionless mesh distribution (ζ_i^+, P_i), as illustrated in Figs. (26–29).

In order to make the best choice, we adopted Akaike's criterion,[82] stating that the model to

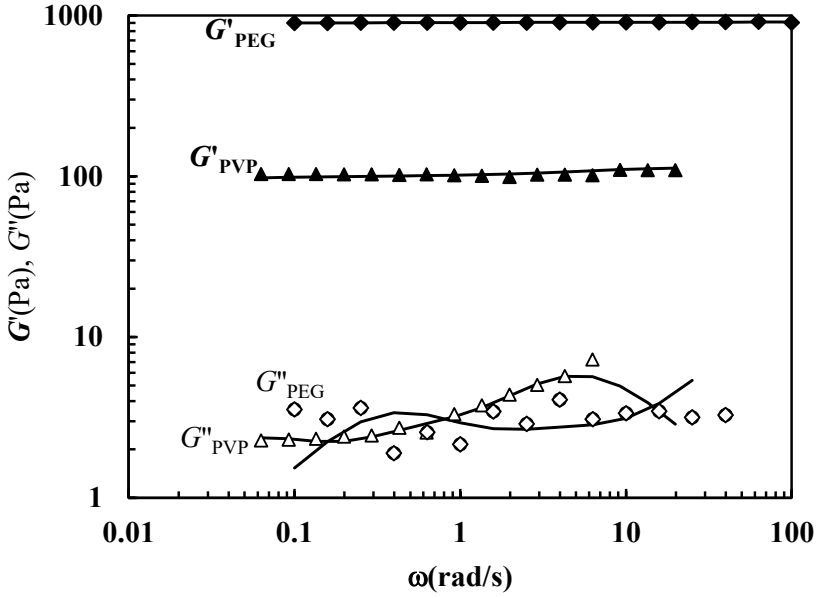

Figure 20: PEG-K90 and PEG-PVP frequency sweep tests. G' (filled symbols) and G'' (open symbols) indicate, respectively, the experimental elastic (or storage) and the viscous (or loss) moduli. The quantity f and ω ($= 2\pi f$) indicate, respectively, the solicitation frequency and angular frequency. The solicitation stress is equal to 2 Pa. Solid lines indicate the best fitting of the generalized Maxwell model (eq. (29) and eq. (30) of the main text).

be preferred is characterized by the smallest Akaike number (AIC):

$$\mathrm{AIC} \;=\; N_e \ln\left(\frac{\chi^2}{N_e}\right) \;+\; 2\,\frac{(N_F+1)(N_e-N_F)}{N_e-N_F-2} \tag{5.6}$$

where N_e is the number of experimental data, N_F is the number of fit parameters and χ^2 is the sum of the squared differences between the experimental data and theoretical (fitting) values. This criterion suggests (see Tabs. 1 and 2 in the main text) that the most probable distribution is the generalized Weibull and that the pierced Gaussian is always preferable to the Gauss distribution.

5.5. Determination of the Mesh Size Distribution

Once the three functional forms (Gaussian, pierced Gaussian, generalized Weibullian) were tested to describe the end-to-end length distribution, one can estimate the average mesh size (ζ_m) of the polymeric network pervading the samples. This target is achieved by confronting the

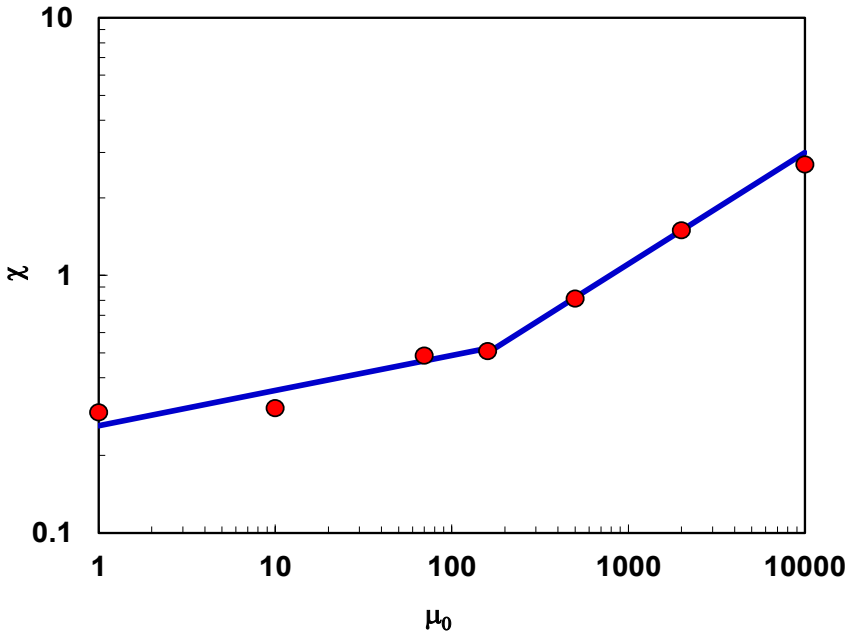

Figure 21: Dependence of $\ln \chi$ vs. $\ln w_{st}$ (red circles) for the alginate 1% sample, chosen here as a representative case. An abrupt slope variation (see blue lines) occurs in the logarithmic plot at about $w_{st} \approx 150$.

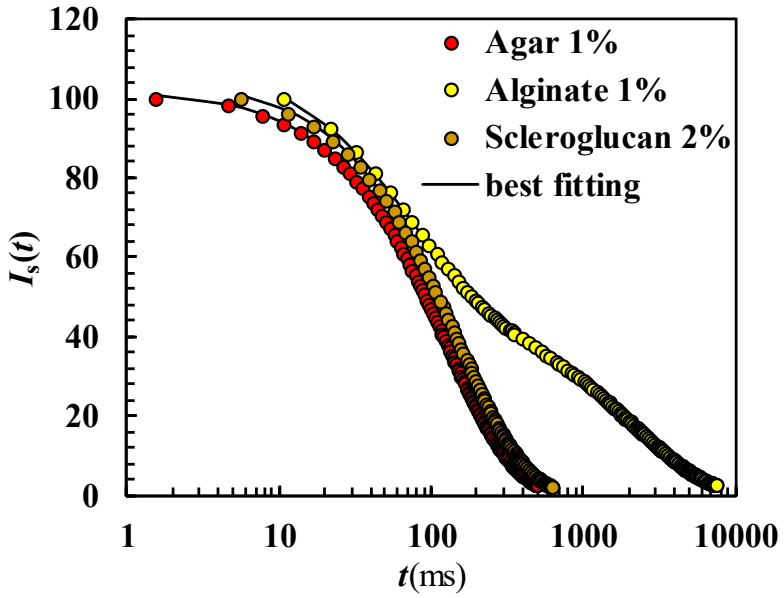

Figure 22: Best fit of Eq. (19) of the main text (solid lines) to the magnetic relaxation data ($I_s(t)$) for agar 1 % (red symbols), alginate 1 % (yellow circles), and scleroglucan 2 % (brown symbols).

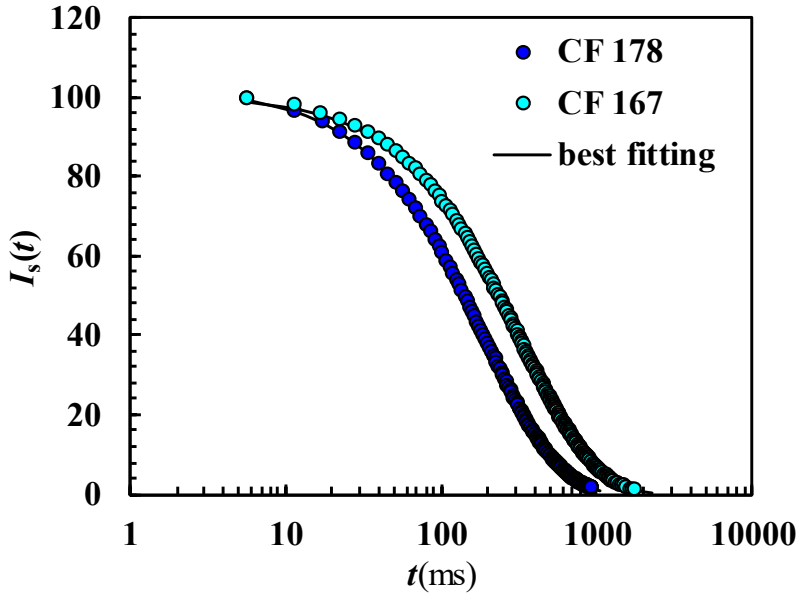

Figure 23: Best fit of Eq. (19) of the main text (solid lines) to the magnetic relaxation data ($I_s(t)$) for sputum samples CF267 (light blue circles) and CF178 (blue circles).

theoretical expressions of the shear modulus related to each distribution with its experimental value, determined by rheology measurements. Such relationships are given respectively in Eq. (1.7) (G), Eq. (1.16) (G_h) and Eq. (1.37) (G_a) where, for experimental reasons, it is convenient replacing the density of crosslink points ρ in the reference state ($\mathrm{Q} = 1$) with $\rho_x = \rho/\mathrm{Q}$, relative to a swollen/shrunken sample ($\mathrm{Q} \neq 1$).

The link between crosslink density and average mesh size is established by the equivalent network theory.[83] Starting from the evidence that a detailed description of a real polymer network is normally rather complicated (if even not impossible), such a theory suggests to replace the real network topology by an idealized one, sharing the same (average) ρ_x. The idealized network is built up by a set of identical spheres, of diameter ζ_m and centered around each cross-link, bringing to a cubic arrangement of ζ_m-sized meshes. The definition of cross-link density (mole number of cross-links per sample unit volume) then implies that the average volume per cross-link in the real network, $1/\rho_x$, should equal the volume of each spherical unit, as the two networks share the same ρ_x. The relation between ζ_m and ρ_x reads is given by Eq. (35) of the main text.

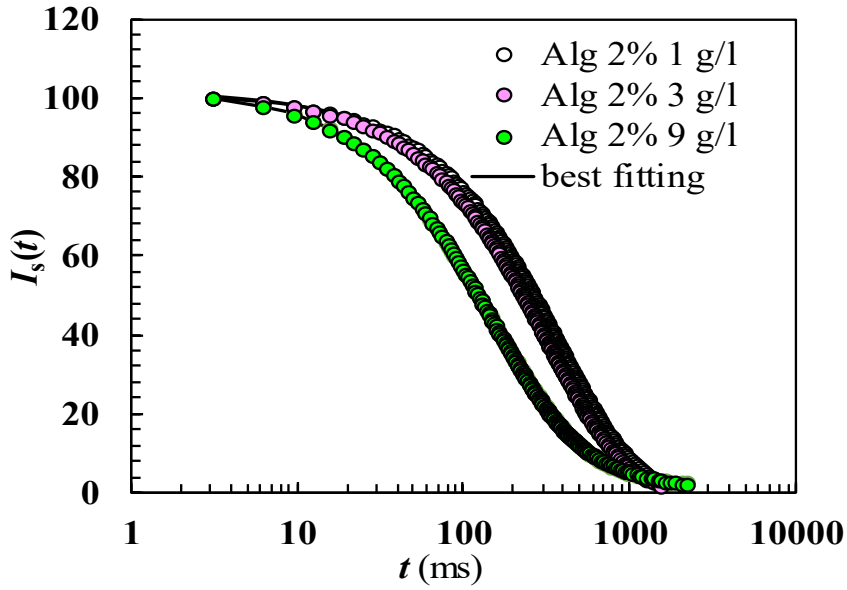

Figure 24: Best fit of Eq. (19) of the main text (solid lines) to the magnetic relaxation data ($I_s(t)$) for alginates 2 % hydrogels and three different crosslinking agent concentrations (white 1 g/l, purple 3 g/l, and light green 9 g/l.

5.6. Determination of the Average Mesh Size from LF-NMR

According to the LF-NMR theory, it is possible to deduce the average mesh (ζ_{mNMR}) of the polymeric network provided that the radius of the polymeric fiber (R_f), the polymer volume fraction (ϕ) and network architecture is regular and known (see Eq. 21 of the main text). Tab. (3), under the hypothesis of a cubical arrangement of the meshes, shows the estimation of ζ_{mNMR} for some of the hydrogels considered in this work.

5.7. Experimental Discussion of the Maxwell-Boltzmann Approximation to the Pierced Gaussian Modulus (Eq. 1.16 vs. Eq. 1.22).

The full expression for the shear modulus in a pierced Gaussian description is quite complicated (Eq. 1.16). It includes a number of swelling contributions (Q) coupled to the perturbation term (q). In unswollen materials ($\mathrm{Q} \to 1$), it reduces to a simpler form, given in Eq. (1.17). We finally proposed a Maxwell-Boltzmann averaging of this equation, which returns the elementary dependence in Eq. (1.22).

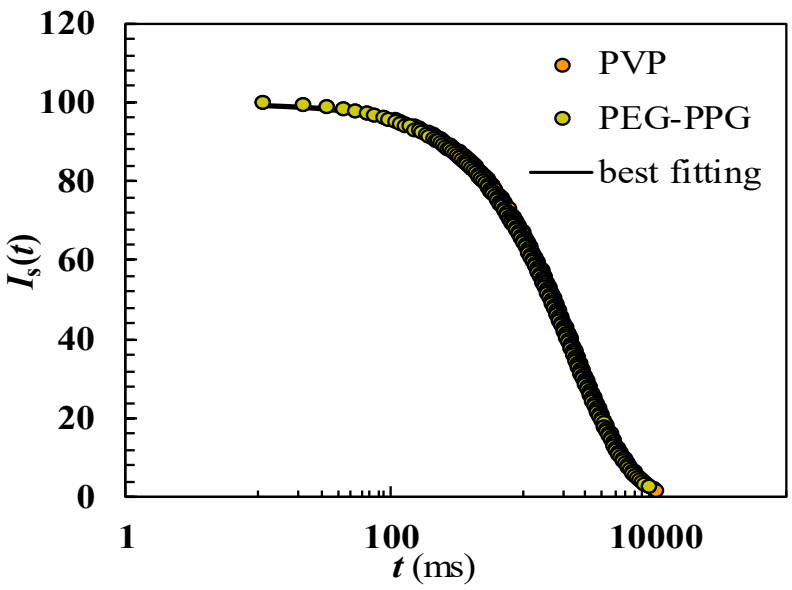

Figure 25: Best fit of Eq. (19) of the main text (solid lines) to the magnetic relaxation data ($I_s(t)$) for hydrogels composed by PVP-K90 (orange) and PEG-PPG (green).

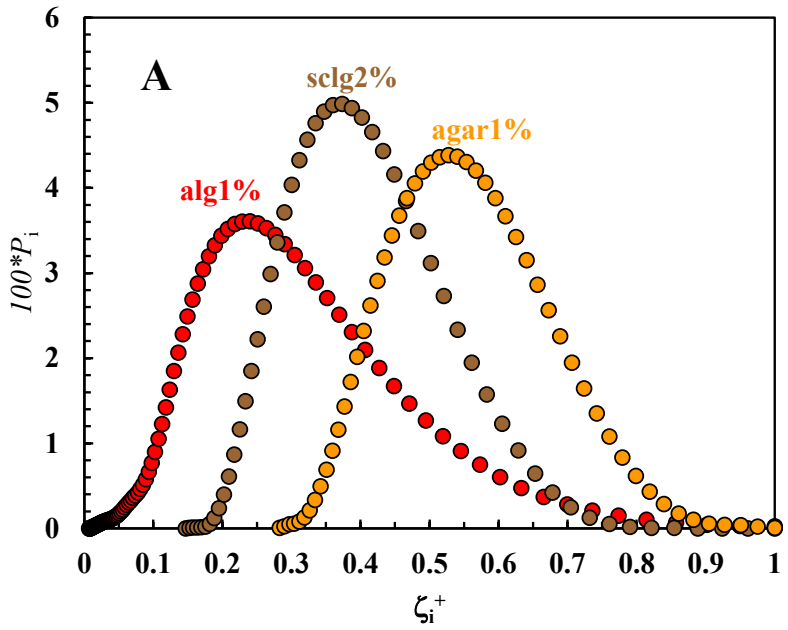

Figure 26: Mesh size distribution in agar 1%, alginate 1% and scleroglucan 2% hydrogels. P_i is the probability of finding a mesh sized ζ_i^+ (in dimensionless units).

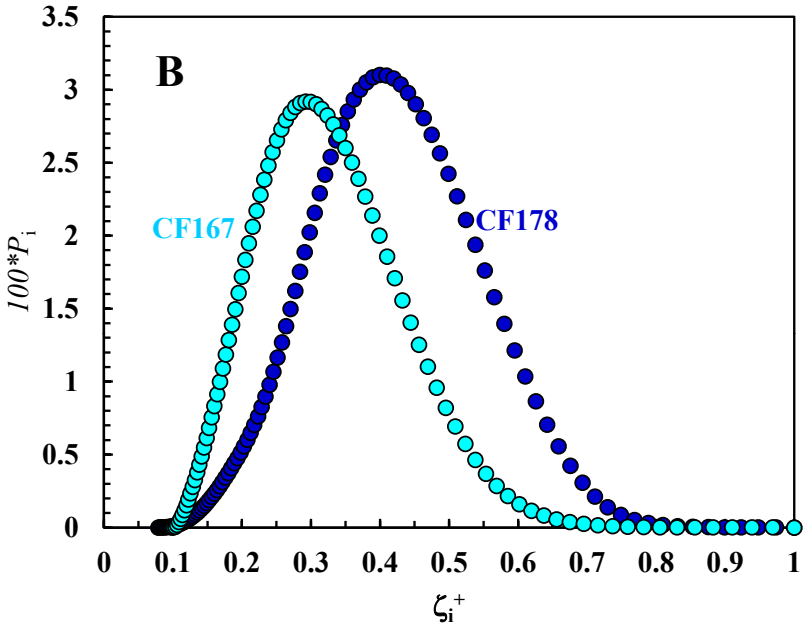

Figure 27: Mesh size distribution in sputum specimens CF167 and CF178. Symbols are set as in Fig. (26).

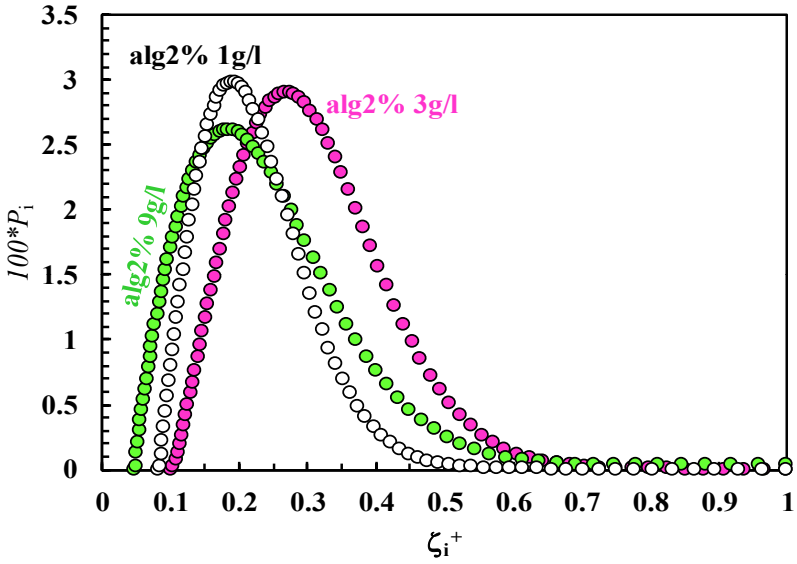

Figure 28: Mesh size distribution in alginate 2 % hydrogels (1 g/l, 3 g/l, 9 g/l). Symbols are set as in Fig. (26).

To estimate the error that affects the last relation when applied to unswollen hydrogels (Q = 1, reference state), Fig. (34) reports the trend of the dimensionless quantity $G_h/(k_B T \rho_x)$

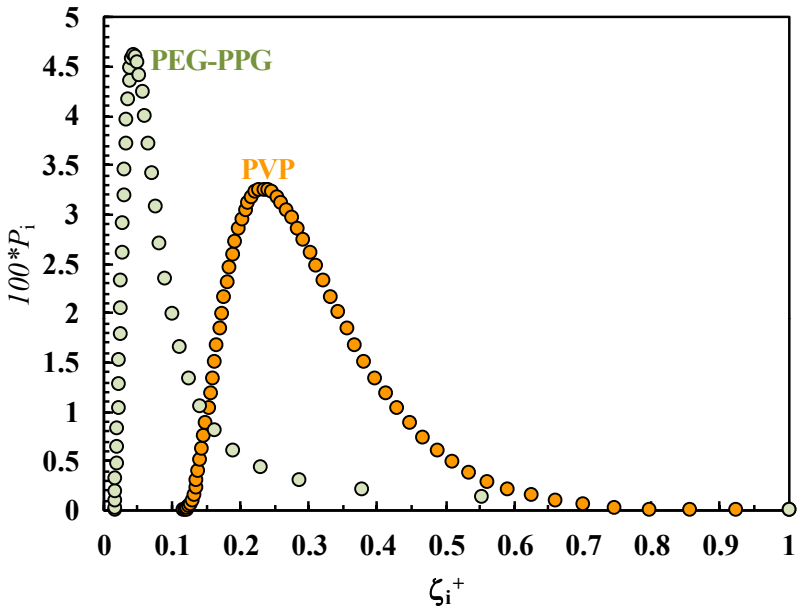

Figure 29: Mesh size distribution in PVP-K90 and PEG-PPG hydrogels. Symbols are set as in Fig. (26).

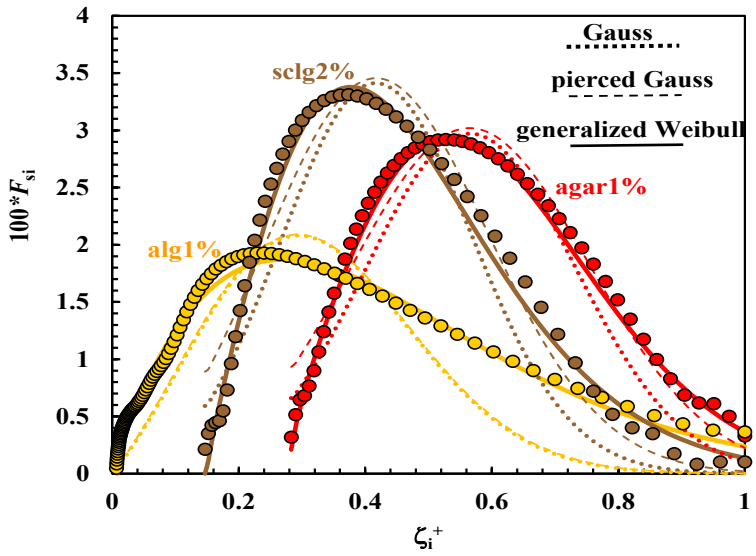

Figure 30: End-to-end distributions (ζ_i^+ , F_{si}) for agar 1 % (red circles), alginate 1 % (yellow circles) and scleroglucan 2 % (brown circles). Dotted, dashed and solid lines represent, respectively the best fitting of the Gauss (Eq. (31) – main text), pierced Gauss (Eq. (32)) and generalized Weibull (Eq. (33)) distributions.

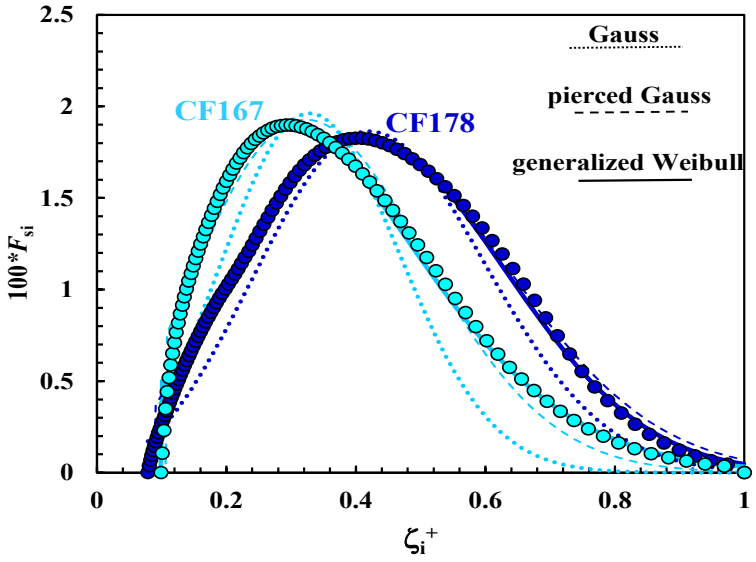

Figure 31: End-to-end distributions (ζ_i^+ , F_{si}) for the sputum samples CF167 (light blue circles) and CF178 (blue circles). Dotted, dashed and solid lines represent, respectively the best fitting of the Gauss (Eq. (31) – main text), pierced Gauss (Eq. (32)) and generalized Weibull (Eq. (33)) distributions.

vs. $q \equiv \beta\zeta_{\min}$, evaluated according to Eq. (1.17) (red line) and Eq. (1.22) (blue line). For simplicity, here it is assumed $\bar{q} = q$. One can see that the percentage error (green line) linearly increase with increasing q from negligible to more significant values ($\approx 33\%$ at $q \approx 0.26$). Experimentally, as in this work $q = 0.03 - 0.36$, we have prudently decided to stick to the exact solution (Eq. 1.17). It is important to remind that assuming different Q values in the range $0.5 - 2$ (shrinking/swelling), the same qualitative conclusions about the comparison of the exact (Eq. 1.16) to the approximate (Eq. 1.22) solutions can be drawn.

Finally, it is worthwhile mentioning that a very good approximation of Eq. (1.16), valid for $\mathrm{Q} = 1$ and $q \leq 0.5$, is achieved by changing the square power of $(1 - q)$ in Eq. (1.22) (still with $\overline{q} = q$) into $\frac{13}{4}$:

$$\frac{G_h}{k_B T} \approx \frac{\rho}{(1-q)^{\frac{13}{4}}\mathrm{Q}^{\frac{1}{3}}} \equiv \frac{\mathrm{Q}^{\frac{2}{3}}\rho_x}{(1-q)^{3.25}} \tag{5.7}$$

In fact, as depicted in Fig. (35), the percentage error is ranging in $\pm$ 4. Notably, Eq. (5.7) can properly approximate Eq. (1.16) also when $\mathrm{Q} \neq 1$. Precisely, for $\mathrm{Q} \geq 0.25$, Eq. (5.7) provides

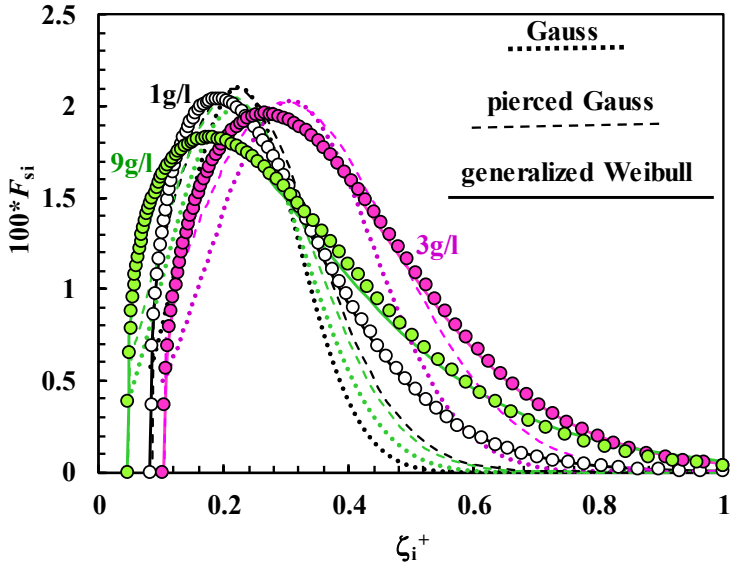

Figure 32: End-to-end distributions (ζ_i^+ , F_{si}) for the alginate 2 % hydrogels characterized by different crosslinking agent ($CaCl_2$) concentrations (1 g/l – white; 3 g/l – purple; 9 g/l - green). Dotted, dashed and solid lines represent, respectively, the best fitting of the Gauss (Eq. (31) - main text), pierced Gauss (Eq. (32)) and generalized Weibull (Eq. (33)) distributions.

a good approximation of Eq. (1.16), as witnessed by Fig. (36). It can be seen that the error dependence on q for three different values of Q is limited to vary within -5% and 9%.

5.8. Which Mesh Size ?

In a recent interesting review on modelling the solute diffusion coefficient within polymeric networks,[87] great attention was paid to the method used to evaluate the average mesh size. In fact, mesh size can be either estimated as the network correlation length (ζ_c) or the end-to-end length of chain segments between two consecutive crosslinks (ζ_{ete}). In addition, the relation between mesh size and mesh radius (r_m), the latter being defined as the maximum radius of a spherical solute passing across a mesh portal, was recently discussed as well.[88] For a chain disposition into a regular tetrahedron around the crosslink (tetra-functional connectivity $f = 4$), r_m is about 82% of the mesh size. For a cubic arrangement (hexa-functional connectivity $f = 6$), r_m is exactly one half of the mesh size and becomes about 35% of it for a octahedral functionality (octa-functional connectivity $f = 8$).

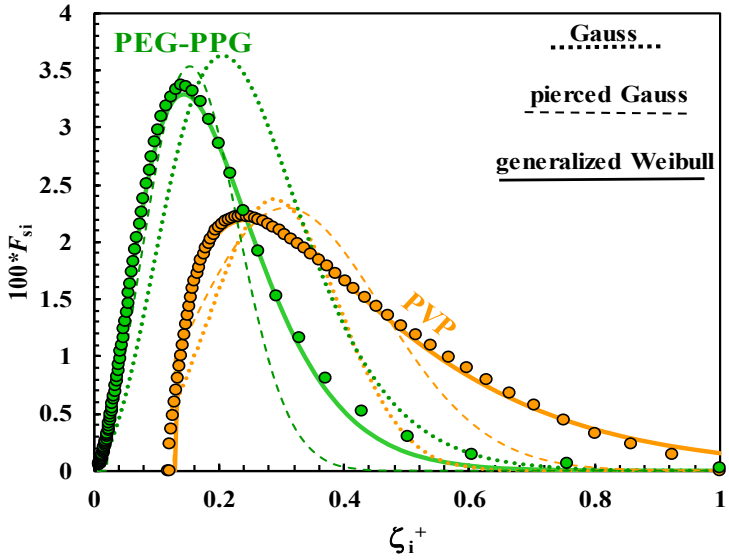

Figure 33: End-to-end distributions (ζ_i^+ , F_{si}) for the PVP-K90 (orange) and PEG-PPG (dark green) hydrogels. Dotted, dashed and solid lines represent, respectively, the best fitting of the Gauss (Eq. (31) - main text), pierced Gauss (Eq. (32)) and generalized Weibull (Eq. (33)) distributions.

5.8.1. Correlation Length

A hydrogel can be considered as a polymer solution at a concentration above the overlap value,[22] $c > c^*$. In this regime (semidilute), macromolecular chains have a high probability to entangle and the average length of polymer segments between two consecutive entanglement points corresponds to the so-called correlation length:

$$\zeta_c \;=\; R_g \left(\frac{c}{c^*}\right)^m \tag{5.8}$$

where R_g is the radius of gyration and m is a scaling coefficient whose value is determined by the polymer-solvent (water) interaction.[87] For non-ionic polymers (such as scleroglucan) m ranges between 0.76, when water is regarded to be a good solvent, to 1 in poor solvent conditions. For polyelectrolytes in water (i.e. alginate) $m = 0.5 - 0.76$ (from low to high salt concentrations).[87]

	Agar 1%	**Alginate 1%**	**Scleroglucan 2%**
ϱ_p (kg/m^3)	1520[84]	1770[85]	1600[56]
ϱ_{H2O} (kg/m^3)	≈ 1000	≈ 1000	≈ 1000
R_f (nm)	0.66[86]	0.8[86]	2.15[53]
C_0 (cubic mesh)	1	1	1
C_1 (cubic mesh)	3π	3π	3π
$10^3\phi$	6.6	5.7	12.6
ζ_{mNMR} (nm)	24.9	32.5	58.6

Table 3: Estimation of the average mesh size following the Low-Field NMR approach (Eq. 21 (main size), ζ_{mNMR}) for the agar, alginate and scleroglucan hydrogels. The symbol ϕ denotes the polymer volume fraction, ϱ_p and ϱ_{H2O} are the polymer and water mass density, R_f is the radius of the polymeric chain schematized by a long cylinder. C_0 and C_1 are two constants depending on the building block of the mesh network (cube, octahedron, tetrahedron).

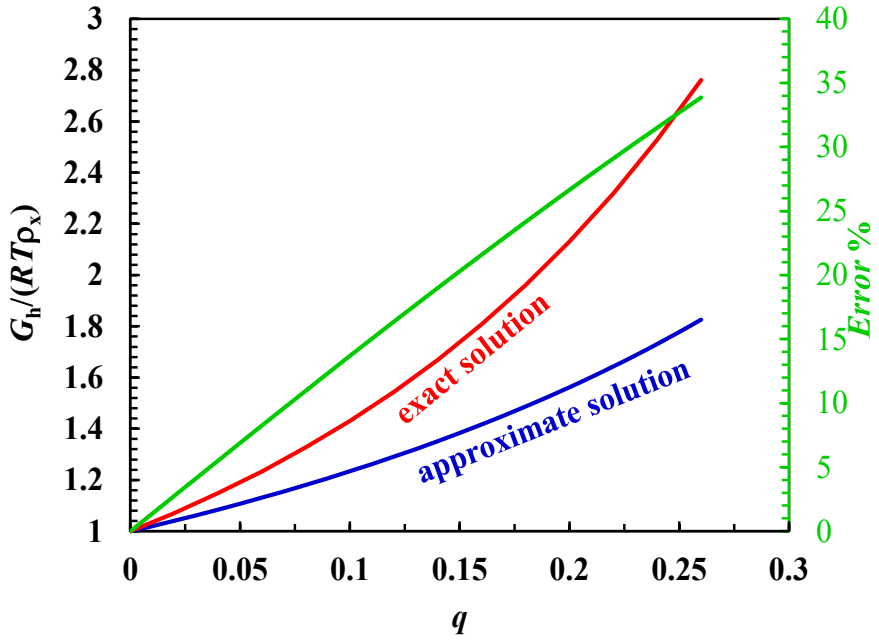

Figure 34: Dependence of the dimensionless quantity $G_h/(k_{_B}T\rho_x)$ vs. q upon setting the swelling/shrinking ratio to Q = 1. The red line gives the exact solution for the pierced Gaussian (Eq. 1.17). The blue line depicts the approximate solution (Eq. 1.22), the behaviour of its percentage error being reported in green.

The overlap concentration then is estimated from the simple molecular mass-volume relationship:

$$c^* = \frac{3M_w}{4\pi N_{_A} R_g^3} \tag{5.9}$$

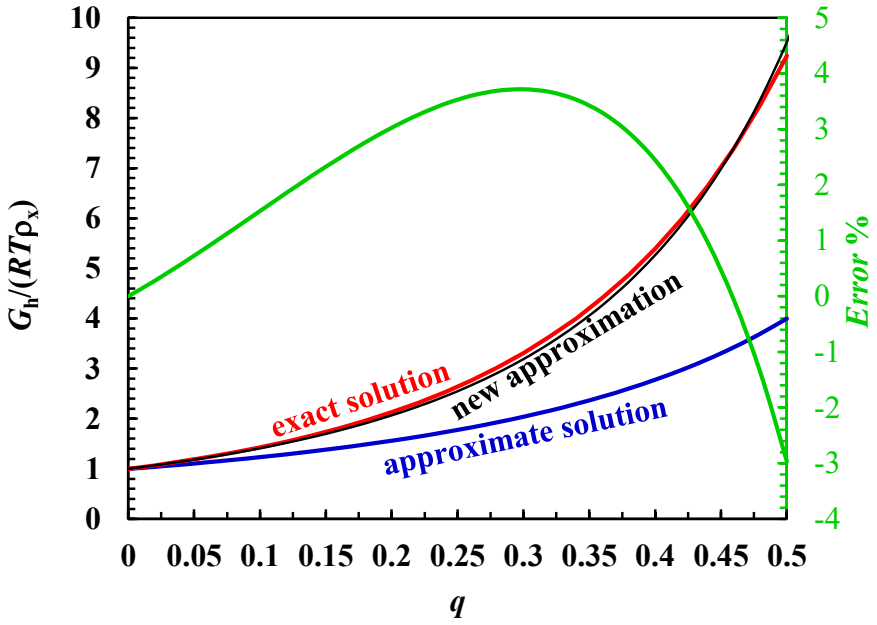

Figure 35: Dependence of the dimensionless quantity $G_h/(k_{_B}T\rho_x)$ vs. q upon setting the swelling/shrinking ratio to $\mathrm{Q} = 1$. The red line gives the exact solution for the pierced Gaussian (Eq. 1.17). The blue line depicts the approximate solution (Eq. 1.22). The black line represents the new approximation in (Eq. 5.7), the behaviour of its percentage error being reported in green.

M_w being the polymer weight-average molecular weight and N_A being the Avogadro's number. For linear flexible chains immersed in a good solvent (Θ conditions), R_g can be derived from:[1,89]

$$R_g^3 \;=\; \frac{[\eta]M_w}{6^{\frac{3}{2}}\Phi_{_0}} \tag{5.10}$$

where $[\eta]$ is the intrinsic viscosity and $\Phi_{_0}$ is the universal Flory constant, equal to $2.1\cdot 10^{23}$ when $[\eta]$ brings the units of ml/g. Finally, the popular Mark-Houwink-Sakurada equation:

$$[\eta] \;=\; K_w M_w^{\overline{\alpha}} \tag{5.11}$$

allows an evaluation of the intrinsic viscosity in terms of the empirical temperature- and composition-dependent parameters, K_w and $\overline{\alpha}$.

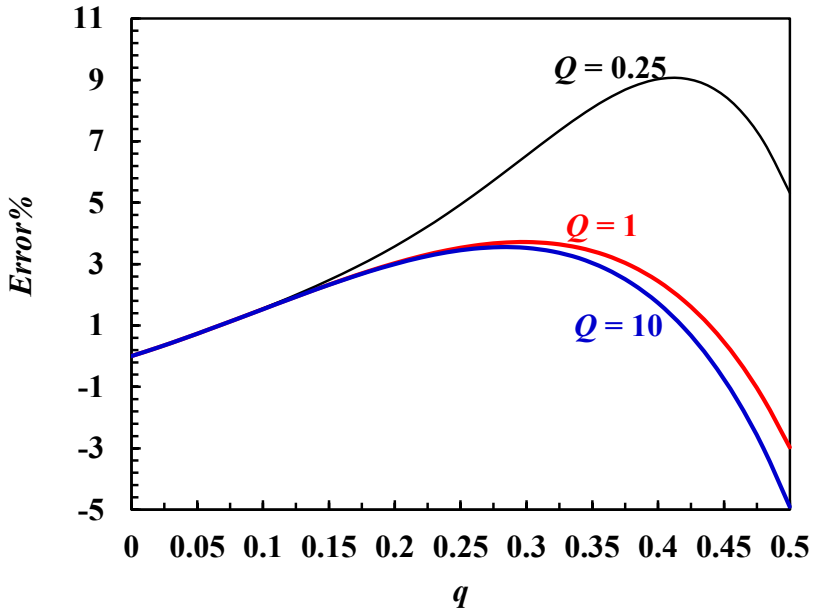

Figure 36: Effect of q ($= \beta\zeta_{\min}$) and Q (swelling/shrinking ratio) on the error produced by approximating Eq. (1.16) with Eq. (5.7). For any $q \leq 0.5$ and $\mathrm{Q} \geq 0.25$, the percentage deviation ranges between -5 and 9 .

5.8.2. End-to-End Length

The length ζ_{ete} is evaluated recurring to the concept of average molecular weight between crosslinks (M_c):[87,88]

$$\zeta_{\mathrm{ete}} = \phi^{-\frac{1}{3}} \sqrt{(1 - \tfrac{2}{f}) C_\infty N_c l^2} \tag{5.12}$$

where l is the repeat unit length, C_∞ is the polymer characteristic ratio, $N_c = M_c/M_r$ is the number of units between crosslinks, each with molecular weight M_r, and f is the crosslink functionality. The product $C_\infty l^2$ can be calculated (in Θ conditions) from:[90]

$$C_\infty l^2 = \left(\frac{[\eta]^2}{M_w \Phi_0^2} \right)^{\frac{1}{3}} M_r \tag{5.13}$$

5.8.3. Alginate (ζ_c vs ζ_{ete})

All the parameters necessary for the derivation of ζ_c and ζ_{ete} in alginate 1% hydrogels are reported in Table (4). In particular, M_c has been determined according to the Brannon &

Peppas' equation:[83]

$$M_c^{-1} = \frac{\rho_x}{\rho_p} + \frac{2}{M_w} \tag{5.14}$$

whereas we believe a better evaluation of R_g can follow from:[91]

$$R_g\,[\text{nm}] = 9.3 \cdot 10^{-2} M_w^{0.53} \tag{5.15}$$

as it was successfully applied to alginates very similar to those regarded by the present work. Use of Eq. (5.10) leads to a smaller, although not so different, value ($R_g = 97$ nm). Finally, the crosslink density (ρ_x) has been inferred from Eq. (1.37) and the experimental shear modulus reported in Tab. (2).

Tab. (4) shows that, while a reasonable agreement between ζ_c and the mesh size (ζ_m) takes place, ζ_{ete} is more than one order of magnitude larger than ζ_c and ζ_m. Employing ζ_c in place of ζ_{ete}, on the other hand, produced a more consistent agreement between experimental data and model predictions of solute diffusion coefficients inside a polymer network,[87] which definitely supports the reliability of the theoretical approach presented in this work. We could also verify that not only ζ_m ($\approx \zeta_c$) and ζ_{ete} significantly differ, but their distributions are different too, as Fig. (37) illustrates. In fact, the distribution of ζ_{ete} values is nothing but the end-to-end length distribution function coming from Eq. (28) (main text), and ζ_m behaves as in Fig. (30).

5.8.4. Agar (ζ_c vs ζ_{ete})

Tab. (5) reports all the parameters for the agar 1% hydrogels. In this case too, M_c was calculated from Eq. (5.14), the crosslink density (ρ_x) from Eq. (1.37), the experimental shear modulus being still reported in Tab. (2). Tab. (5) again shows the reasonable agreement between ζ_c and the mesh size (ζ_m) determined in this work, ζ_{ete} being still more than one order of magnitude larger than ζ_c and ζ_m. The difference between their distributions well emerges from Fig. (38), according to the same arguments explained in the agar case (see still Eq. (28) of the main text and Fig. (30).

M_w	10^6	K_w (dL/g)	$5.9 \cdot 10^{-4}$ [91]
M_r	198 [90]	$\overline{\alpha}$	0.78 [91]
M_c	192933	$[\eta]$ (dL/g)	28.2
N	974	R_g (nm)	141†
ρ_p (g/cm^3)	1.77 [85]	c^* (g/mL)	$1.42 \cdot 10^{-3}$
ϕ	$5.7 \cdot 10^{-3}$	c (g/mL)	10^{-2}
$l^2 C_\infty$ (mol/cm^3)	11.2	m	0.5 [87]
ρ_x (mol/cm^3)	$5.63 \cdot 10^{-6}$	ζ_c (nm)	16.7
ζ_{ete} (nm)	534	ζ_m (nm)	8.5

Table 4: Evaluation of correlation (ζ_c) and end-to-end (ζ_{ete}) lengths for alginate 1% hydrogels assuming a hexafunctional (or cubical, $f = 6$) network. M_w is the polymer molecular weight, M_r the molecular weight of the repeat unit, M_c and N are respectively the average molecular weight and repeat unit number, both between crosslinks, ρ_p, ϕ and c are the polymer mass density, volume fraction and concentration, l is the repeat unit length, C_∞ the characteristic ratio, K_w and $\overline{\alpha}$ are the Mark-Houwink-Sakurada's parameters (Eq. 5.11), $[\eta]$ is the intrinsic viscosity, R_g the gyration radius of the polymer chain, c^* the overlap concentration, m the correlation scaling exponent (Eq. 5.8), ρ_x the crosslink density (evaluated through Eqs. 1.37) and ζ_m is the average mesh size hereby evaluated. The above numerical data refer to the quantities to their left [†evaluated from Eq. 5.15 and not from Eq. 5.10].

M_w	$0.12 \cdot 10^6$	K_w (dL/g)	$5.9 \cdot 10^{-4}$ [91]
M_r	306 [92]	$\overline{\alpha}$	0.78 [91]
M_c	59097	$[\eta]$ (dL/g)	5.4 [91,93]
N	193	R_g (nm)	27.6
ρ_p (g/cm^3)	1.52 [84]	c^* (g/mL)	$1.42 \cdot 10^{-3}$
ϕ	$6.6 \cdot 10^{-3}$	c (g/mL)	10^{-2}
$l^2 C_\infty$ (mol/cm^3)	11.6	m	0.593 [94]
ρ_x (μmol/cm^3)	0.387	ζ_c (nm)	11.4
ζ_{ete} (nm)	231	ζ_m (nm)	20.2

Table 5: Evaluation of correlation (ζ_c) and end-to-end (ζ_{ete}) lengths for agar 1% hydrogels assuming a hexafunctional (or cubical, $f = 6$) network. Symbols and references to equations are as in Tab. (4).

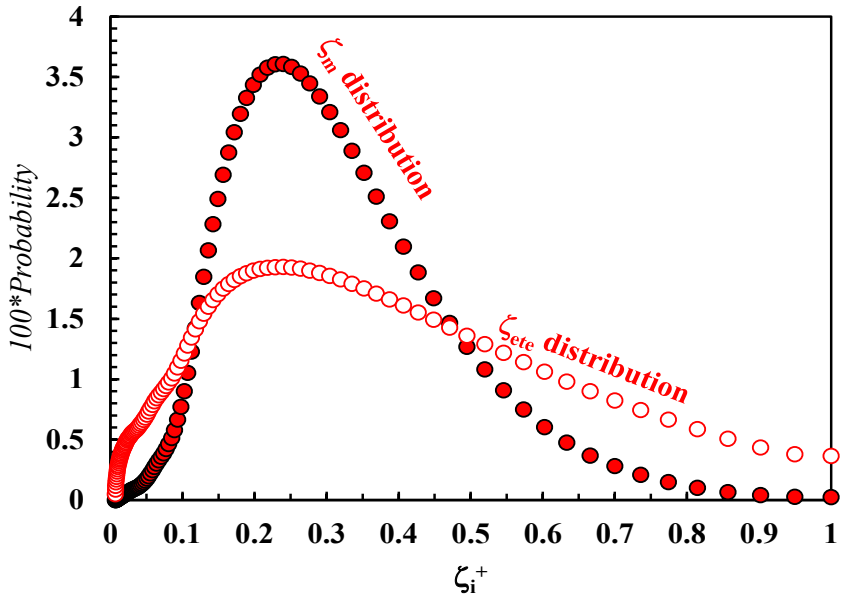

Figure 37: Comparison between the ζ_m ($\approx \zeta_c$) (red dots) and the ζ_{ete} (open dots) distributions for alginate hydrogels at 1 .

5.8.5. Scleroglucan (ζ_c vs ζ_{ete})

Tab. (6) reports all the scleroglucan 2% hydrogels parameters essential for evaluating ζ_c and ζ_{ete}. In the present case ζ_m is much closer to ζ_c than ζ_{ete} but their distributions are different, as shown in Fig. (39). Again, the distribution of ζ_{ete} values is nothing in fact but the end-to-end length distribution coming from Eq. (28) (main text) whereas ζ_m behaves as in Fig. (30).

5.9. Free Water Relaxation

It is well known that the magnetic relaxation time depends on many physical parameters such as magnetic field intensity, temperature and time separation (τ) between the 90 °C and 180 °C pulses of the CPMG sequence.[95] In particular, a decrease in τ implies an increase in the relaxation time. As this effect becomes more and more pronounced in samples relaxing with long characteristic times, its determination requires particular care when dealing with water (i.e. the substance with the longest relaxation time in water-based materials such as hydrogels). Fig. (40) reports the water FID decay ($I_s(t)$) for three increasing values of τ. It is qualitatively

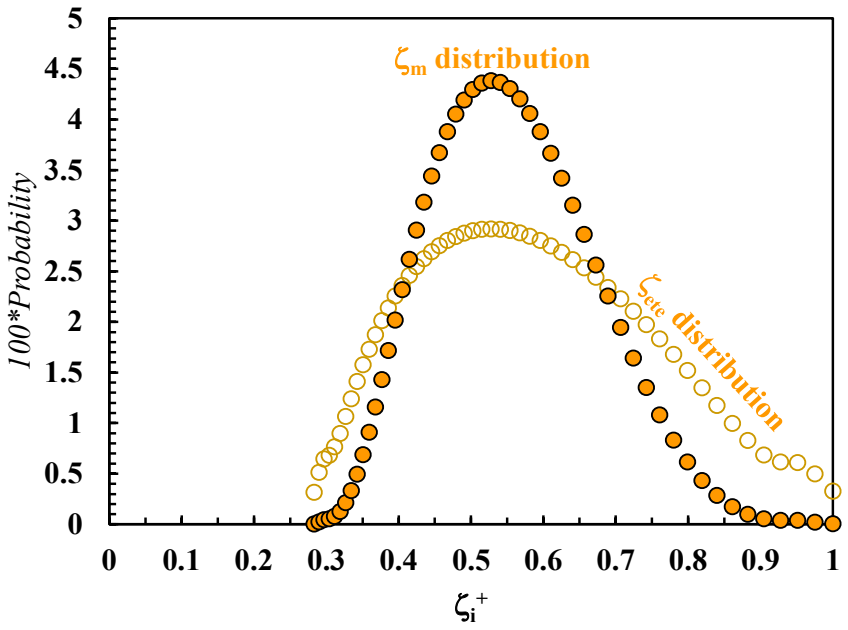

Figure 38: Comparison between the ζ_m ($\approx \zeta_c$) (orange dots) and the ζ_{ete} (open dots) distributions for agar hydrogels at 1%.

evident that increasing τ leads to a faster relaxation process, as it is proved by a gradually smaller intercept of the $I_s(t)$ curve onto the x-axis.

An analysis of the three decay curves by means of Eq. (19) (main text) allows to quantify their differences in terms of relaxation spectra (Fig. 41), and we note that an increase in τ shifts the whole distribution towards lower values. Fig. (42) reports the displacements of the distribution peak and its extremal points, i.e. the minimum and maximum relaxation times when $A_i = 0$. Their positions turn out to increase almost linearly with decreasing τ. The actual distribution spectrum, corresponding to $\tau = 0$, ranges from 2980 to 4540 ms, to show its peak at 3711 ms. Accordingly, we adopted the peak upper part (4540 ms) for the free water relaxation time at 37 °C and 20 MHz. We remind, however, this picture is somehow more complex than the one hitherto discussed. In fact the smoothing factor value (w_{st}, Eq. 20, main text), adopted to determine the distribution form, is also affecting the distribution width.

As an example, Fig. (43) displays the variation of the water relaxation spectrum with changing w_{st}, which here assumes five different values. It may be seen that the peak does not substan-

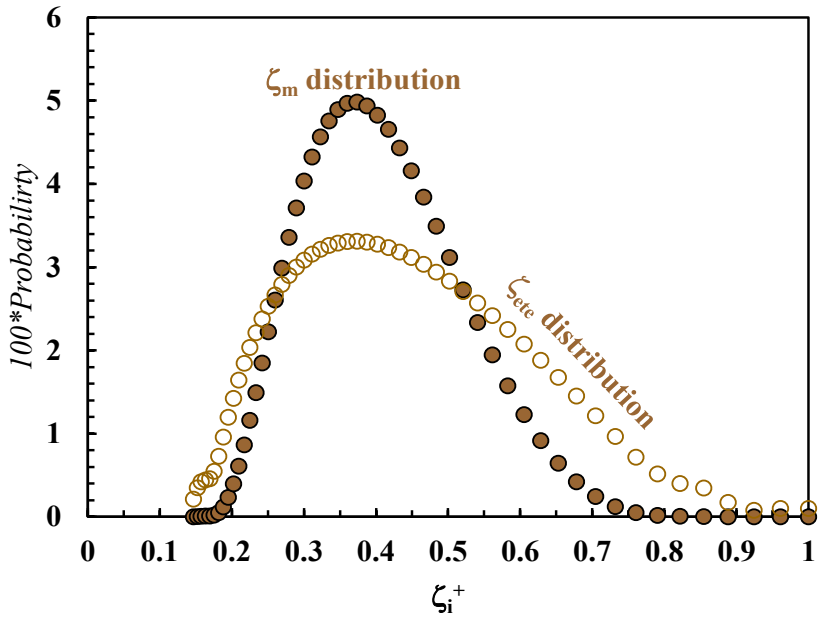

Figure 39: Comparison between the ζ_m ($\approx \zeta_c$) (brown dots) and the ζ_{ete} (open dots) distributions for scleroglucan hydrogels at 2%.

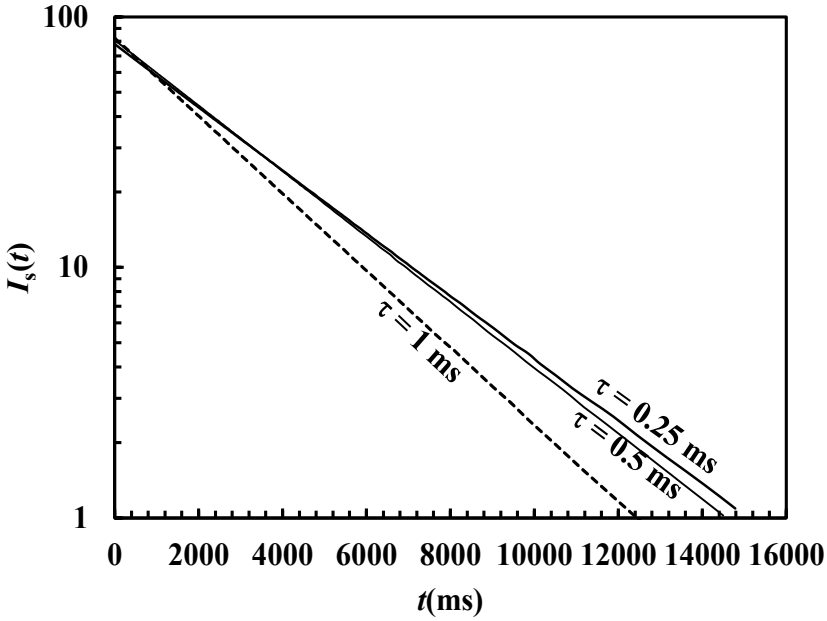

Figure 40: FID ($I_s(t)$) decay dependence on the time separation τ between pulses at 90° and 180° of the CPMG sequence for Milli-Q water at 37° C and 20 MHz.

M_w	$1.2 \cdot 10^6$	K_w (dL/g)	$3.9 \cdot 10^{-4}$ [52]
M_r	636 [96]	$\overline{\alpha}$	1.1 [52]
M_c	593537	$[\eta]$ (dL/g)	19.1 [52]
N	993	R_g (nm)	27.6
ρ_p (g/cm^3)	1.6 [97]	c^* (g/mL)	$0.6 \cdot 10^{-3}$
ϕ	$12.6 \cdot 10^{-3}$	c (g/mL)	$2.0 \cdot 10^{-2}$
$l^2 C_\infty$ (mol/cm^3)	26.1	m	0.76 [87]
ρ_x (μmol/cm^3)	0.03	ζ_c (nm)	6.6
ζ_{ete} (nm)	612	ζ_m (nm)	47.5

Table 6: Evaluation of correlation (ζ_c) and end-to-end (ζ_{ete}) lengths for scleroglucan 2% hydrogels assuming a hexa-functional (or cubical, $f = 6$) network. Symbols and references to equations are as in Tab. (4).

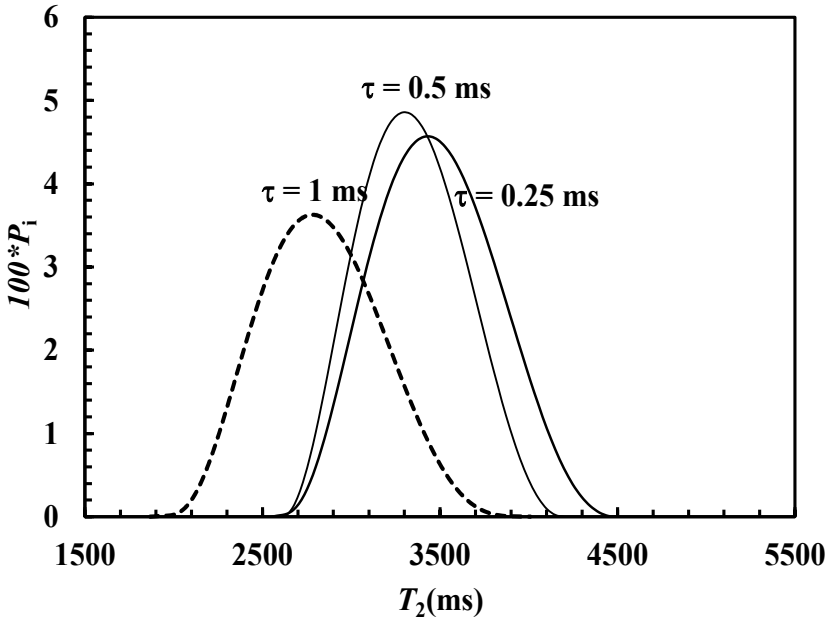

Figure 41: Relaxation spectra of the three decay curves depicted in Fig. (40).

tially shift, but the distribution width increases with w_{st}. Accordingly, while the extrapolation of the peak position at $\tau = 0$ holds whatever the value of w_{st}, in principle the width calculation needs an evaluation at every w_{st}. In the specific case of polymeric hydrogels, it is found that the optimal w_{st} normally ranges between 100 and 300.[81] For this domain, $w_{st} = 150$ may be taken as a representative value, as the distribution width remains substantially unchanged (Fig. 43). Clearly, the effect of time separation (τ) on the $T_{2\text{H}_2\text{0}}$ spectrum occurs whatever the temperature considered. In particular, at $T = 25$ °C, it was found[39] that in the limit $\tau \to 0$ the $T_{2\text{H}_2\text{0}}$

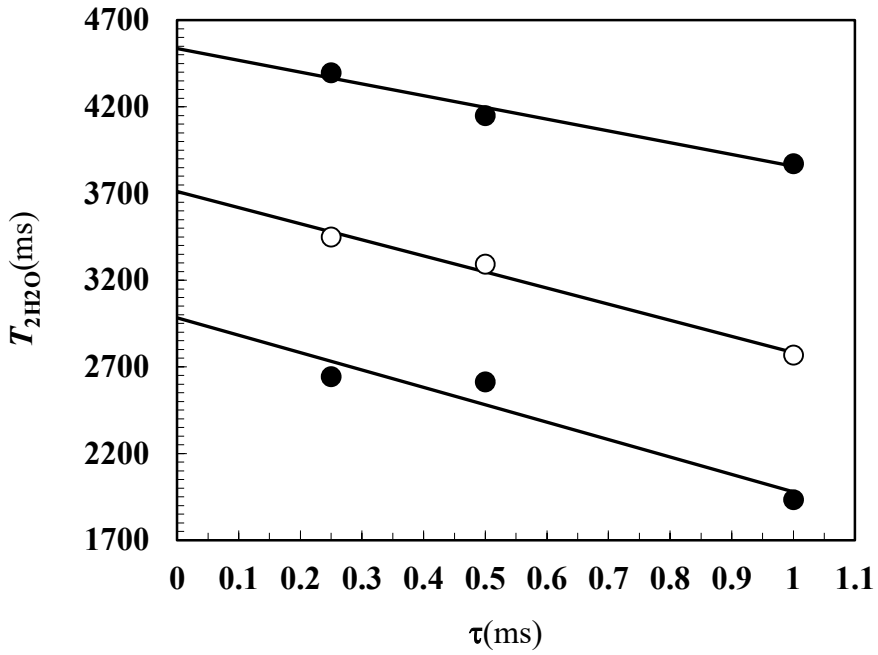

Figure 42: The effect of increasing τ on the displacement of the peak (white circles) and the two extremes (black circles) is observed across the three distributions in Fig. (41), with solid lines illustrating the linear interpolants.

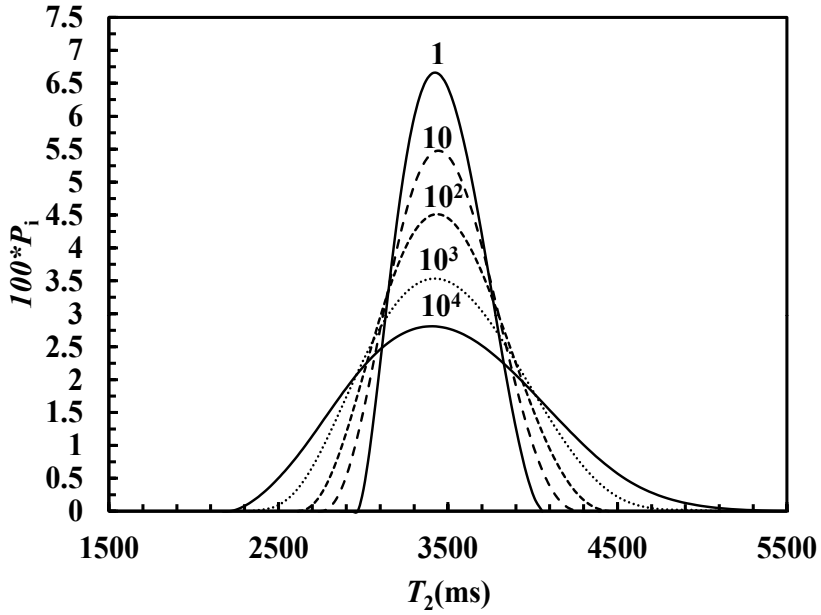

Figure 43: How increasing the smoothing factor (w_{st} = 1, 10, 10^2, 10^3, 10^4) affects the distribution of water relaxation times (solid and dotted lines) at $\tau = 0.25$ ms, 37° C and 20 MHz.

spectrum spans from 2546 ms to 3634 ms, showing its peak at 3022 ms. Thus, we assume 3634 ms as the free water relaxation time at 25 °C and 20 MHz.

5.10. Mesh Size Effect on the Diffusion Coefficient

A practical/clinical inquiry that demands attention concerns the impact of varying mesh size distributions on the diffusion coefficient of solutes within the network. While a precise resolution of this matter necessitates the numerical solution of Fick's second equation in three dimensions, a reasonable approximation can be provided through a simpler approach.

We can begin by converting the mesh size distribution $100P_i - \zeta_i$, for instance the one depicted in Fig. (27) for the sputum of CF patient 178, into the corresponding distribution of diffusion coefficients. To this purpose, it is convenient to employ the Lustig & Peppas model,[98] successively implemented by Abrami et al as:[68]

$$\frac{D_i}{D_0} = \left(1 - \frac{2r_s}{\zeta_i}\right) \mathrm{e}^{-\left[\frac{Y}{\left(\frac{\zeta_i}{r_f}\right)^2}\frac{c_0}{c_1} - 0.42\right]} \tag{5.16}$$

Here, r_s is the radius of the diffusing solute assumed to be a sphere, r_f denotes the radius of the polymeric chains constituting the network, c_0 and c_1 are the former constants (SI 5.1) related to the mesh architecture (for a cubic mesh $c_0 = 1$ and $c_1 = 3\pi$), Y is a model parameter, which, in the absence of further information, can be set[98] to 1, D_0 is the solute diffusion coefficient in the solvent (water) pervading the network, and D_i represents the solute diffusion coefficient through a mesh sized ζ_i. Eq. (5.16) facilitates the establishment of a straightforward connection between D_i and the corresponding mesh size ζ_i present in the network with probability P_i. Assuming the typical value[86] $r_f = 0.8$ nm, Fig. (44) depicts the distribution of D_i for three different values of r_s in the case of Gauss (green lines) and generalized Weibull (red lines) end-to-end distributions. To generalize the results, the solute diffusion coefficient distribution is shown in (D_i/D_0) units.

Fig. (44) then illustrates that, regardless of the value of r_s, the distribution of D_i/D_0 resulting from the generalized Weibull end-to-end distribution (Eq. 16, main text) is skewed towards larger values of the diffusion coefficient. This discrepancy is minor for smaller solutes ($r_s = 1$

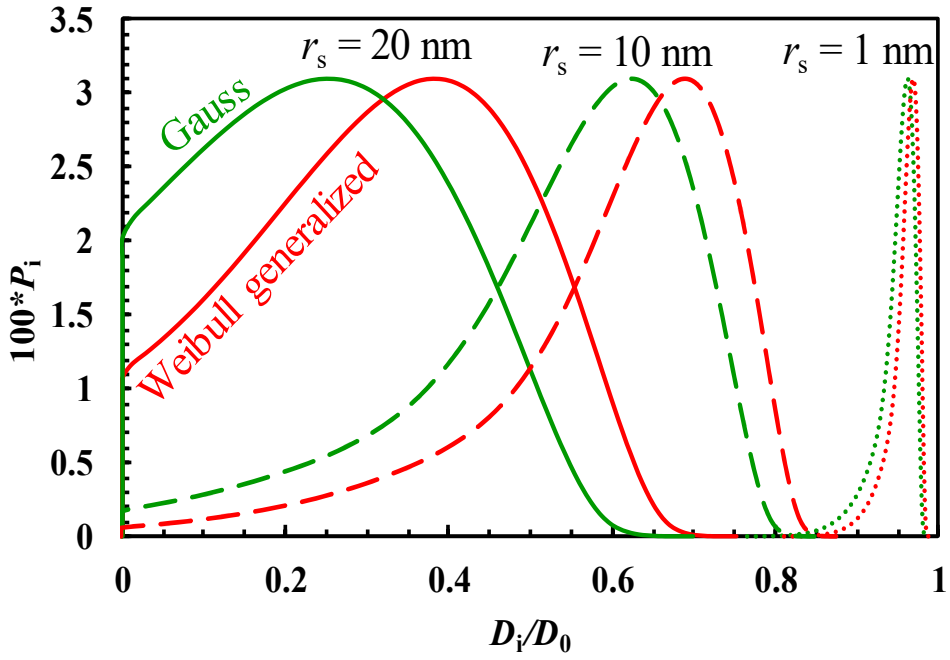

Figure 44: The effect of solute radius (r_s) on its relative diffusion coefficient (D_i/D_0) distribution, derived from the mesh size statistics depicted in Fig. (31) and referring to the sputum of CF patient 178, is investigated. This simulation relies on Eq. (5.16) with $r_f = 0.8$ nm, $Y = 1$, $c_0 = 1$, and $c_1 = 3\pi$. P_i represents the probability of finding a mesh of size ζ_i inside the network.

nm) to become increasingly significant for larger ones, which is a common scenario encountered in gene delivery when the drug needs to be encapsulated within a carrier to shield it from various environmental factors such as enzymes (main text, section 4.4). It is worth noting that similar overall trends can be observed for different Y and r_f values within their typical ranges ($1 \leq Y \leq 30$;[99] 0.5 nm $\leq r_f \leq 5$ nm[86]). To further bolster the previous observations, it is beneficial to analyze the average relative diffusion coefficient $(D/D_0)_m$ characterizing the D_i/D_0 distributions illustrated in Fig. (44):

$$\left(\frac{D}{D_0}\right)_m = \frac{\sum_i \left(\frac{D_i}{D_0}\right) P_i}{\sum_i P_i} \tag{5.17}$$

and defining the percentage difference ($\Delta\%$) between that coming from the generalized Weibullian $(D/D_0)_m^{(W)}$ and Gaussian $(D/D_0)_m^{(G)}$ distributions:

$$\Delta\% \;=\; 100\,\frac{\left(\frac{D}{D_0}\right)_m^{(W)} - \left(\frac{D}{D_0}\right)_m^{(G)}}{\left(\frac{D}{D_0}\right)_m^{(G)}} \tag{5.18}$$

Fig. (45) shows that, for small r_s, $\Delta\%$ is negligible while it rapidly increases for larger r_s (blue line).

Once the effect of different mesh size distributions on the diffusion coefficient has been evaluated, it is important to estimate how this reflects on solute diffusion. Assuming that solute transport is mainly affected by diffusion with constant D (possible chemical-physical interactions

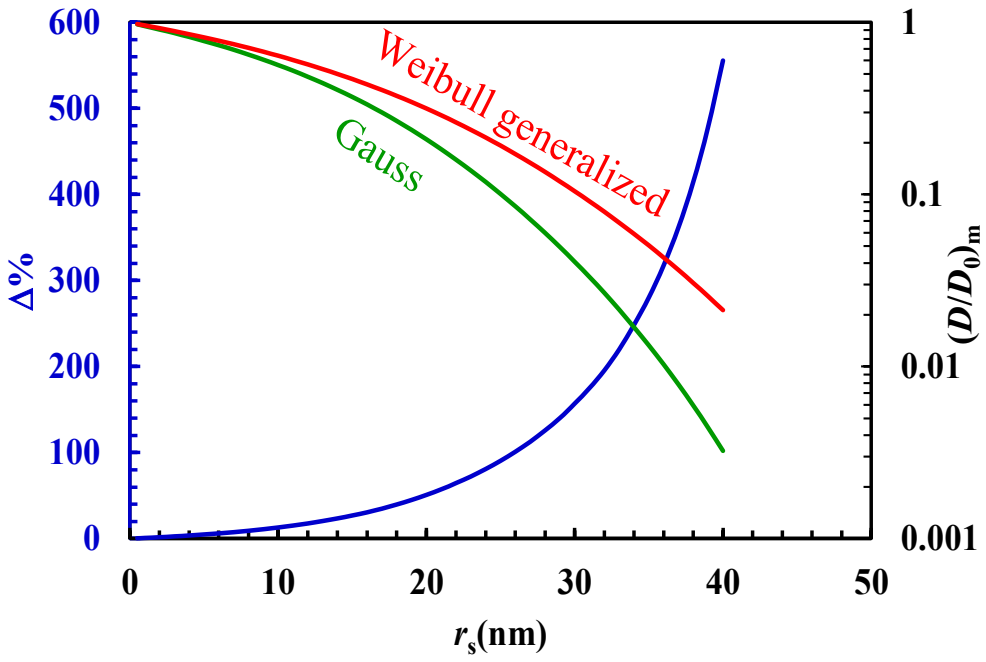

Figure 45: The effect of solute radius (r_s) on the percentage difference ($\Delta\%$, Eq. 5.18, blue line, left vertical axis) between the average relative diffusion coefficient derived from the generalized Weibull $(D/D_0)_m^{(W)}$ and Gaussian distributions $(D/D_0)_m^{(G)}$ is examined, as shown in Fig. (44). Red and green lines represent respectively the trends of $(D/D_0)_m^{(W)}$ and $(D/D_0)_m^{(G)}$ versus r_s (right vertical axis).

between solute and polymeric chains are neglected or occur very quickly compared to diffusional processes), the prediction of solute penetration inside the airway surface layer (ASL) can be obtained by solving the one-dimensional Fick's equation with proper initial and boundary conditions. In particular, it is assumed that at time $t = 0$ (deposition on ASL via inhalation of a liquid phase containing the solute), the solute is not present inside the ASL and it is uniformly distributed at the known concentration $C = C_0$, in the liquid phase (of thickness δ) topping the ASL. Boundary conditions involve the existence of an impermeable wall at position $X = 0$ (solutes cannot diffuse towards the negative X direction) and the possibility of diffusion in the positive direction up to $X \to \infty$ (i.e. drugs can diffuse inside cells too). According to these hypotheses, the time evolution of the drug profile concentration inside ASL can be properly approximated by:[100]

$$\frac{C}{C_0} = \frac{\delta}{\sqrt{4\pi D t}} \, \mathrm{e}^{-\left(\frac{X^2}{4Dt}\right)} \tag{5.19}$$

The solute diffusion coefficient D is calculated by Eq. (5.16), after taking the average mesh size from Tab. (3) ($\zeta_m = 51.4$ nm for Gauss; $\zeta_m = 62.2$ nm for generalized Weibull), setting $r_s = 25$ nm, $D_0 = 1.31 \times 10^{-11}$ m^2/s (Stokes & Einstein's equation at $T = 37$ °C), $\delta = 3$ μm and an ASL thickness of 27 μm (typical value for CF patients and healthy subjects[101]), with all other parameters as adopted in Fig. (44) ($r_f = 0.8$ nm, $Y = 1$, $c_0 = 1$, $c_1 = 3\pi$).

Fig. (46) shows the solute profile concentration (Eq. 5.19) at increasing times (8 s, 32 s, 128 s) by adopting the mesh size distribution derived from the Gauss (green line) and generalized Weibull (red line) end-to-end distributions. It is evident that when large solutes are regarded ($r_s/\zeta_m = 0.486$ for Gauss; $r_s/\zeta_m = 0.402$ for Weibull), different distributions result in considerable differences in diffusion inside the ASL, which becomes much more permeable to solute when the Weibullian statistics is considered. Indeed, for $X \leq 4$, the green lines in Fig. (46) always exceed the corresponding red lines (generalized Weibull). The improved ASL permeability conferred by the generalized Weibull end-to-end distribution can be further emphasized by looking at Fig. (47), showing the time evolution of solute concentration on the epithelial cell surface ($X = 30$ μm). It is clear that the concentration evolution following the generalized Weibullian

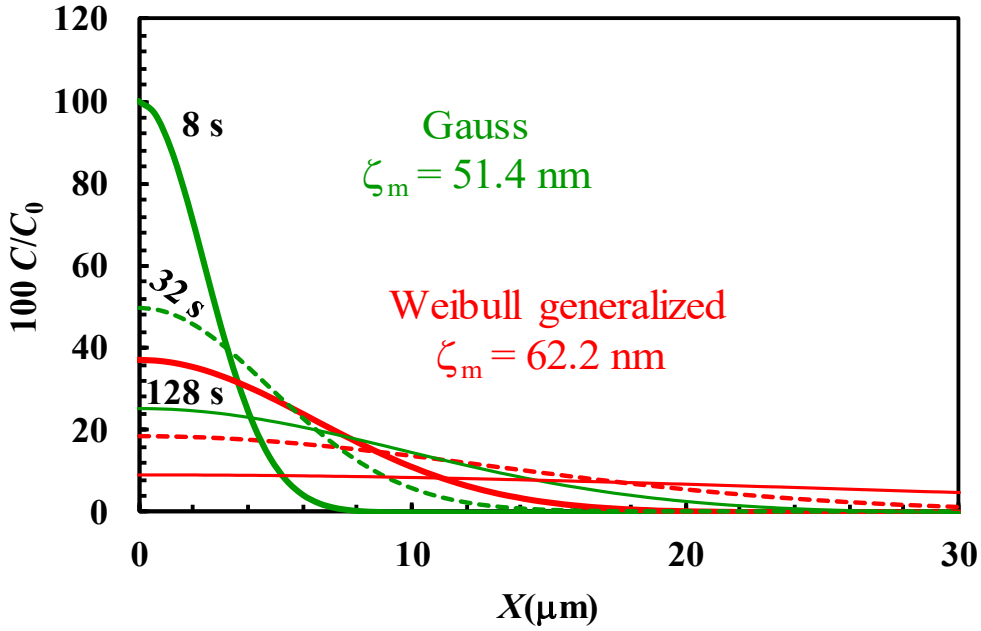

Figure 46: The solute profile concentration (Eq. 5.19) is depicted relative to the Gaussian (green line, average mesh size $\zeta_m = 51.4$ nm) and generalized Weibull distribution (red line, average mesh size $\zeta_m = 62.2$ nm). Thick solid line refers to 8 s, the dashed line to 32 s, and the solid thin line to 128 s. The position of the surface of epithelial cells is given by $X = 30$ μm.

(red line) greatly anticipates that derived from the Gauss end-to-end distribution (green line). Obviously, the lower the r_s/ζ_m ratio, the smaller the effect of the chosen distribution on the diffusion process.

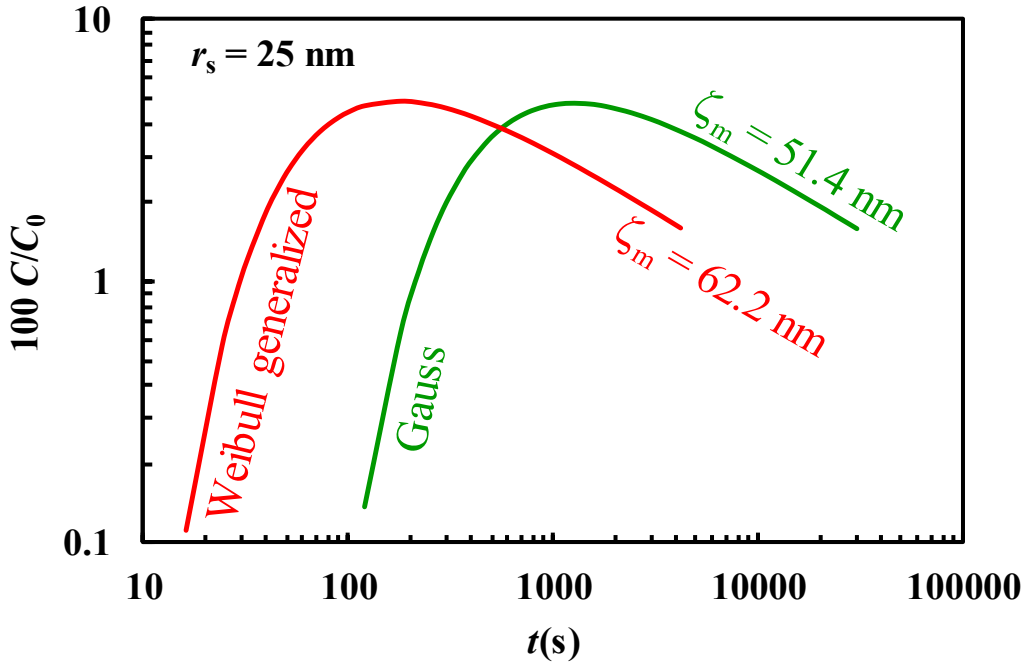

Figure 47: Temporal variation of the dimensionless solute concentration (C/C_0) on the surface of epithelial cells, $X = 30$ μm (Eq. 5.19), relative to the Gaussian (green line, average mesh size $\zeta_m = 51.4$ nm) and the generalized Weibullian (red line, average mesh size $\zeta_m = 62.2$ nm) end-to-end distributions. All parameter values are as in Fig. (46).

Supporting Information References

[1] P. Flory, Principles of Polymer Chemistry, Baker lectures 1948, Cornell University Press, Ithaca, New York, USA, 1953.

[2] M. F. Beatty, Topics in Finite Elasticity: Hyperelasticity of Rubber, Elastomers, and Biological Tissues—With Examples, Appl. Mech. Rev. 40 (12) (1987) 1699–1734. doi:10.1115/1.3149545.

[3] H. M. James, E. Guth, Theory of the increase in rigidity of rubber during cure, J. Chem. Phys. 15 (9) (1947) 669–683. doi:10.1063/1.1746626.

[4] L. R. G. Treloar, The Physics of Rubber Elasticity, 3rd Edition, Clarendon Oxford, 1975.

[5] B. Erman, P. J. Flory, Relationships between stress, strain, and molecular constitution of polymer networks. comparison of theory with experiments, Macromolecules 15 (3) (1982) 806–811. doi:10.1021/ma00231a023.

[6] S. A. Mezzasalma, M. Abrami, G. Grassi, M. Grassi, Rubber elasticity of polymer networks in explicitly non-gaussian states. statistical mechanics and lf-nmr inquiry in hydrogel systems, Int. J. Eng. Sci. 176 (2022) 103676. doi:10.1016/j.ijengsci.2022.103676.

[7] A. Y. Grosberg, A. Khokhlov, Statistical Physics of Macromolecules, AIP series in polymers and complex materials, AIP Press, 1994.

[8] T. Witten, P. Pincus, Structured Fluids: Polymers, Colloids, Surfactants, Oxford University Press, 2010.

[9] P. J. Flory, Molecular theory of rubber elasticity, Polymer 20 (11) (1979) 1317–1320, jabtonna Conference on Polymer Networks. doi:10.1016/0032-3861(79)90268-4.

[10] E. M. Arruda, M. C. Boyce, A three-dimensional constitutive model for the large stretch behavior of rubber elastic materials, J. Mech. Phys. Solids 41 (2) (1993) 389–412. doi:10.1016/0022-5096(93)90013-6.

[11] M. Rubinstein, R. Colby, Polymer Physics, Oxford University Press, 2003.

[12] F. Reif, Fundamentals of Statistical and Thermal Physics, McGraw Hill, 1965.

[13] J.-Y. Fortin, M. Clusel, Applications of extreme value statistics in physics, J. Phys. A: Math. Theor. 48 (18) (2015) 183001. doi:10.1088/1751-8113/48/18/183001.

[14] N. Johnson, S. Kotz, Continuous Univariate Distributions, no. v. 1 in Continuous Univariate Distributions, J. Wiley, 1970.

[15] I. S. Gradshteyn, I. M. Ryzhik, Table of integrals, series, and products, seventh Edition, Elsevier/Academic Press, Amsterdam, 2007, translated from the Russian.

[16] Desmos Graphing Calculator (at https://www.desmos.com/calculator).

[17] M. Clusel, E. Bertin, Global fluctuations in physical systems: a subtle interplay between sum and extreme value statistics, Int. J. Mod. Phys. B (22) (2008) 3311. doi:10.48550/arXiv.0807.1649.

[18] E. Bertin, M. Clusel, Generalized extreme value statistics and sum of correlated variables, J. Phys. A: Math. Gen. 39 (24) (2006) 7607. doi:10.1088/0305-4470/39/24/001.

[19] The Sage Developers, SageMath, the Sage Mathematics Software System (Version 8.7), https://www.sagemath.org (2019).

[20] M. E. Fisher, Shape of a Self-Avoiding Walk or Polymer Chain, J. Chem. Phys. 44 (2) (2004) 616–622. doi:10.1063/1.1726734.

[21] J. des Cloizeaux, Lagrangian theory for a self-avoiding random chain, Phys. Rev. A 10 (1974) 1665–1669. doi:10.1103/PhysRevA.10.1665.

[22] P. de Gennes, Scaling Concepts in Polymer Physics, Cornell University Press, Ithaca, New York, USA, 1979.

[23] S. Mezzasalma, Macromolecules in Solution and Brownian Relativity, Academic Press-Elsevier, London, 2008. doi:10.1016/S1573-4285(07)00009-9.

[24] J. des Cloizeaux, Lagrangian theory for a self-avoiding random chain, Phys. Rev. A 10 (1974) 1665–1669. doi:10.1103/PhysRevA.10.1665.

[25] A. Papoulis, S. U. Pillai, Probability, Random Variables, and Stochastic Processes, 4th Edition, McGraw Hill, Boston, 2002.

[26] S. N. Majumdar, A. Pal, G. Schehr, Extreme value statistics of correlated random variables: A pedagogical review, Phys. Rep. 840 (2020) 1–32, extreme value statistics of correlated random variables: A pedagogical review. doi:10.1016/j.physrep.2019.10.005.

[27] E. Bertin, Global fluctuations and gumbel statistics, Phys. Rev. Lett. 95 (2005) 170601. doi:10.1103/PhysRevLett.95.170601.

[28] M. Doi, S. Edwards, The Theory of Polymer Dynamics, International series of monographs on physics, Clarendon Press, Oxford, 1988.

[29] W. W. Graessley, R. C. Hayward, G. S. Grest, Excluded-volume effects in polymer solutions. comparison of experimental results with numerical simulation data, Macromolecules 32 (10) (1999) 3510–3517. doi:10.1021/ma981915p.

[30] A. Hajikhani, P. Wriggers, M. Marino, Chemo-mechanical modelling of swelling and crosslinking reaction kinetics in alginate hydrogels: A novel theory and its numerical implementation, J. Mech. Phys. Solids 153 (2021) 104476. doi:10.1016/j.jmps.2021.104476.

[31] Q. Lei, M. Zhang, L. Shen, R. Li, B. Q. Liao, H. Lin, A novel insight into membrane fouling mechanism regarding gel layer filtration: Flory-huggins based filtration mechanism, Sci. Rep. 6 (2016) 33343. doi:10.1038/srep33343.

[32] E. Aasprong, O. Smidsr, B. T. Stokke, Swelling, mechanical properties and effect of annealing of scleroglucan gels, Carbohydr. Polym. 60 (3) (2005) 363–378. doi:10.1016/j.carbpol.2005.01.016.

[33] E. W. Merrill, K. A. Dennison, C. Sung, Partitioning and diffusion of solutes in hydrogels of poly(ethylene oxide), Biomaterials 14 (15) (1993) 1117–1126. doi:10.1016/0142-9612(93)90154-T.

[34] A. K. Das, D.-Y. Hsu, P.-D. Hong, Dynamic viscosity of peg:peg-ran-ppg blends through stress relaxation, Macromol. Theory Simul. 20 (1) (2011) 19–30. doi:10.1002/mats.201000053.

[35] W. R. Good, H.-J. Cantow, One and two component hydrogels, 3. deswelling and compression measurements on one component hydrogels, Makromol. Chem. 180 (11) (1979) 2605–2613. doi:10.1002/macp.1979.021801105.

[36] A. P. Safronov, F. A. Blyakhman, T. F. Shklyar, T. V. Terziyan, M. A. Kostareva, S. A. Tchikunov, G. H. Pollack, The influence of counterion type and temperature on flory-huggins

binary interaction parameter in polyelectrolyte hydrogels, Macromol. Chem. Phys. 210 (7) (2009) 511–519. doi:10.1002/macp.200800495.

[37] P. Matricardi, F. Alhaique, T. Coviello, Polysaccharide Hydrogels: Characterization and Biomedical Applications, Taylor Francis Group, CRC Press, Boca Raton, USA, 2016.

[38] P. Marizza, M. Abrami, S. Keller, P. Posocco, E. Laurini, K. Goswami, A. Skov, A. Boisen, D. Larobina, G. Grassi, M. Grassi, Synthesis and characterization of uv photocrosslinkable hydrogels with poly(n-vinyl-2-pyrrolidone): Determination of the network mesh size distribution, Int. J. Polym. Mater. Polym. Biomater. 65 (10) (2016) 516–525. doi:10.1080/00914037.2015.1129964.

[39] M. Abrami, F. Bignotti, F. Baldi, G. Spagnoli, A. Biasin, L. Grassi, G. Grassi, M. Grassi, Rheological and low field nmr characterization of hydrophobically-modified peg hydrogels for drug delivery, Int. J. Pharm. 637 (2023) 122882. doi:10.1016/j.ijpharm.2023.122882.

[40] I. Donati, S. Paoletti, Alginates: Biology and Applications, Vol. 13, 2009, Ch. Material Properties of Alginates, pp. 1–53. doi:10.1007/978-3-540-92679-5(1).

[41] K. I. Draget, O. Smidsr, G. Skjåk-Bræk, Alginates from Algae, Vol. 6, John Wiley Sons, Ltd, 2005. doi:10.1002/3527600035.bpol6008.

[42] P. de Vos, M. Bučko, P. Gemeiner, M. Navrátil, J. Švitel, M. Faas, B. L. Strand, G. Skjak-Braek, Y. A. Morch, A. Vikartovská, I. Lacík, G. Kolláriková, G. Orive, D. Poncelet, J. L. Pedraz, M. B. Ansorge-Schumacher, Multiscale requirements for bioencapsulation in medicine and biotechnology, Biomaterials 30 (13) (2009) 2559–2570. doi:10.1016/j.biomaterials.2009.01.014.

[43] P. Matricardi, C. Di Meo, T. Coviello, W. E. Hennink, F. Alhaique, Interpenetrating polymer networks polysaccharide hydrogels for drug delivery and tissue engineering, Adv. Drug Deliv. Rev. 65 (9) (2013) 1172–1187, polysaccharide-based systems in drug and gene delivery. doi:10.1016/j.addr.2013.04.002.

[44] J. Totten, H. Alhadrami, E. Jiffri, C. McMullen, F. Seib, H. Carswell, Towards clinical translation of 'second-generation' regenerative stroke therapies: hydrogels as game changers?, Trends Biotechnol. (Nov. 2021). doi:10.1016/j.tibtech.2021.10.009.

[45] S. Arnott, A. Fulmer, W. Scott, I. Dea, R. Moorhouse, D. Rees, The agarose double helix and its function in agarose gel structure, J. Mol. Biol. 90 (2) (1974) 269–284. doi:10.1016/0022-2836(74)90372-6.

[46] K. Labropoulos, D. Niesz, S. Danforth, P. Kevrekidis, Dynamic rheology of agar gels: theory and experiments. part i. development of a rheological model, Carbohydr. Polym. 50 (4) (2002) 393–406. doi:10.1016/S0144-8617(02)00084-X.

[47] T. Kopač, M. Abrami, M. Grassi, A. Ručigaj, M. Krajnc, Polysaccharide-based hydrogels crosslink density equation: A rheological and lf-nmr study of polymer-polymer interactions, Carbohydr. Polym. 277 (2022) 118895. doi:10.1016/j.carbpol.2021.118895.

[48] M. Djabourov, A. H. Clark, D. W. Rowlands, S. B. Ross-Murphy, Small-angle x-ray scattering characterization of agarose sols and gels, Macromolecules 22 (1) (1989) 180–188. doi:10.1021/ma00191a035.

[49] M. Kouwijzer, S. Pérez, Molecular modeling of agarose helices, leading to the prediction of crystalline allomorphs, Biopolymers 46 (1) (1998) 11–29. doi:10.1002/(SICI)1097-0282(199807)46:1¡11::AID-BIP2¿3.0.CO;2-0.

[50] M. Rinaudo, M. Vincendon, 13c nmr structural investigation of scleroglucan, Carbohydr. Polym. 2 (2) (1982) 135–144. doi:10.1016/0144-8617(82)90059-5.

[51] T. L. Bluhm, Y. Deslandes, R. H. Marchessault, S. Pérez, M. Rinaudo, Solid-state and solution conformation of scleroglucan, Carbohydr. Res. 100 (1) (1982) 117–130. doi:10.1016/S0008-6215(00)81030-7.

[52] J. Fariña, F. Siñeriz, O. Molina, N. Perotti, Isolation and physicochemical characterization of soluble scleroglucan from sclerotium rolfsii. rheological properties, molecular weight and

conformational characteristics, Carbohydr. Polym. 44 (1) (2001) 41–50. doi:10.1016/S0144-8617(00)00189-2.

[53] A. Palleschi, G. Bocchinfuso, T. Coviello, F. Alhaique, Molecular dynamics investigations of the polysaccharide scleroglucan: first study on the triple helix structure, Carbohydr. Res. 340 (13) (2005) 2154–2162. doi:10.1016/j.carres.2005.06.026.

[54] M. Grassi, R. Lapasin, S. Pricl, A study of the rheological behavior of scleroglucan weak gel systems, Carbohyd. Polym. 29 (2) (1996) 169–181. doi:10.1016/0144-8617(95)00120-4.

[55] R. Lapasin, S. Pricl, Rheology of Industrial Polysaccharides: Theory and Applications; Blackie Academic & Professional, 1995. doi:10.1007/978-1-4615-2185-3.

[56] T. Coviello, M. Grassi, R. Lapasin, A. Marino, F. Alhaique, Scleroglucan/borax: characterization of a novel hydrogel system suitable for drug delivery, Biomaterials 24 (16) (2003) 2789–2798. doi:10.1016/S0142-9612(03)00087-5.

[57] M. Grassi, R. Lapasin, T. Coviello, P. Matricardi, C. Di Meo, F. Alhaique, Scleroglucan/borax/drug hydrogels: Structure characterisation by means of rheological and diffusion experiments, Carbohydr. Polym. 78 (3) (2009) 377–383. doi:10.1016/j.carbpol.2009.04.025.

[58] P. Matricardi, I. Onorati, T. Coviello, F. Alhaique, Drug delivery matrices based on scleroglucan/alginate/borax gels, Int. J. Pharm. 316 (1) (2006) 21–28. doi:10.1016/j.ijpharm.2006.02.024.

[59] S. C. Viñarta, N. J. François, M. E. Daraio, L. I. Figueroa, J. I. Fariña, Sclerotium rolfsii scleroglucan: The promising behavior of a natural polysaccharide as a drug delivery vehicle, suspension stabilizer and emulsifier, Int. J. Biol. Macromol. 41 (3) (2007) 314–323. doi:10.1016/j.ijbiomac.2007.04.001.

[60] B. P. O'Sullivan, S. D. Freedman, Cystic fibrosis, Lancet 373 (9678) (2009) 1891–1904. doi:10.1016/S0140-6736(09)60327-5.

[61] P. M. Farrell, The prevalence of cystic fibrosis in the european union, J. Cyst. Fibros. 7 (5) (2008) 450–453. doi:10.1016/j.jcf.2008.03.007.

[62] O. Ciofu, T. Tolker-Nielsen, P. Østrup Jensen, H. Wang, N. Hby, Antimicrobial resistance, respiratory tract infections and role of biofilms in lung infections in cystic fibrosis patients, Adv. Drug Deliv. Rev. 85 (2015) 7–23, inhaled antimicrobial chemotherapy for respiratory tract infections: Successes, challenges and the road ahead. doi:10.1016/j.addr.2014.11.017.

[63] N. Vij, G. P. Downey, The yin and yang of cystic fibrosis transmembrane conductance regulator function, Am. J. Respir. Crit. Care Med. 187 (2) (2013) 120–122. doi:10.1164/rccm.201211-2011ED.

[64] J. Emerson, M. Rosenfeld, S. McNamara, B. Ramsey, R. L. Gibson, Pseudomonas aeruginosa and other predictors of mortality and morbidity in young children with cystic fibrosis, Pediatr. Pulmonol. 34 (2) (2002) 91–100. doi:10.1002/ppul.10127.

[65] D. Yang, K. S. Jones, Effect of alginate on innate immune activation of macrophages, J. Biomed. Mater. Res. A 90A (2) (2009) 411–418. doi:10.1002/jbm.a.32096.

[66] M. Iwamoto, M. Kurachi, T. Nakashima, D. Kim, K. Yamaguchi, T. Oda, Y. Iwamoto, T. Muramatsu, Structure–activity relationship of alginate oligosaccharides in the induction of cytokine production from raw264.7 cells, FEBS Lett. 579 (20) (2005) 4423–4429. doi:10.1016/j.febslet.2005.07.007.

[67] L. M. Cobb, J. C. Mychaleckyj, D. J. Wozniak, Y. S. Lopez-Boado, Pseudomonas aeruginosa Flagellin and Alginate Elicit Very Distinct Gene Expression Patterns in Airway Epithelial Cells: Implications for Cystic Fibrosis Disease1, J. Immun. 173 (9) (2004) 5659–5670. doi:10.4049/jimmunol.173.9.5659.

[68] M. Abrami, M. Maschio, M. Conese, M. Confalonieri, F. Salton, F. Gerin, B. Dapas, R. Farra, A. Adrover, G. Milcovich, C. Fornasier, A. Biasin, M. Grassi, G. Grassi, Effect of chest physiotherapy on cystic fibrosis sputum nanostructure: an experimental and theoretical approach, Drug Deliv. Transl. Res. 12 (2022) 1943–1958. doi:10.1007/s13346-022-01131-8.

[69] C. Fung, S. Naughton, L. Turnbull, P. Tingpej, B. Rose, J. Arthur, H. Hu, C. Harmer, C. Harbour, D. J. Hassett, C. B. Whitchurch, J. Manos, Gene expression of pseudomonas aeruginosa in a mucin-containing synthetic growth medium mimicking cystic fibrosis lung sputum, J. Med. Microbiol. 59 (9) (2010) 1089–1100. doi:10.1099/jmm.0.019984-0.

[70] B. Posocco, E. Dreussi, J. De Santa, G. Toffoli, M. Abrami, F. Musiani, M. Grassi, R. Farra, F. Tonon, G. Grassi, B. Dapas, Polysaccharides for the delivery of antitumor drugs, Materials 8 (5) (2015) 2569–2615. doi:10.3390/ma8052569.

[71] P. G. Woodruff, A. Agusti, N. Roche, D. Singh, F. J. Martinez, Current concepts in targeting chronic obstructive pulmonary disease pharmacotherapy: making progress towards personalised management, Lancet 385 (9979) (2015) 1789–1798. doi:10.1016/S0140-6736(15)60693-6.

[72] G. M. Solomon, L. Fu, S. M. Rowe, J. F. Collawn, The therapeutic potential of cftr modulators for copd and other airway diseases, Curr. Opin. Pharmacol. 34 (2017) 132–139. doi:10.1016/j.coph.2017.09.013.

[73] S. V. Raju, G. M. Solomon, M. T. Dransfield, S. M. Rowe, Acquired cystic fibrosis transmembrane conductance regulator dysfunction in chronic bronchitis and other diseases of mucus clearance, Clin. Chest Med. 37 (1) (2016) 147–158. doi:10.1016/j.ccm.2015.11.003.

[74] J. Witten, K. Ribbeck, The particle in the spider's web: transport through biological hydrogels, Nanoscale 9 (2017) 8080–8095. doi:10.1039/C6NR09736G.

[75] M. Mitchell, M. Billingsley, R. Haley, M. Wechsler, N. Peppas, R. Langer, Engineering precision nanoparticles for drug delivery, Nat. Rev. Drug Discov. 20 (2021) 101–124. doi:10.1038/s41573-020-0090-8.

[76] V. Bühler, Kollidon: Polyvinylpyrrolidone for Pharmaceutical Industry, BASF, Ludwigshafen, Germany, 1996.

[77] F. Bignotti, F. Baldi, M. Grassi, M. Abrami, G. Spagnoli, Hydrophobically-modified peg hydrogels with controllable hydrophilic/hydrophobic balance, Polymers 13 (9) (2021). doi:10.3390/polym13091489.

[78] S. Meiboom, D. Gill, Modified spin-echo method for measuring nuclear relaxation times, Rev. Sci. Instr. 29 (8) (1958) 688–691. doi:10.1063/1.1716296.

[79] P. Sacco, M. Borgogna, A. Travan, E. Marsich, S. Paoletti, F. Asaro, M. Grassi, I. Donati, Polysaccharide-based networks from homogeneous chitosan-tripolyphosphate hydrogels: Synthesis and characterization, Biomacromolecules 15 (9) (2014) 3396–3405. doi:10.1021/bm500909n.

[80] M. Abrami, G. Chiarappa, R. Farra, G. Grassi, P. Marizza, M. Grassi, Use of low-field nmr for the characterization of gels and biological tissues, ADMET DMPK 6 (1) (2018) 34–46. doi:10.5599/admet.6.1.430.

[81] X. Wang, Q. Ni, Determination of cortical bone porosity and pore size distribution using a low field pulsed nmr approach, J. Orthop. Res. 21 (2) (2003) 312–319. doi:10.1016/S0736-0266(02)00157-2.

[82] K. Burnham, D. Anderson, Model Selection and Multimodel Inference: A Practical Information-Theoretic Approach, Springer New York, 2002.

[83] J. Schurz, Rheology of polymer solutions of the network type, Progr. Polym. Sci. 16 (1) (1991) 1–53. doi:10.1016/0079-6700(91)90006-7.

[84] M. D. De'Nobili, A. M. Rojas, M. Abrami, R. Lapasin, M. Grassi, Structure characterization by means of rheological and nmr experiments as a first necessary approach to study the l-(+)-ascorbic acid diffusion from pectin and pectin/alginate films to agar hydrogels that mimic food materials, J. Food Eng. 165 (2015) 82–92. doi:10.1016/j.jfoodeng.2015.05.014.

[85] E. Pasut, R. Toffanin, D. Voinovich, C. Pedersini, E. Murano, M. Grassi, Mechanical and

diffusive properties of homogeneous alginate gels in form of particles and cylinders, J. Biomed. Mater. Res. A 87A (3) (2008) 808–818. doi:10.1002/jbm.a.31680.

[86] B. Amsden, Solute diffusion within hydrogels. mechanisms and models, Macromolecules 31 (23) (1998) 8382–8395. doi:10.1021/ma980765f.

[87] B. G. Amsden, Hydrogel mesh size and its impact on predictions of mathematical models of the solute diffusion coefficient, Macromolecules 55 (18) (2022) 8399–8408. doi:10.1021/acs.macromol.2c01443.

[88] N. R. Richbourg, N. A. Peppas, The swollen polymer network hypothesis: Quantitative models of hydrogel swelling, stiffness, and solute transport, Progr. Polym. Sci. 105 (2020) 101243. doi:10.1016/j.progpolymsci.2020.101243.

[89] A. Banerjee, R. De, B. Das, Hydrodynamic and conformational characterization of aqueous sodium alginate solutions with varying salinity, Carbohydr. Polym. 277 (2022) 118855. doi:10.1016/j.carbpol.2021.118855.

[90] A. W. Chan, R. J. Neufeld, Modeling the controllable ph-responsive swelling and pore size of networked alginate based biomaterials, Biomaterials 30 (30) (2009) 6119–6129. doi:10.1016/j.biomaterials.2009.07.034.

[91] H. Storz, K. J. Müller, F. Ehrhart, I. Gómez, S. G. Shirley, P. Gessner, G. Zimmermann, E. Weyand, V. L. Sukhorukov, T. Forst, M. M. Weber, H. Zimmermann, W.-M. Kulicke, U. Zimmermann, Physicochemical features of ultra-high viscosity alginates, Carbohydr. Res. 344 (8) (2009) 985–995. doi:10.1016/j.carres.2009.02.016.

[92] G. Sen, G. Rani, S. Mishra, Microwave assisted synthesis of poly(2-hydroxyethylmethacrylate) grafted agar (ag-g-p(hema)) and its application as a flocculant for wastewater treatment, Front. Chem. Sci. Eng. 7 (2013) 312–321. doi:10.1007/s11705-013-1344-3.

[93] E. Marinho-Soriano, E. Bourret, M. de Casabianca, L. Maury, Agar from the reproductive and vegetative stages of gracilaria bursa-pastoris, Bioresour. Technol. 67 (1) (1999) 1–5. doi:10.1016/S0960-8524(99)00092-9.

[94] S. Boral, H. Bohidar, Hierarchical structures in agar hydrogels, Polymer 50 (23) (2009) 5585–5588. doi:10.1016/j.polymer.2009.09.033.

[95] A. Abragam, The Principles of Nuclear Magnetism, International series of monographs on physics, Clarendon Press, 1961.

[96] M. Sletmoen, B. T. Stokke, Structural properties of polyc–scleroglucan complexes, Biopolymers 79 (3) (2005) 115–127. doi:10.1002/bip.20340.

[97] T. Coviello, P. Matricardi, F. Alhaique, R. Farra, G. Tesei, S. Fiorentino, F. Asaro, G. Milcovich, M. Grassi, Guar gum/borax hydrogel: Rheological, low field nmr and release characterizations, Express Polym. Lett. 7 (2013) 733–746. doi:10.3144/expresspolymlett.2013.71.

[98] S. R. Lustig, N. A. Peppas, Solute diffusion in swollen membranes. ix. scaling laws for solute diffusion in gels, J. Appl. Polym. Sci. 36 (4) (1988) 735–747. doi:10.1002/app.1988.070360401.

[99] M. Abrami, P. Marizza, F. Zecchin, P. Bertoncin, D. Marson, R. Lapasin, F. de Riso, P. Posocco, G. Grassi, M. Grassi, Theoretical importance of pvp-alginate hydrogels structure on drug release kinetics, Gels 5 (2) (2019). doi:10.3390/gels5020022.

[100] J. Crank, The Mathematics of Diffusion, Oxford science publications, Clarendon Press, 1979.

[101] D. V. Olivença, L. L. Fonseca, E. O. Voit, F. R. Pinto, Thickness of the airway surface liquid layer in the lung is affected in cystic fibrosis by compromised synergistic regulation of the enac ion channel, J. R. Soc. Interface 16 (157) (2019) 20190187. doi:10.1098/rsif.2019.0187.